TRAWL GEAR PERFORMANCE AND NET DRAG ANALYSIS WITH APPLICATION TO SMALL TRAWLS AND VESSELS

DAVID A. SMITH

TRAWL GEAR PERFORMANCE AND NET DRAG ANALYSIS WITH APPLICATION TO SMALL TRAWLS AND VESSELS

BY

(c) DAVID A. SMITH, B.Eng.

A thesis submitted to the School of Graduate Studies in partial fulfillment of the requirements for the degree of

Master of Engineering

Faculty of Engineering & Applied Science
Memorial University of Newfoundland

DECEMBER (1986)

St. John's Newfoundland Canada

ISBN 0-315-37011-4

To my wife Deborah
and daughter Victoria

Acknowledgement

I should like to thank my supervisors Mr. J.J. Foster and Dr. G.R. Peters for their patient guidance at every stage of my work. I am grateful for the helpful suggestions of Mr. V. Neelakantan and Mr. M. Francis R. Cooray in solving computer problems. I am indebted for the helpful suggestions of Mr. Mervin Marshall and Mr. Wayne Raman-Nair. In addition, I gratefully acknowledge the financial support of the School of Graduate Studies and the Faculty of Engineering and Applied Science.

Finally, I express my sincere thanks to Mr. Frazer Smith, Mr. T. Dyer, and Mr. J. B. Brown for drafting figures. Many thanks, as well, to Mr. T. Lanning and various other technical staff at Memorial University for helping with the experimental work. Special thanks to Mary, Randy, Marg and Gina at Computing Services.

Abstract

In the following thesis a procedure is developed to determine the engineering performance of an inshore trawling system from an analysis of the forces acting on the towing warps and bridle system. Equilibrium force balance equations are derived for each warp and solved using a fourth-order Runge kutta numerical analysis method. The procedure is then applied to an inshore trawl and the results are used in the comparison of vessel power and gear drag.

In addition towing tank drag measurements were made on small polyethylene nets. The effect of the development of turbulent flow around the net on the drag of the net is investigated. Empirical drag coefficients are also derived for polyethylene netting from these measurements. The coefficients are then used in empirical trawl net drag calculations using methods developed by Dickson, Kowalski and Fridman. In addition the relationship between the orientation of a mesh and the drag of the net is investigated. It is shown how mesh orientation can explain the reduced drag of a square mesh net as compared to a diamond mesh net.

Table of Contents

List of Tables

List of Figures

Nomenclature

A	area
a	twine bar length
A_f	inside area of holding frame
A_k	average knot area
A_{mh}	mesh hole area
A_p	projected area
A_t	twine area
b	number of twine bars
bhp	brake horsepower
c_d	coefficient of pressure drag
$c_{d\alpha}$	coefficient of pressure drag at α° to the flow
c_f	coefficient of friction drag
c_l	coefficient of lift of an otter board
d	diameter as noted
d_k	knot diameter
dhp	delivered horsepower
E	output voltage
e	mean standard error

F	force as noted
F_p	pressure drag force
F_f	friction drag force
F_l	spreading force of an otter board
Fx	force in the x direction
Fy	force in the y direction
Fz	force in the z direction
J	advance coefficient
k	number of knots
k_1	trawl net area reduction factor
kg	kilograms
k_q	Torque coefficient
k_t	Thrust coefficient
$\|M\|$	determinant of matrix M
m	meters
mm	millimeters
m/s	meters per second
mV	millivolt
N	newtons
n	number of trawl net panels
$N-m$	newton meters
R	drag
RPM	revolutions per minute

R_α	drag at α° to the flow
Q	torque
$Qmax$	maximum torque
S	Mesh Solidity
T	thrust (chapter 6)
T	tension (chapter 2)
$tmax$	thrust limit
u_1	first mesh hanging coefficient
u_2	second mesh hanging coefficient
V	velocity
W	weight of a cable element per unit length
w	wake coefficient

Greek Letters

α	Angle of attack
β	Warp declination angle
ϕ	Angle between cable and direction of towing
π	3.1416
θ	Mesh opening angle
ρ	density
ω	Warp divergence angle
ψ	Angle between twine bar and direction of towing

Chapter 1

INTRODUCTION

1.1. Background

A typical otter trawl used for fishing on the sea bed is shown in Figure 1-1. The majority of fish harvested on a world wide basis are caught in various sizes of fishing gear of this type. Both large and small vessels are used to tow appropriately sized gear. In North America large vessels, usually owned by large fishing companies, travel to deep waters and fish for extended periods of time. Smaller, privately owned vessels are involved in inshore activities.

Observations by divers using underwater cameras have shown that in a typical trawling process the fish swim ahead of the gear for a short period of time before eventually falling back into the bag type net. Fish are therefore gathered in the net rather than being entangled as in the case of passive type fishing. The gear must be towed at a speed greater than the swimming speed of the fish species sought. This translates into a towing speed of 2.5 to 5.0 knots. Overpowering the vessel must however be avoided since it results in extra capital expenditure and reduces the overall efficiency of the fishing operation [10].

Procedures for determining the drag of the gear, and its implications on vessel power are considered in this thesis. In particular the drag of a trawling system used by the Western Newfoundland inshore trawling fleet is investigated.

1.2. Bottom trawl description

The trawl net shown in figure 1-1 has two *wings* at the front which guide fish into the net. The middle section is divided into two upper panels called the *square* and *baiting* while the two bottom panels are known as the *belly* and lower *bailing*. These panels are laced together along their transverse edges and form a passage for fish to the rear of the trawl net, or *codend*, where they are finally trapped.

A *headline* rope is attached to the front of the netting along the square and the two upper *wings*. Special floats tied along the *headline* keep the trawl mouth open in the vertical plane during towing. The bottom front edge of the netting is joined to a rope called a *fishing line*. It is attached to the *belly* and the two lower *wings*. In order to protect the netting of the trawl from rubbing against the sea bottom the fishing line is joined onto a *groundrope* made from steel wire. Cylindrical or spherical rollers strung along the *groundrope* protect the trawl net by rolling over obstacles encountered along the bottom. A full set of gear component definitions is provided in Bridger [3].

Otter boards are attached on either side of the trawl mouth forty or more meters ahead of the wing tips. The steel wires connecting the boards to the wings are called *bridles*. These otter boards are rigged so that when the gear is being towed they spread open the mouth of the net. A variety of otter board designs are used in groundfish fisheries around the world including flat, oval and v-shape [8].

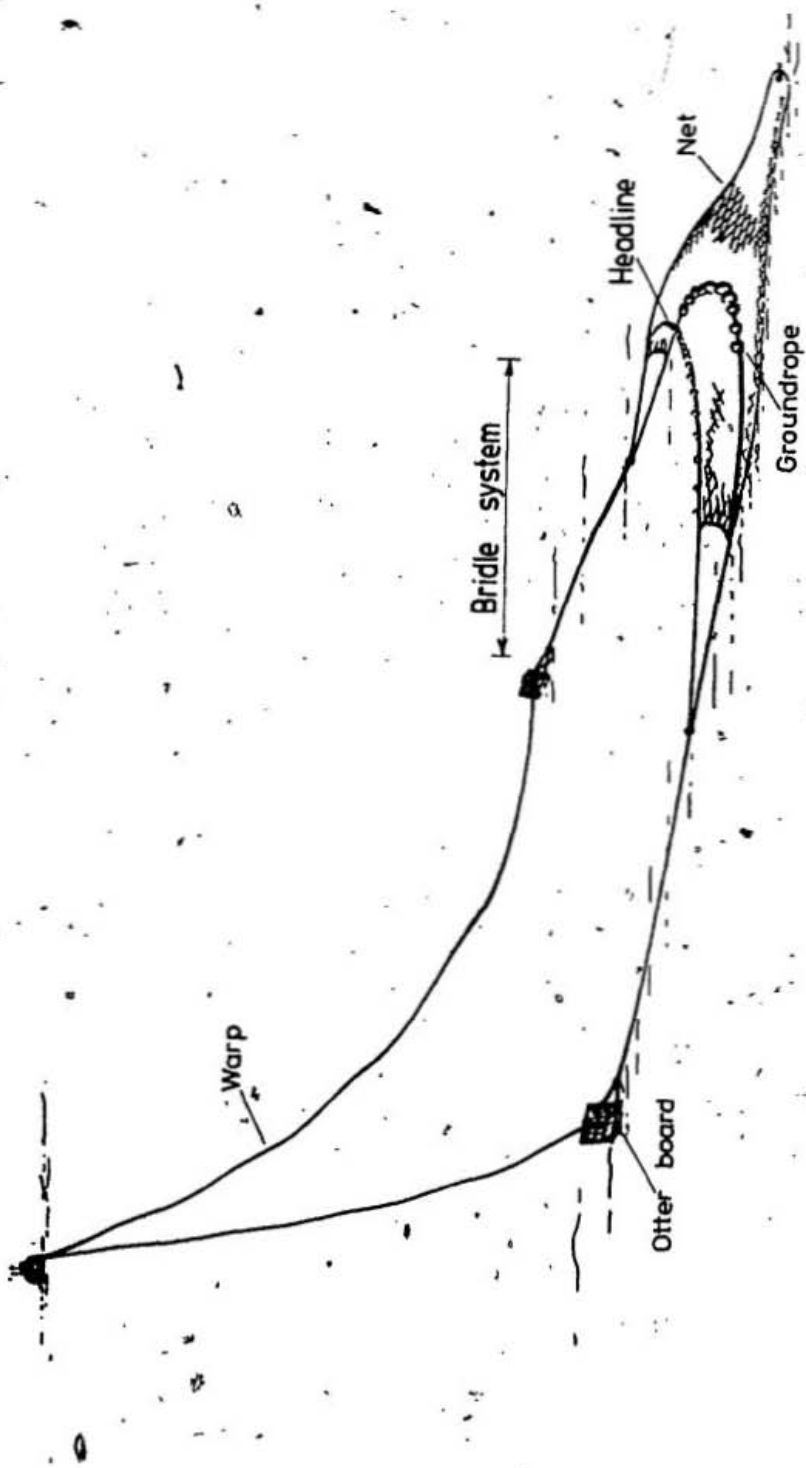

Figure 1-1 : A typical Bottom Trawl
(Courtesy of Bridger (3))

The entire net and otter board combination is towed with steel *towing warps* which are wrapped onto winches on the vessel. The length of the warps is chosen to suit the depth of the water and the required spread of the otter boards. A rule of thumb is to use a warp length equal to three times the water depth.

1.3. Trawl gear drag - A literature review

A drag force acts on a trawl gear when it is towed along the sea bed. This drag results from the hydrodynamic interaction between the gear and the water and also from the contact between the gear and the sea bed. The total drag of the gear can be calculated as the sum of the drag of the individual components because the major components are separated sufficiently to limit interactions [2].

Measurements at sea have shown that the trawl net drag is the largest component of the total gear drag. In the case of a bottom trawl it can be as high as 70% [21]. Because of the flexibility of the net structure it is also the least understood and difficult to predict. A major portion of this thesis deals with the determination of trawl net drag, both from a theoretical and experimental point of view.

Theoretically, it should be possible to derive a system of geometric and force equations which could be solved simultaneously to obtain the drag forces acting on a trawl net. The development of these equations has however been delayed because of the large number of unknowns involved [21]. According to the literature, trawl net drag calculations are made using standard type drag equations with an empirical drag coefficient. The use of these equations is

illustrated in section 4.3. A review of literature pertaining to empirical net drag coefficients is given in the following section.

1.3.1. Geometry of a mesh

A standard mesh as shown in figure 1-2 is formed by four bars of twine of equal length knotted at four corners. A basic mesh element consists of two twine bars and a knot because each mesh in a net is completed by adding two bars of twine and a knot.

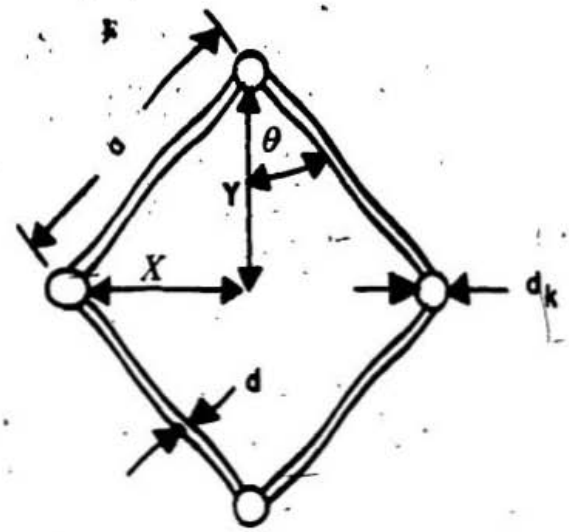

Figure 1-2: A standard net mesh.

A twine bar has a nominal diameter, d, and a length, a, which is the center to center distance between two knots. A knot is schematically represented as a twine wound around another. The knot diameter, d_k, is therefore approximately three times the diameter of the twine [2].

The exact shape of a mesh can be described by its hanging coefficients, u_1 and u_2 [11]. These hanging coefficients are determined from figure 1-2 as follows:

$$u_1 = \sin\theta = x/a \tag{1.1}$$

$$u_2 = \cos\theta = y/a . \tag{1.2}$$

The relative mesh area, or *solidity*, of a mesh is defined as the ratio of the area covered by the twine making up a mesh element to the total area enclosed by the mesh. Referring to figure 1-2, it can be seen that the area enclosed by the mesh can be calculated using the following equation:

$$A_{mesh} = 2u_1u_2a^2 . \tag{1.3}$$

The twine area of a mesh element is sometimes estimated as the area of two twine bars, i.e. $(2da)$. In this case the solidity is given by the following equation:

$$S = \frac{A_{twine}}{A_{mesh}} = (d/a)(1/u_1u_2) . \tag{1.4}$$

The area of a mesh element including the knot area is as follows [18]:

$$A_{twine} = 2da + \pi d_k^2/4 . \tag{1.5}$$

and the solidity including the knot area is therefore defined as follows:

$$S = \frac{2da + \pi d_k^2/4}{2u_1u_2a^2} . \tag{1.6}$$

1.3.2. Empirical net drag coefficients

Drag measurements on small pieces of nets measuring less than one-half a square meter have been used to develop empirical formulae for the calculation of the drag nets. A representative sample of these formulae is given in the following section.

The majority of net drag measurements have been made with the net held perpendicular to the flow. Baranov [2], for example, reported that the drag of a net held perpendicular to the flow was approximated by the following expression:

$$R_{90} = 75\, l\, d\, V^{1.75} \tag{1.7}$$

where:

l = total length of twine from which the net is made (not including knots)

V = velocity.

He later derived the following equation from the same data:

$$R_{90} = 180\,(d/a)\, F V^{2.0}. \tag{1.8}$$

where:

F = the overall area of the net.

For the case of perpendicular flow Tauti [26] proposed the following formula:

$$R_{90} = 191\,(d/a)\, F V^{2}. \tag{1.9}$$

An equation derived by Revin [23] for the drag of a net held perpendicular to the flow has the following form:

$$R_{90} = 108\,(d/a)\,(1/u_1 u_2)\,F V^2 . \qquad (1.10)$$

Fridman [11] performed wind tunnel tests on a net panel with a d/a ratio of 0.05 and summarized the results with the following formula:

$$R_{90} = 200\,(d/a)\,F\ \mathrm{v}^2 . \qquad (1.11)$$

Further experiments by Fridman indicated that the drag of a net held perpendicular to the flow was best calculated using the following formula:

$$R_{90} = 1/2\,C_x F_t V^2 . \qquad (1.12)$$

where:

$$C_x = f(Re^d, F)$$

and

F = total area of the net

F_t = actual twine area of the net sample

Re^d = Reynolds number (calculated using the diameter of the twine as the characteristic linear net dimension).

There are fewer measurements reported on the drag of nets which are held such that the plane of the netting is not perpendicular to the flow. For nets held parallel to the flow Tauti [26] gives the following expression:

$$R_0 = 1.8\,F V^2 \qquad (1.13)$$

Revin [23] reports the following elaborate formula for the drag of a net held parallel to the flow:

$$R_0 = 1.4 l^{-0.14}(1 + 5\,d/a)$$
$$(0.9 + 0.04\,u_1\,u_2 + 0.55\,l^{-2.4u_1/u_2})\,F\,V^{1.96} \qquad (1.14)$$

where:

l = Length of the net.

For a very elongated net held parallel to the flow the following equation is found in Baranov [2]:

$$R_0 = 0.79\,F\,V^{1.72} \qquad (1.15)$$

For the case where the net is held at some angle between the perpendicular and parallel case Tauti [26] recommends the following formula:

$$R_\alpha = R_0 + (R_{90} - R_0)\,\alpha/90 \qquad (1.16)$$

while Revin [23] proposes the following equation

$$R_\alpha = R_0 + (R_{90} - R_0)\sin\alpha. \qquad (1.17)$$

Measurements made by Stengel and Fischer [25] indicate that the drag of nets cannot be calculated using a constant drag coefficient as implied by equations (1.7) to (1.15). Stengel's analysis also showed that the drag of a net was dependent upon the twine type and its surface structure and that the mesh opening angle has an effect on the drag of nets.

It was therefore concluded that absolute relationships between the drag of a net and the velocity of flow around and through the net have not been established. Also, exhaustive data on the drag of nets is clearly not available and

very few recent measurements are reported. In particular, information on the drag of a wide variety of twine types, including polyethylene twine, is not reported. Measurements were made on polyethylene twine and the results are reported in this thesis.

1.4. Scope of work

The majority of work included in this thesis is applicable to all towed fishing trawls. However, the study is focused on an inshore trawling fleet operating off Western Newfoundland.

The intent of the present work is to investigate the compatibility of the vessel and gear combinations used in the Newfoundland fishery. The trawling system most commonly used in this fishery is a bottom otter trawl manufactured by Iver Christensen (I.C.). The construction details of the trawl net used with this gear are shown in chapter 4.0.

Calculations of the compatibility of vessel power and gear drag have not been reported for vessels operating off Western Newfoundland. Although very few measurements have been made on the I.C. trawl gear as used in this area, engineering performance measurements made by Kingsley and Hearn [14] are suitable for these calculations. The drag of the I.C. gear is derived from these measurements in chapter 2.0. A particular method of trawl gear analysis based on steady-state towing cable theory is developed in chapter 2.0 for this purpose. Although this theory seems to have been seldom used in this type of work very good results are obtained.

It has been verified through experiments at sea that the drag of a trawl net is the largest single component of the total gear drag. However, very little progress has been made in the development of accurate methods of calculating this drag. In fact, no literature could be found that deals with the calculation of the drag of trawl nets made from polyethylene nets. In this thesis, empirical drag coefficients are derived for polyethylene nets from measurements made on full scale pieces of polyethylene netting in a towing tank. A considerable part of the present work is based on the analysis of these new experimental measurements. The use of these coefficients in calculating trawl net drag is illustrated in section 4.3. Experimental procedures are contained in chapter 3.0 along with the net drag measurements. Drag coefficient derivations are given in chapter 4.0.

In addition, the unique relationship between the orientation of the mesh in a net to the flow and the drag of the net is examined in chapter 5.0. An analysis of measurements made on a square mesh net, which is an example of a special mesh orientation, is also included in chapter 5.0.

Finally, in chapter 6.0, the drag of the I.C. trawl gear is compared to the towing power of two typical inshore trawling vessels used off Western Newfoundland. The results have important practical implications which are discussed in chapter 7.0 together with other conclusions and a summary.

Chapter 2

TRAWL GEAR PERFORMANCE ANALYSIS

Performance measurements have been made on the 350 mesh I. C. trawl in areas typically trawled off the west coast of Newfoundland [14]. Measurements taken include the tension in the main warps, bridle and ground wire. The spread of the wing ends and the headline height were also measured. These measurements are shown in figures 2-3 to 2-5. The tension measurements were made at points one, four and five as shown on figures 2-1 and 2-2. Also shown are the locations of the wing spread and headline height measurements. The measurements appear to be insensitive to speed in addition to there being some scatter, neither of which was explained by Kingsley and Hearn [14].

The drag of the total gear and that of the trawl net were derived from the measurements shown in figures 2-3, 2-4 and 2-5. The spread of the doors and the warp angles at the towing block were not included in these measurements. A method of analysis was therefore developed which did not require a knowledge of these variables. Theoretical equations describing the steady-state configuration of a towing cable were utilised in the analysis [7]. Researchers have made very little use of this theory for trawl gear analysis purposes. Steady-state towing cable theory is, however, very applicable to trawl gear analysis.

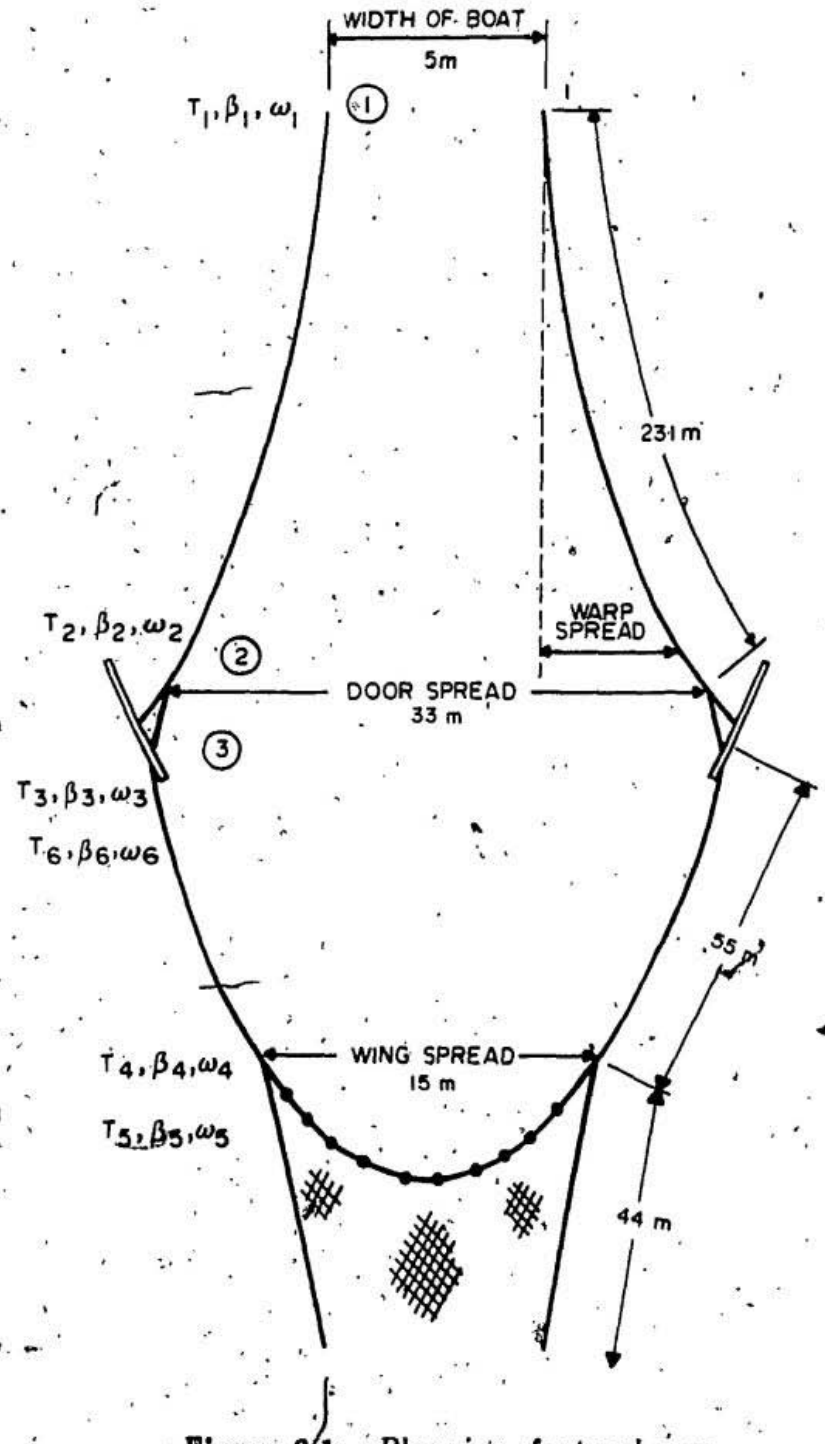

Figure 2.1: Plan view of a trawl gear.

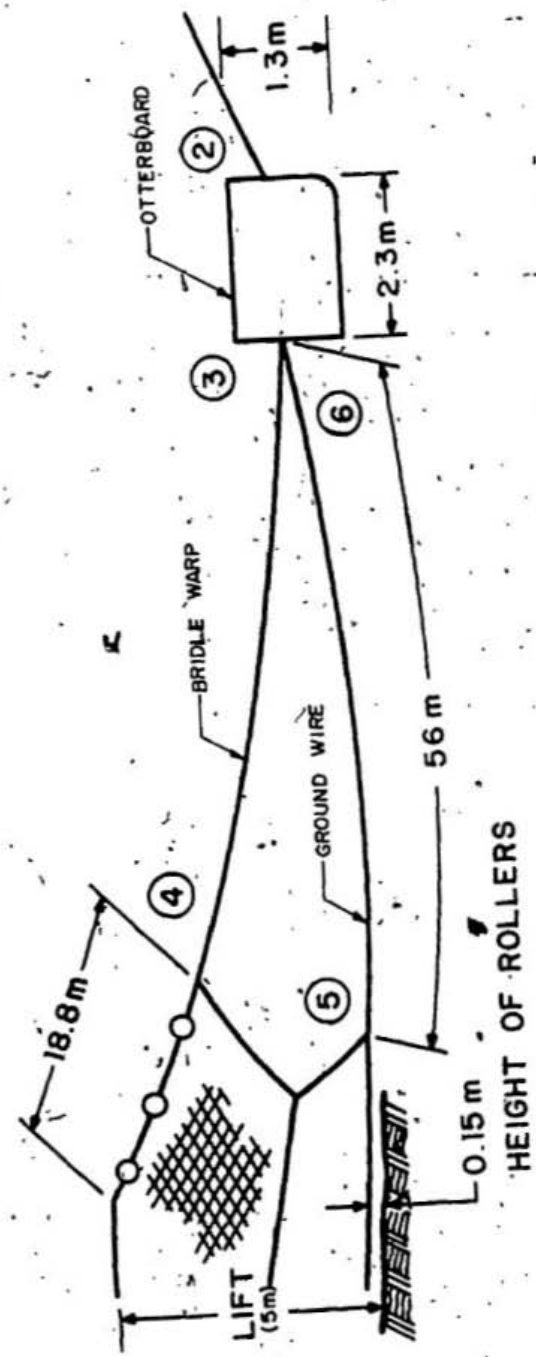

Figure 2-2: Sectional view of a trawl net

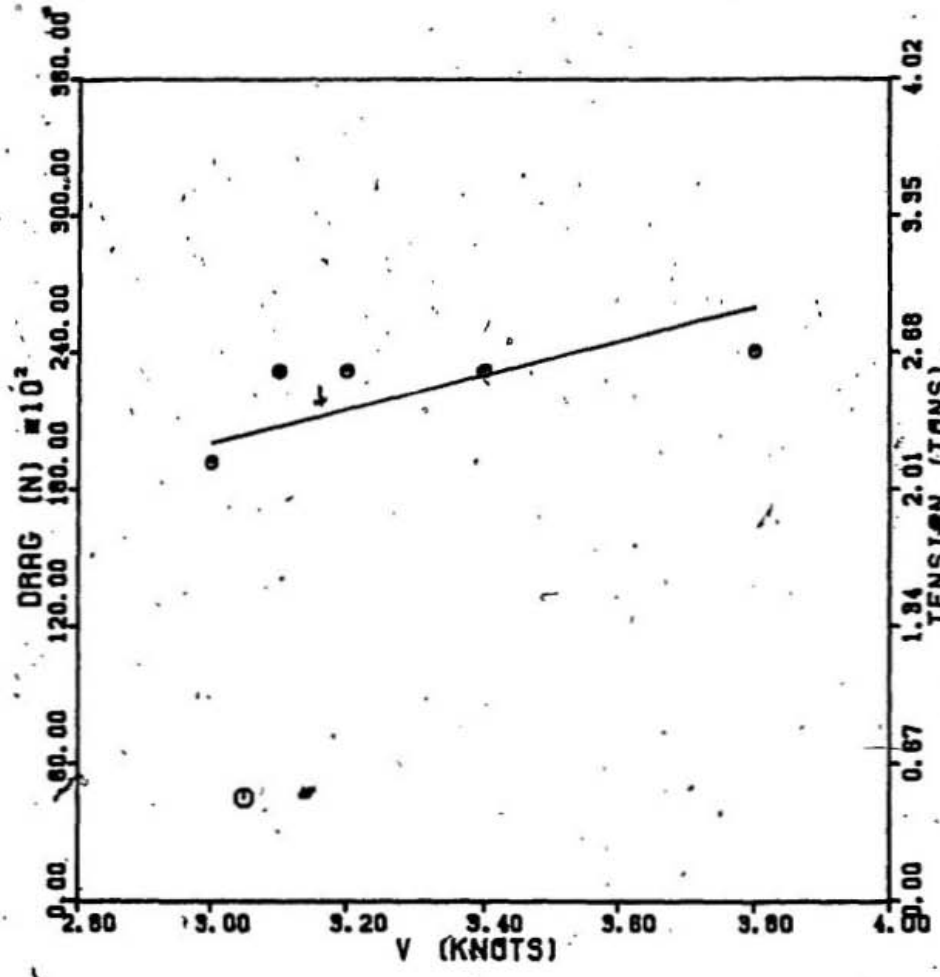

Figure 2-3: 350 I.C. trawl gear performance
Total gear tension
(Courtesy of Kingsley and Hearn(14))

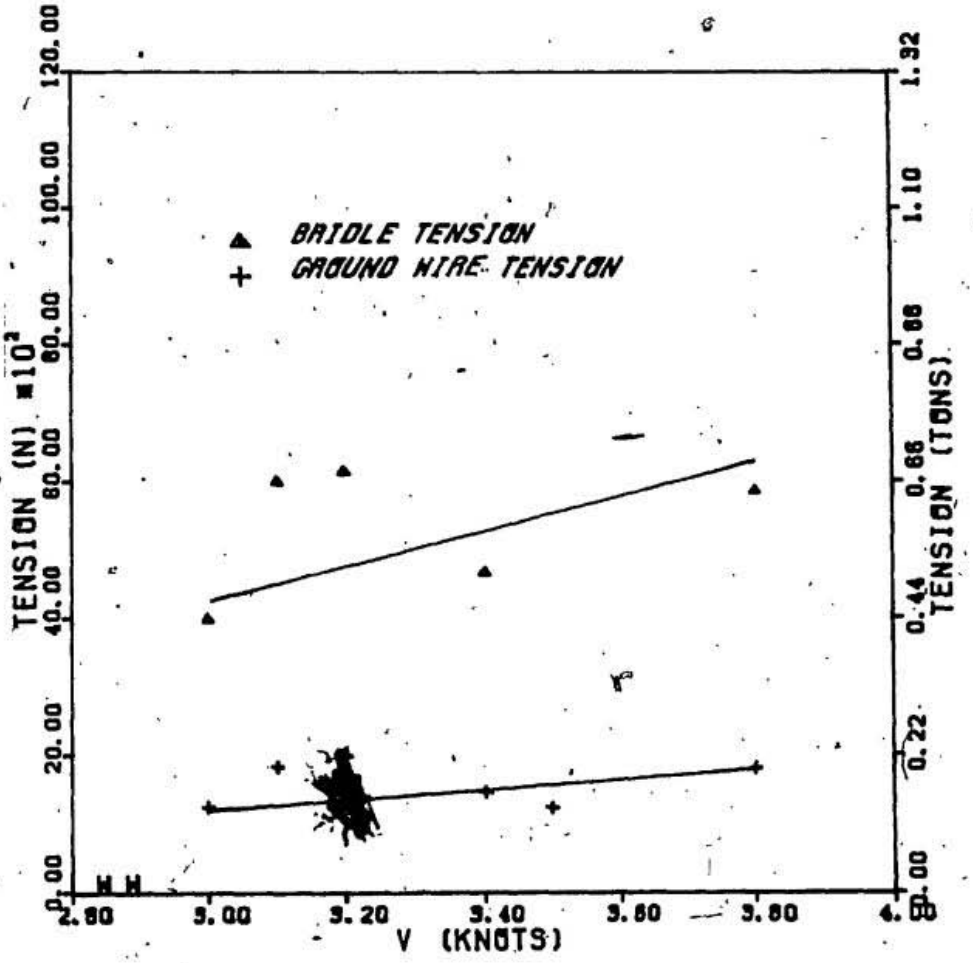

Figure 2-4: 350 I.C. trawl gear performance. Bridle/ground wire tension (Courtesy of Kingsley and Hearn(14))

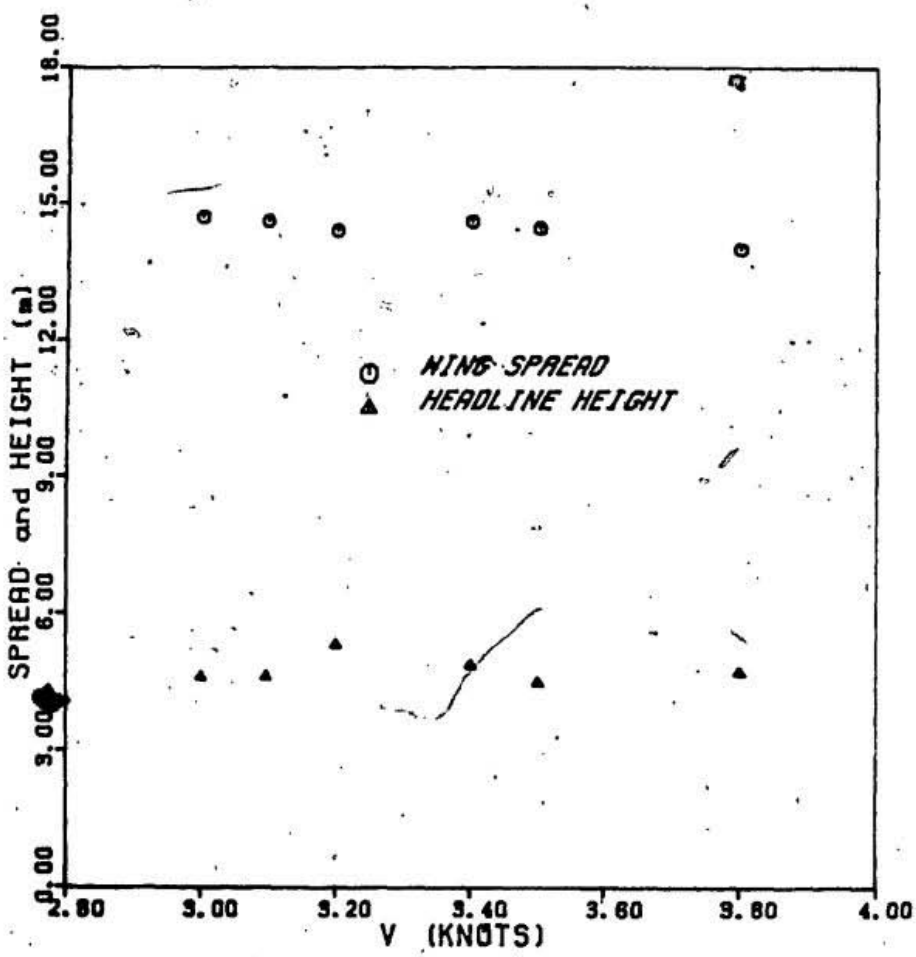

Figure 2-5: 350 I.C. trawl gear performance
Wing spread and Headline height
(Courtesy of Kingsley and Hearn(14))

2.1. Steady-state theory of a towing cable

An approximate method of analyzing a warp as towed behind a fishing vessel is to neglect the small angle of divergence between the plane containing the warp and the direction of motion [18] [11]. The angle of divergence, ω, is shown in figure 2-1. Another method is to use steady-state towing cable theory [20]. According to this theory an element of cable is subjected to external hydrodynamic and gravity forces which must be in equilibrium with its internal tension [7]. These forces include the weight of the cable, pressure drag and friction drag [7]. The tangential components of the external forces act to increase the tension while the normal components cause the cable to bend, changing the line of action but not the magnitude of the tension [7].

The tangential component of the velocity is assumed to have negligible effect on the pressure distribution around the section of cable, and therefore the pressure drag is a result of the normal velocity component only [7]. Also, the friction drag is assumed to be unaffected by the pressure distribution and acts in the direction of flow regardless of the cable configuration [7].

An element of cable is shown in figure 2-6. The internal tension, T, is in equilibrium with the weight of the element, W, the pressure drag, F_d, and the friction drag, f_f. The element forms a divergence angle of ω with the xz plane and a declination angle of β with the xy plane. The tension changes by an amount dT over the length of the element while the angles ω and β change by an amount $d\omega$ and $d\beta$. The angle ϕ is the geometric combination of ω and β, i.e.

$$\cos\phi = \cos\omega\cos\beta. \tag{2.1}$$

2.1.1. Numerical analysis of a steady-state towing cable

A summation of the internal tension, T, and external forces along the x, y and z axes yields the following general equilibrium equations:

$$\frac{d}{dl}(T\cos\beta\cos\omega) = \sum Fx \tag{2.2}$$

$$\frac{d}{dl}(T\cos\beta\sin\omega) = \sum Fy \tag{2.3}$$

$$\frac{d}{dl}(T\sin\beta) = \sum Fz \tag{2.4}$$

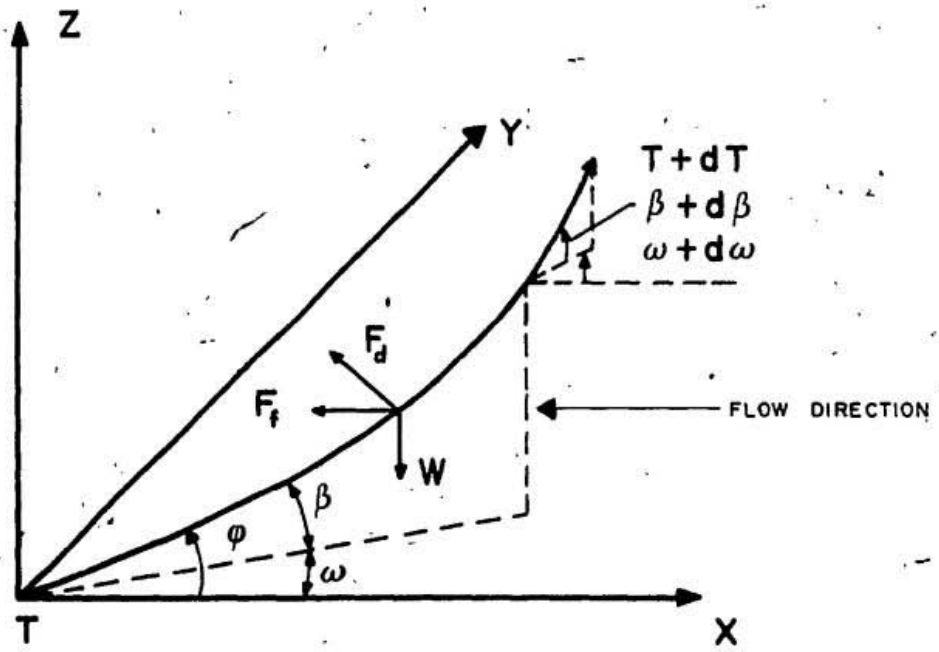

Figure 2-6: An element of towing cable.

Given the initial tension, T, and the angles, β and ω, at one end of a cable

element, the value of these variables at the other end is obtained by solving equations (2.2), (2.3) and (2.4) numerically. The first step in the solution procedure is to expand the derivatives on the left hand side of equations (2.2), (2.3) and (2.4) as follows:

$$-T\sin\beta\cos\omega\frac{d\beta}{dl} - T\cos\beta\sin\omega\frac{d\omega}{dl} + \cos\beta\cos\omega\frac{dT}{dl} = \sum Fx \qquad (2.5)$$

$$-T\sin\beta\sin\omega\frac{d\beta}{dl} + T\cos\beta\cos\omega\frac{d\omega}{dl} + \cos\beta\sin\omega\frac{dT}{dl} = \sum Fy \qquad (2.6)$$

$$T\cos\beta\frac{d\beta}{dl} + \sin\beta\frac{dT}{dl} = \sum Fz \qquad (2.7)$$

Equations (2.5), (2.6) and (2.7) are then rewritten in the following matrix form:

$$\begin{bmatrix} a_1 & b_1 & c_1 \\ a_2 & b_2 & c_2 \\ a_3 & b_3 & c_3 \end{bmatrix} \begin{bmatrix} \frac{d\beta}{dl} \\ \frac{d\omega}{dl} \\ \frac{dT}{dl} \end{bmatrix} = \begin{bmatrix} \sum Fx \\ \sum Fy \\ \sum Fz \end{bmatrix} \qquad (2.8)$$

where:

$$a_1 = -T\sin\beta\cos\omega, \quad a_2 = -T\sin\beta\sin\omega, \quad a_3 = T\cos\beta$$

$$b_1 = -T\cos\beta\sin\omega, \quad b_2 = T\cos\beta\cos\omega, \quad b_3 = 0.0$$

$$c_1 = \cos\beta\cos\omega, \quad c_2 = \cos\beta\sin\omega, \quad c_3 = \sin\beta$$

Application of Cramer's rule leads to the following system of first-order differential equations:

$$\frac{d\beta}{dl} = \frac{|M_1|}{|M|}, \quad \frac{d\omega}{dl} = \frac{|M_2|}{|M|}, \quad \frac{dT}{dl} = \frac{|M_3|}{|M|}$$

where the matrix M_i is obtained by replacing the i^{th} column in matrix M with the column matrix $\sum F$ as follows:

$$M = \begin{bmatrix} a_1 & b_1 & c_1 \\ a_2 & b_2 & c_2 \\ a_3 & b_3 & c_3 \end{bmatrix}$$

$$M_{i=1} = \begin{bmatrix} \sum Fx & b_1 & c_1 \\ \sum Fy & b_2 & c_2 \\ \sum Fz & b_3 & c_3 \end{bmatrix}$$

The determinant of the a matrices is given by the following equation:

$$M = [a_1b_2c_3 + a_2b_3c_1 + a_3b_1c_2] - [a_1b_3c_2 + a_2b_1c_3 + a_3b_2c_1] \qquad (2.9)$$

2.1.2. Application of steady-state towing cable theory to the trawling warps

The steady-state analysis procedure as described above was developed into a computer program and used to determine the incremental change in tension along the I.C. trawl warp down to the otter boards. From these calculations the spread of the otter boards and the tension in the main warp just in front of the otter board were derived.

An element of warp is shown in figure 2-7. The co-ordinate axes are placed around the element so that the angles ω and β correspond to those shown in figure 2-6. Also, the origin is placed at the point where the tension is known.

Maclennan [20], gives the forces F_d and F_f in terms of the dimensionless drag coefficients c_d and c_f as follows:

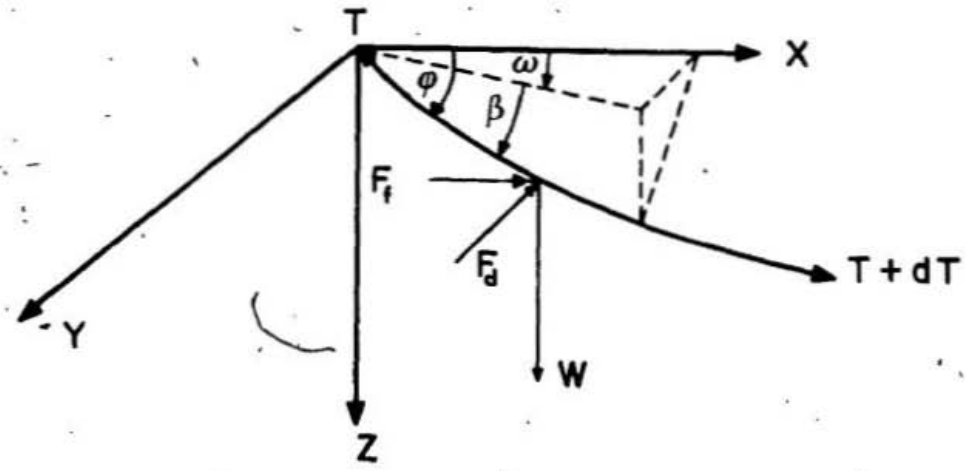

Figure 2-7: An element of warp.

$$F_d = \frac{\rho}{2}(V \sin \phi)^2 D c_d \tag{2.10}$$

$$F_f = \frac{\rho}{2} V^2 \pi D c_f \tag{2.11}$$

where:

D = cable diameter

$\cos \phi$ = $\cos \omega \cos \beta$.

Since the boat moves in the negative x-direction, the flow relative to the warp is in the positive x-direction. The pressure and friction drag forces therefore act in the positive x-direction. The following equations give the sum of external forces acting in the x, y and z directions respectively:

$$\frac{d}{dl}(T \cos \beta \cos \omega) = -\frac{\rho}{2} V^2 D (\pi c_f + c_d \sin^3 \phi) \tag{2.12}$$

$$\frac{d}{dl}(T\cos\beta\sin\omega) = \frac{\rho}{2}V^2 D c_d \cos\beta \sin\omega \cos\phi \sin\phi \qquad (2.13)$$

$$\frac{d}{dl}(T\sin\beta) = \frac{\rho}{2}V^2 D c_d \sin\beta \sin\phi\cos\phi - W \qquad (2.14)$$

The computer program developed to solve equations (2.12), (2.13) and (2.14) is shown in appendix A. A fourth-order Runge Kutta method was used to solve the set of first-order differential equations derived in the analysis. Starting with the known tension at the vessel, as given in figure 2-3, the program estimates the change in the tension at small increments down the warp to the otter boards. For the purposes of these calculations the total gear tension is assumed to be divided equally between the two warps. In addition, the total displacement of the cable from the starting point is calculated by adding up the projected lengths of each cable element in the x, y and z directions. The initial angles ω and β used in the analysis were estimated from measurements made on trawl gears similar in size to the 350 I.C. gear [4].

Other inputs to the program include the coefficients of drag and friction, c_d and c_f, which are given values of 1.1 and 0.007 respectively [20]. The velocity, V, and the weight of the cable per unit length, W, are also required inputs.

2.1.3. Application of steady-state towing cable theory to the bridle system

An element of bridle warp and ground wire is shown in figures 2-8 and 2-9 respectively.

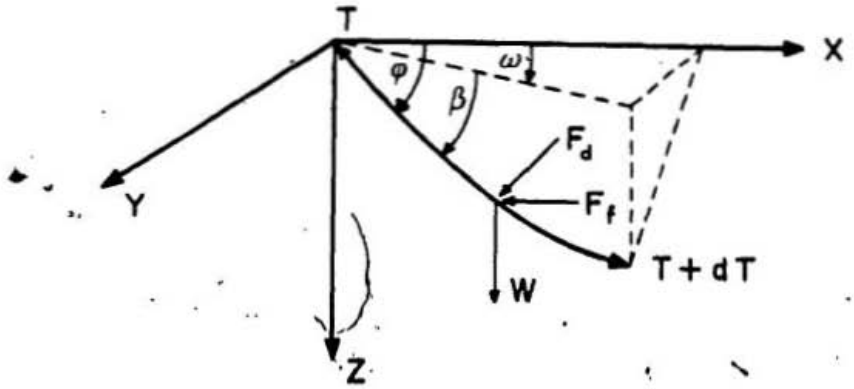

Figure 2-8: An element of bridle warp.

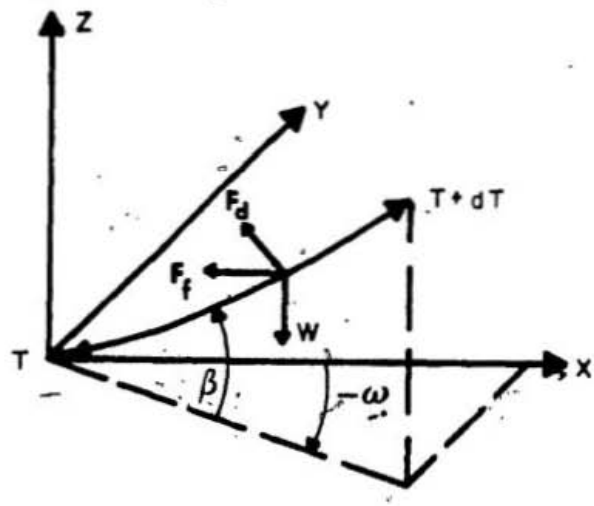

Figure 2-9: An element of ground wire.

The following equilibrium equations were derived for each element in the x, y and z directions respectively:

bridle equilibrium equations

$$\frac{d}{dl}(\mathrm{T}\cos\beta\cos\omega) = \frac{\rho}{2}\mathrm{V}^2 D(\pi c_f + c_d \sin^3\phi) \tag{2.15}$$

$$\frac{d}{dl}(T\cos\beta\sin\omega) = -\frac{\rho}{2}V^2 D\, c_d \cos\beta \sin\omega \cos\phi \sin\phi \tag{2.16}$$

$$\frac{d}{dl}(T\sin\beta) = -\frac{\rho}{2}V^2 D\, c_d \sin\beta \sin\phi \cos\phi - W \tag{2.17}$$

ground wire equilibrium equations

$$\frac{d}{dl}(\mathrm{T}\cos\beta\cos\omega) = \frac{\rho}{2}\mathrm{V}^2 D(\pi c_f + c_d \sin^3\phi) \tag{2.18}$$

$$\frac{d}{dl}(T\cos\beta\sin\omega) = -\frac{\rho}{2}V^2 D\, c_d \cos\beta \sin\omega \cos\phi \sin\phi \tag{2.19}$$

$$\frac{d}{dl}(T\sin\beta) = -\frac{\rho}{2}V^2 D\, c_d \sin\beta \sin\phi \cos\phi + W \tag{2.20}$$

The above equations were used to derive the variation in the tension in the bridle and ground wire beginning at the mouth of the trawl net. The inital tension in these warps at the trawl net is given in figure 2-4 and the angles β and ω were estimated as before.

2.1.4. Results of equilibrium trawl analysis

The results of the equilibrium analysis are shown in tables 2-1 to 2-9. These tables outline the configuration of the trawl gear by defining the location of both ends of each cable with respect to the points shown on figures 2-1 and 2-2. Theoretically, the spreading force of an otter board can be calculated using the following equation:

$$F_l = \frac{\rho}{2} V^2 A c_l \qquad (2.21)$$

where:

A = the area of the otter boards

c_l = the coefficient of lift of the boards

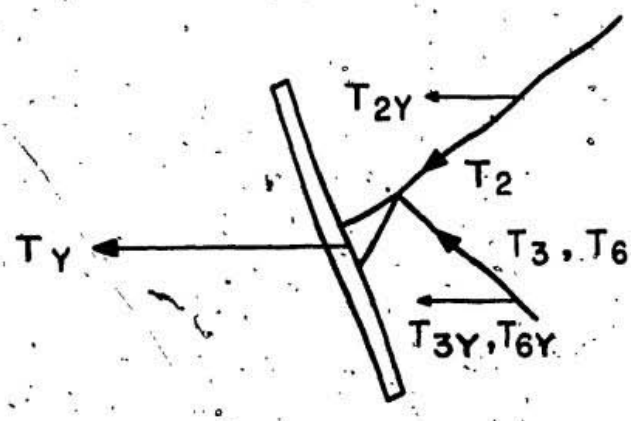

Figure 2-10: The forces acting on an otter board

The coefficient of lift is nearly constant for a properly rigged door at board angles of attack typical for trawling [8]. The spreading force of the boards, as illustrated in figure 2-10, is given as follows:

$$F_l = T_{2y} + T_{3y} + T_{6y} \quad (2.22)$$

where:

$$T_{2y} = T_2 \cos\beta_2 \cos\omega_2$$

$$T_{3y} = T_3 \cos\beta_3 \cos\omega_3$$

$$T_{6y} = T_6 \cos\beta_6 \cos\omega_6$$

The final cable configuration data shown in tables 2-1 to 2-9 were arrived at by varying the inital estimates of β and ω until the spreading force required from the boards, as given by equation (2.22), matched that obtainable from the boards. The force obtainable from the boards was calculated using equation (2.21) with a coefficient of lift of 0.8 [8].

2.2. Total gear and net drag

The total drag of the gear is defined as the x-component of the tension in the main warps at the vessel, see figure 2-1. Also, the drag of the trawl net is equal to the sum of the tensions in the bridle and ground wire at the mouth of the net, see figure 2-2. Calculations were therefore made of the total gear and net drag using the following equations and the data given in tables 2-1 to 2-9:

$$\textit{Total gear drag} = 2\,T_1 \cos\beta_1 \cos\omega_1 \quad (2.23)$$

$$\textit{Trawl net drag} = 2\,T_4 \cos\beta_4 \cos\omega_4 + 2\,T_5 \cos\beta_5 \cos\omega_5 \quad (2.24)$$

The subscripts in equations (2.23) to (2.24) refer to points shown on figures 2-1

and 2-2, Figure 2-11 shows the results of the calculations. The total gear drag is used in the comparison of vessel power and gear drag in chapter 6.0 and the net drag is compared to empirical net drag calculations in chapter 4.0. Additional net drag analysis is given in the following chapters.

Table 2-1: Warp configuration speed 3.0 knots

Length (m)	Tension (N)	β°	ω°	X (m)	Z (m)	Y (m)
pt. 1 0.0	9584.37	18.00	3.00	0.00	0.00	0.00
32.9	9530.57	17.53	3.06	31.29	10.03	1.66
65.9	9477.73	17.03	3.12	62.75	19.83	3.35
98.9	9426.05	16.52	3.18	94.30	29.35	5.09
131.9	9375.60	15.98	3.25	125.94	38.58	6.87
164.9	9326.42	15.42	3.31	157.65	47.51	8.68
pt. 2 231.0	9232.03	14.22	3.42	221.44	64.41	12.43

Table 2-2: Warp configuration speed 3.4 knots

Length (m)	Tension (N)	β°	ω°	X (m)	Z (m)	Y (m)
pt. 1 0.0	11595.40	17.45	3.50	0.00	0.00	0.00
32.9	11539.45	17.13	3.57	31.43	9.77	1.94
65.9	11484.06	16.79	3.65	63.02	19.39	3.93
98.9	11429.59	16.44	3.72	94.66	28.83	5.97
131.9	11375.73	16.07	3.79	126.35	38.06	8.05
164.9	11322.86	15.68	3.87	158.11	47.08	10.17
pt. 2 231.0	11219.74	14.86	4.02	221.32	64.49	14.57

Table 2-3: Warp configuration speed 3.8 knots

Length (m)	Tension (N)	β°	ω°	X (m)	Z (m)	Y (m)
pt. 1 0.0	12036.80	17.12	4.00	0.00	0.00	0.00
32.9	11977.97	16.88	4.09	31.38	9.62	2.23
65.9	11919.51	16.63	4.19	62.90	19.13	4.53
98.9	11861.66	16.37	4.29	94.46	28.49	6.88
131.9	11804.43	16.09	4.39	126.04	37.71	9.29
164.9	11747.84	15.80	4.48	157.69	46.77	11.76
pt. 2 231.0	11636.62	15.17	4.68	221.18	64.42	16.88

Table 2-4: Bridle configuration speed 3.0 knots

Length (m)		Tension (N)	β°	ω°	X (m)	Z (m)	Y (m)
pt. 4	0.0	4067.00	5.20	7.90	0.00	0.00	0.00
	7.7	4067.92	4.71	7.86	7.60	0.66	1.05
	15.5	4069.14	4.21	7.82	15.30	1.27	2.12
	23.3	4070.65	3.72	7.78	23.01	1.81	3.17
	31.1	4072.43	3.22	7.74	30.73	2.28	4.22
	38.9	4074.50	2.74	7.70	38.45	2.68	5.27
	46.7	4076.84	2.25	7.66	46.17	3.02	6.31
pt. 3	54.5	4079.64	1.77	7.62	53.90	3.30	7.42

Table 2-5: Bridle configuration speed 3.4 knots

Length (m)		Tension (N)	β°	ω°	X (m)	Z (m)	Y (m)
pt. 4	0.0	4750.00	4.90	9.40	0.00	0.00	0.00
	7.7	4751.49	4.47	9.33	7.57	0.63	1.25
	15.5	4753.24	4.04	9.27	15.25	1.21	2.50
	23.3	4755.25	3.61	9.20	22.93	1.72	3.75
	31.1	4757.50	3.18	9.14	30.62	2.19	4.99
	38.9	4759.99	2.75	9.08	38.31	2.59	6.22
	46.7	4762.73	2.33	9.01	46.00	2.93	7.45
pt. 3	54.5	4765.91	1.92	8.96	53.70	3.22	8.67

Table 2-6: Bridle configuration speed 3.8 knots

Length (m)		Tension (N)	β°	ω°	X (m)	Z (m)	Y (m)
pt. 4	0.0	5970.00	4.60	11.10	0.00	0.00	0.00
	7.7	5972.14	4.25	10.91	7.48	0.59	1.4
	15.5	5974.52	3.90	10.82	15.07	1.15	2.92
	23.3	5977.11	3.55	10.74	22.66	1.65	4.38
	31.1	5979.90	3.20	10.66	30.26	2.11	5.82
	38.9	5982.88	2.85	10.58	37.86	2.52	7.26
	46.7	5986.07	2.51	10.50	45.47	2.89	8.68
pt. 3	54.5	5989.68	2.18	10.42	53.57	3.21	10.10

Table 2-7: Ground wire configuration speed 3.0 knots

Length (m)		Tension (N)	β°	ω°	X (m)	Z (m)	Y (m)
pt. 5	0.0	1269.00	-4.90	-8.25	0.00	0.00	0.00
	7.7	1269.28	-3.33	-8.10	7.62	-0.55	-1.09
	15.5	1270.48	-1.78	-7.95	15.35	-0.90	-2.18
	23.3	1272.59	-0.25	-7.82	23.07	-1.03	-3.25
	31.1	1275.58	1.25	-7.69	30.79	-0.96	-4.30
	38.9	1279.44	2.72	-7.56	38.50	-0.69	-5.33
	46.7	1284.15	4.16	-7.43	46.20	-0.22	-6.35
pt. 6	55.0	1290.07	5.65	-7.29	54.38	0.49	-7.41

Table 2-8: Ground wire configuration speed 3.4 knots

Length (m)		Tension (N)	β°	ω°	X (m)	Z (m)	Y (m)
pt. 5	0.0	1490.00	-4.10	-10.20	0.00	0.00	0.00
	7.7	1491.39	-2.75	-9.87	7.56	-0.46	-1.33
	15.5	1493.58	-1.42	-9.65	15.24	-0.74	-2.65
	23.3	1496.55	-0.12	-9.44	22.93	-0.84	-3.94
	31.1	1500.28	1.16	-9.25	30.63	-0.77	-5.21
	38.9	1504.74	2.40	-9.06	38.33	-0.53	-6.45
	46.7	1509.92	3.61	-8.87	46.02	-0.12	-7.66
pt. 6	55.0	1516.19	4.86	-8.66	54.21	0.5	-8.92

Table 2-9: Ground wire configuration speed 3.8 knots

Length (m)		Tension (N)	β°	ω°	X (m)	Z (m)	Y (m)
pt. 5	0.0	1840.00	-3.20	-12.05	0.00	0.00	0.00
	7.7	1842.66	-2.10	-11.73	7.49	-0.35	-1.58
	15.5	1846.00	-1.02	-11.43	15.11	-0.57	-3.15
	23.3	1849.97	0.03	-11.15	22.75	-0.63	-4.67
	31.1	1854.56	1.06	-10.87	30.42	-0.56	-6.16
	38.9	1859.73	2.05	-10.61	38.10	-0.34	-7.61
	46.7	1865.49	3.03	-10.36	45.78	0.00	-9.03
pt. 6	55.0	1872.22	4.03	-10.10	53.97	0.51	-10.50

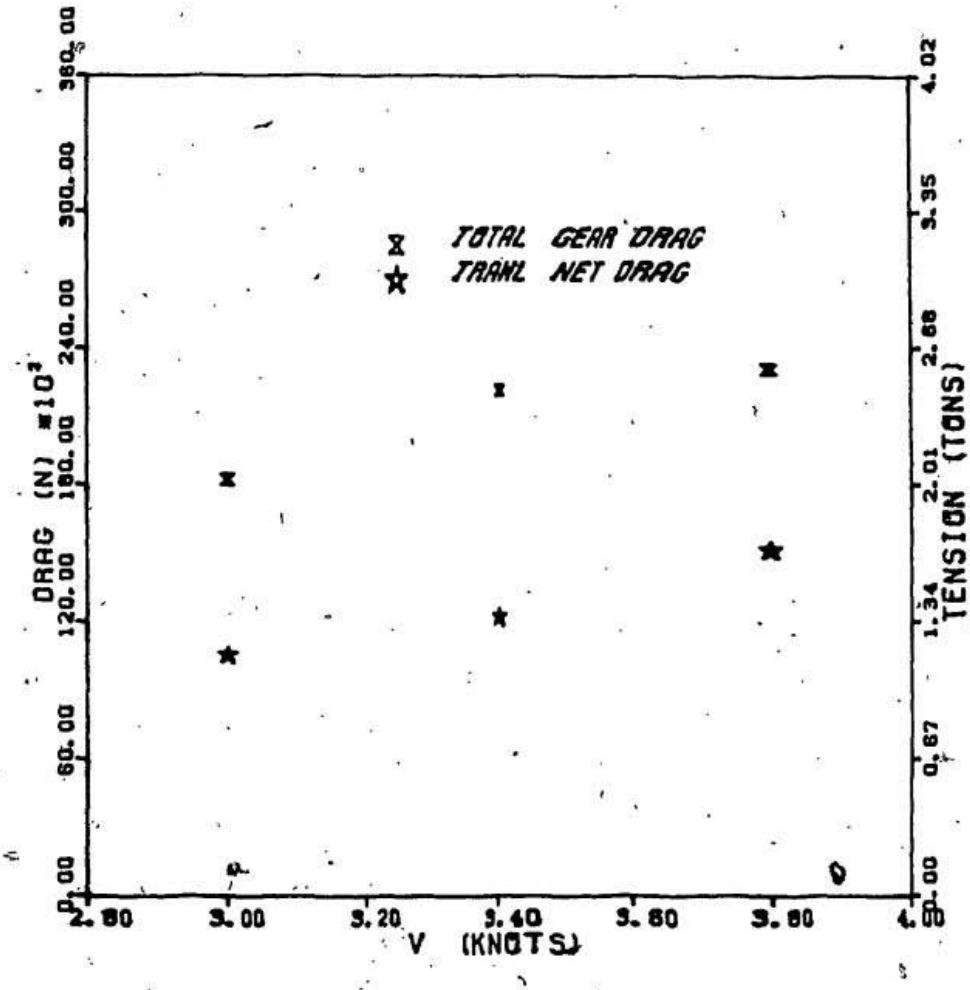

Figure 2-11: Total gear and net drag.

Chapter 3

TOWING TANK DRAG MEASUREMENTS ON SAMPLES OF POLYETHYLENE NETTING

Polyethylene netting, from which the I.C. trawl net is constructed, is a relatively new fishing net material and very little information concerning its drag properties is available. An attempt has been made to obtain this information by conducting a series of towing tank drag measurements on samples of polyethylene netting. These measurements are used to derive drag coefficients in chapter 4.0, and also for net drag analysis in chapter 5.0. Empirical trawl net drag calculations are also made in chapter 4.0 using the derived drag coefficients.

3.1. Experimental apparatus

The drag measurements were made in a towing tank at Memorial University. The towing tank has dimensions of 61 m length, 4.5 m width and 3 m depth and is equipped with a towing carriage as shown in figure 3-2.

The polyethylene nets were attached to a frame which was suspended from the towing carriage and towed through the water. A frame size was determined from the size and shape of the meshes and the rating of the instruments to be used. The frame was constructed from aluminum pipe and aluminum rectangular bar to the specifications shown in figure 3-1.

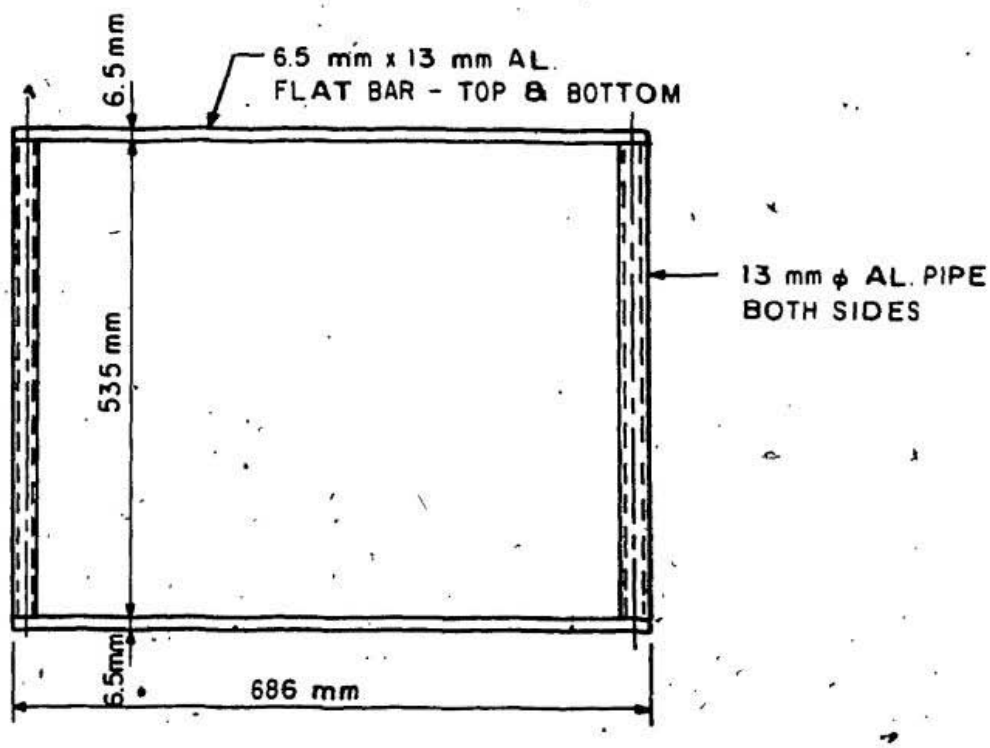

Figure 3-1: Net holding frame.

The nets were cut slightly smaller than the inside dimensions of the frame and stretched to avoid net curvature during testing. Initially each mesh was attached loosely to the frame in its approximate position by looping electrical cable wraps around a side of the frame and through a mesh as shown in figure 3-3. The nets were then stretched in the frame by systematically tightening the wraps holding meshes on opposite sides of the frame. Electrical cable wraps are ideal for this purpose because it was possible to tighten a net gradually while maintaining a uniform mesh pattern.

A holding assembly was fabricated and used to suspend the net and frame from the carriage into the water. This assembly consists of a rectangular plate which straddles the carrying rails of the towing carriage (figure 3-4). A shaft and

bearing arrangement was attached to a length of pipe which extends down from the rectangular plate and is used to support a pivoting pole which holds the frame and net suspended in the water below (figure 3-5). When the carriage is in motion the drag force of the water on the net and frame tends to rotate the pivoting pole and shaft in the opposite direction of motion. A force gauge equipped with a variable-reluctance displacement transducer is attached to the upper end of the pivoting pole as shown in figure 3-7. This force gauge provides a reaction force which prevents the rotation of the pivoting pole and generates a DC output voltage that is a linear function of the applied force. The net is suspended approximately 15 cm below the surface of the water. There was no indication of free surface effects at this depth.

The pivoting pole has a circular disk welded to its submerged end. Matching holes drilled in the disk and frame allow the frame to be bolted to the pivoting pole. The bolt hole positions, as shown in figure 3-6, were preset to form specific angles with the direction of motion when the holding assembly is attached to the carriage. This disk allowed precise changes of the angle of attack between tests. The angle of attack was defined as the horizontal angle between the plane of the net and the direction of motion.

The experimental instrumentation is shown in figure 3-4 and a circuit diagram illustrating the wiring of the instruments is shown in figure 3-8.

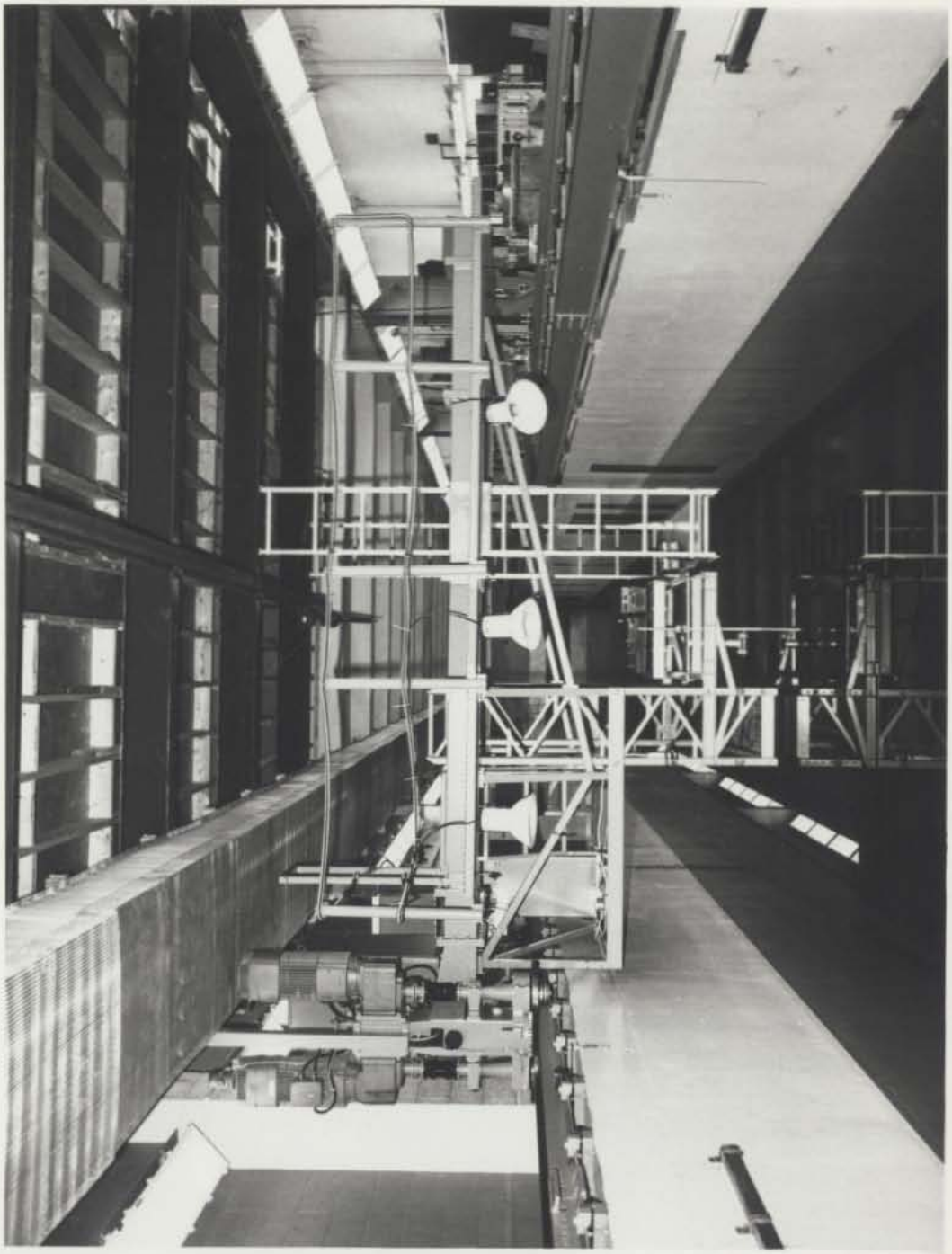

Figure 3-2 : Towing carriage and tank

Figure 3-3 : Electrical cable wraps used to attach nets to frame

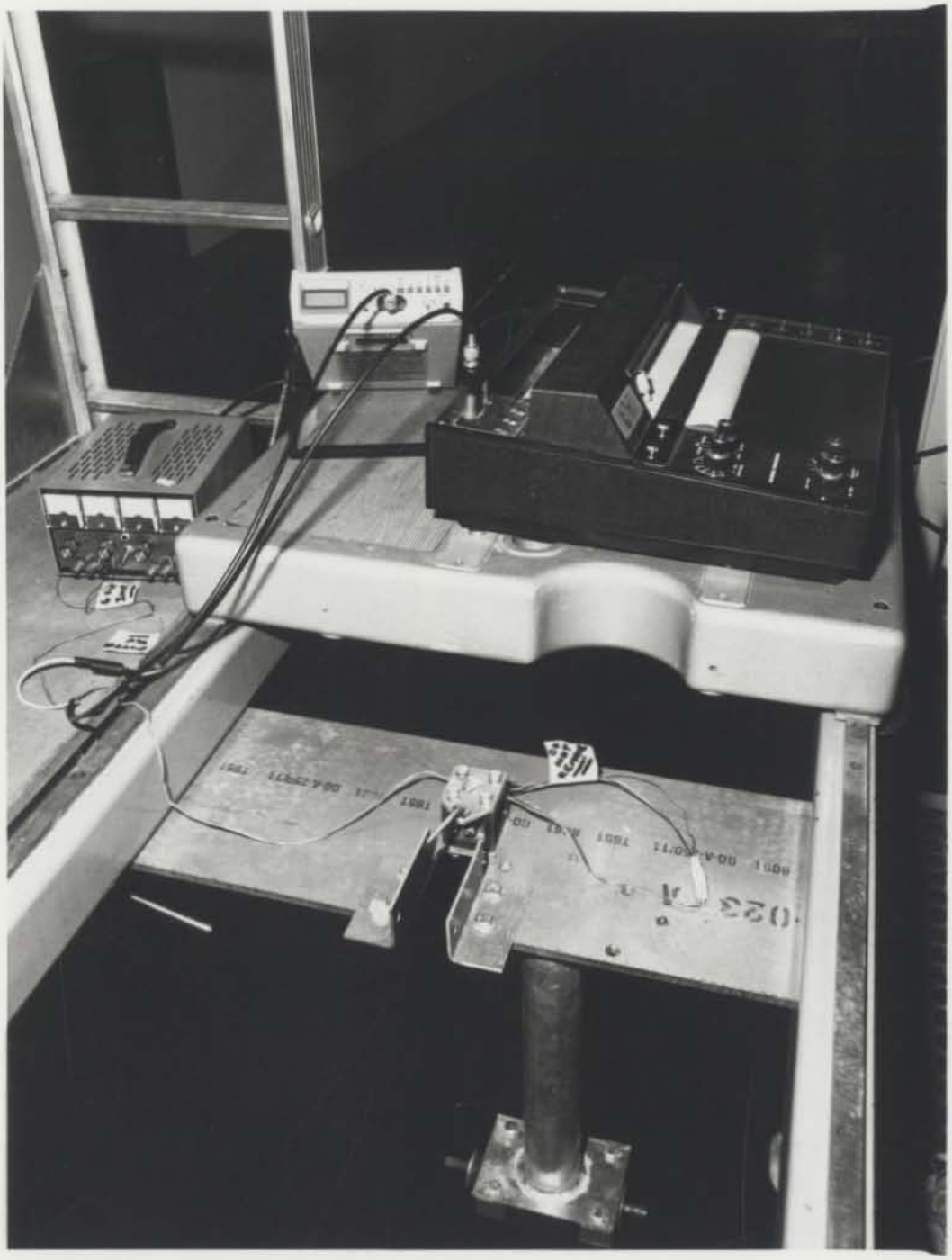

Figure 3-4 : Holding assembly

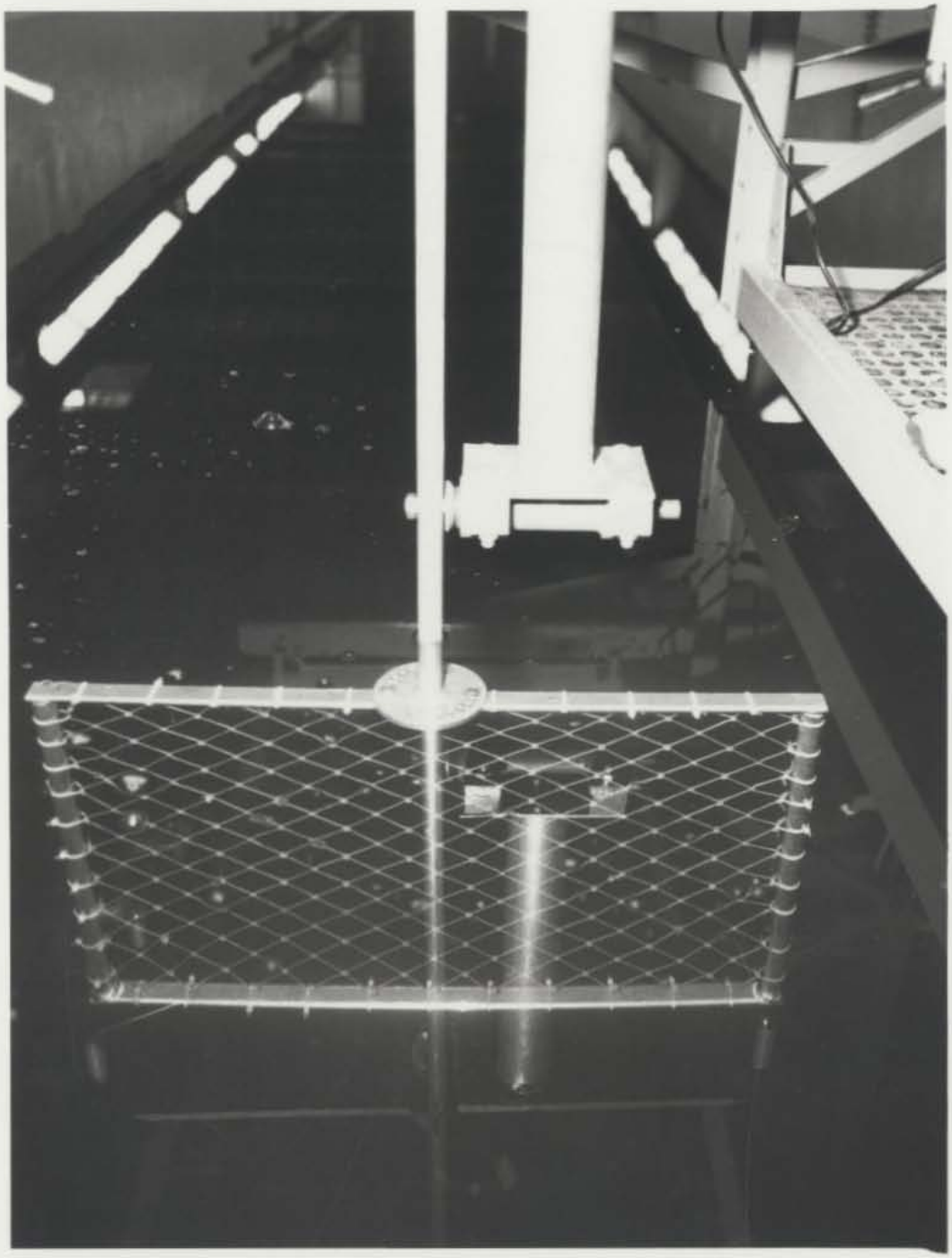

Figure 3-5 : Frame suspended in water

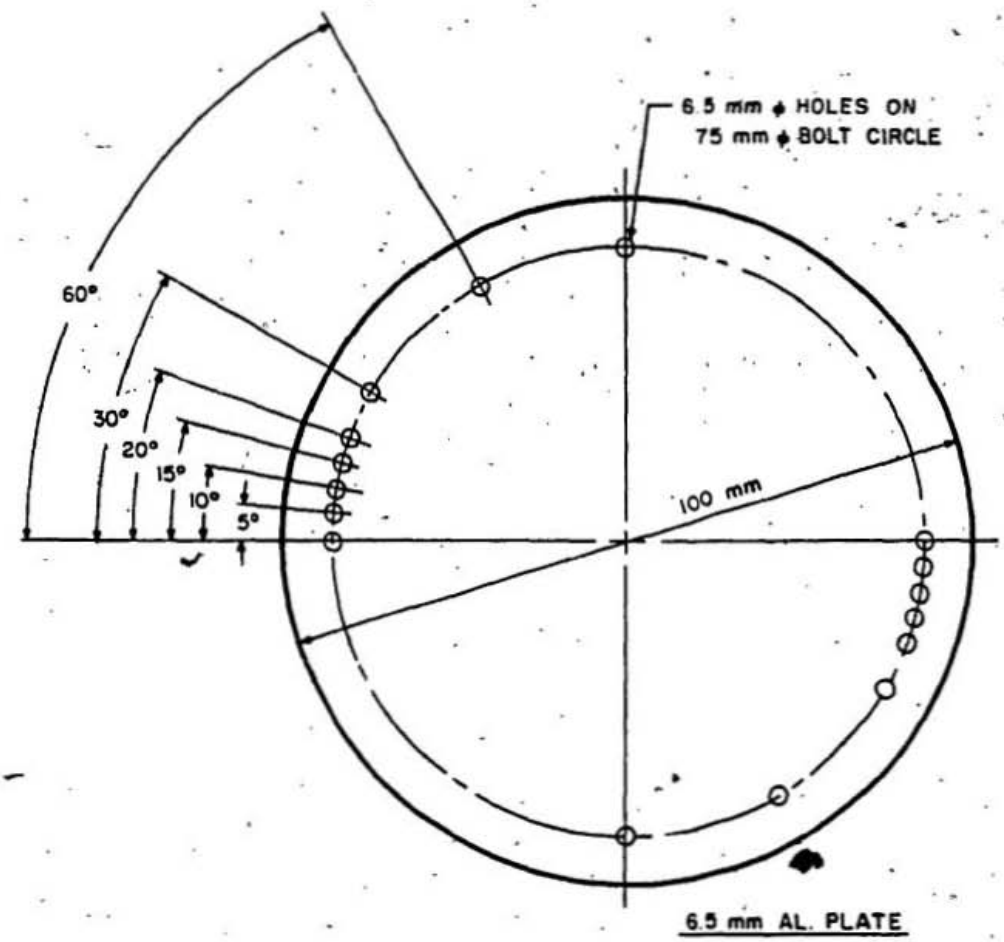

Figure 3-6: Circular disk with preset bolt hole positions.

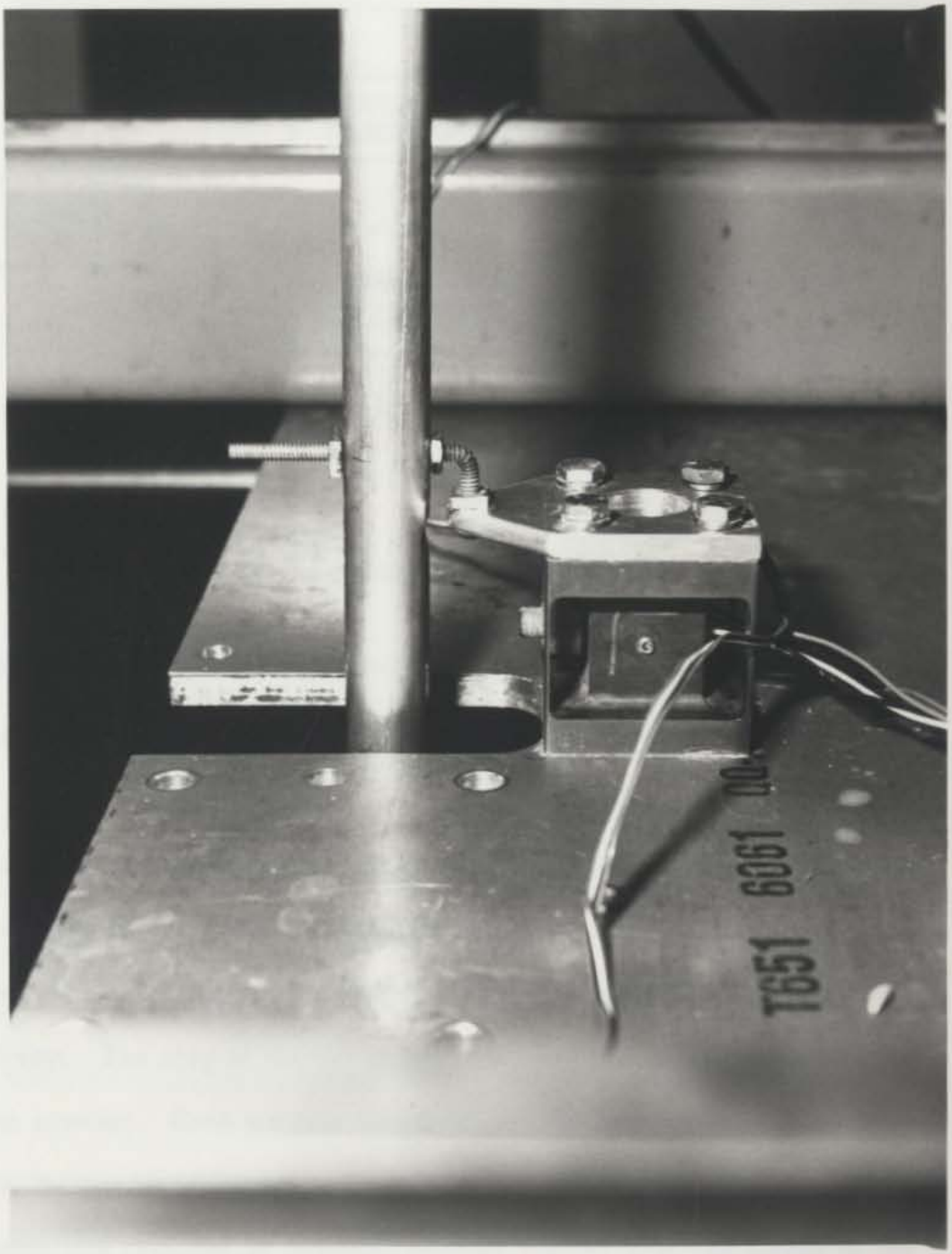

Figure 3-7 : Variable-reluctance displacement transducer

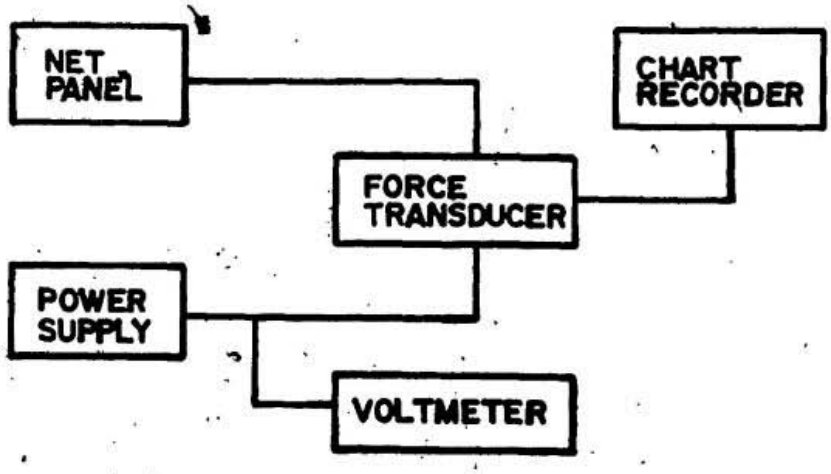

Figure 3-8: Experimental circuit diagram.

3.2. Experimental procedure and measurements

Drag measurements were made on the nets listed in Table 3-1 and are shown in appendix B. Included in each table in appendix B is the drag of the net and frame combination expressed in millivolts, *net/frame(mv)*, the drag of the frame alone, *frame(mv)*, and the drag of the net alone, *net(mv)*. The drag of the net is calculated by subtracting the drag of the frame from the total drag of the net and frame. The drag of the net in newtons, *net(N)*, was calculated using a calibration constant. Each net was tested at velocities ranging from 1.0 *m/s* to 2.0 *m/s* in increments of 0.2 *m/s* over a full range of attack angles. Each drag measurement was recorded at constant carriage velocity over the length of the tank.

Table 3-1: Mesh parameters of the nets tested.

NET	a (*mm*)	d (*mm*)	b	k	$\theta°$
# 1	75.0	3.0	144	85	30
# 2	75.0	4.0	144	85	30
# 3	75.0	3.0	142	80	SQ
# 4	75.0	3.0	130	71	43
# 5	75.0	3.0	132	78	48
# 6	75.0	3.0	150	88	60
# 7	75.0	3.0	252	150	79

The millivolt readings shown in appendix B are the mean numerical values for each trace. A large number of readings were made at small increments along a typical trace and a sample mean, a standard deviation and the mean standard error calculated. A 95% confidence interval was established by calculating the mean standard error using two standard deviations. The mean standard error was calculated to be ±.48%. This mean standard error is expressed as a percentage in appendix B. It is reasonable to assume that the numerical mean of all other traces lies within two standard errors of its sample mean.

The mean standard error of the difference of two measured quantities each having a mean m_1 and m_2 and mean standard errors e_1 and e_2 is given as follows [27]:

$$e = \sqrt{e_1^2 + e_2^2} \tag{3.1}$$

where:

e = the combined mean standard error.

Thus, the new mean is calculated using the following equation:

$$m = m_1 - m_2 + \sqrt{e_1^2 + e_2^2} \tag{3.2}$$

where:

m = the combined mean.

Equation (3.2) was used to calculate the drag of the various nets with m_1 as the drag of the net and frame and m_2 as the drag of the frame. As shown by equation (3.2), the mean standard error will be large if the individual means are nearly equal. As a result the mean standard error of the net drag is highest at low angles of attack.

The resulting mean standard error is given as a percentage in each table in appendix B. The value shown is the maximum occurring at that angle of attack.

Calibration measurements were made at regular intervals throughout the testing period. These calibration measurements were combined and a least squares curve fitting routine used to determine the mean linear calibration constant of the transducer. A plot of the resulting calibration curve is shown in figure 3-9 along with the initial calibration measurements. The calibration curve is defined by the following relationship:

$$F = (0.63 \pm 0.0012)(\Delta E) \tag{3.3}$$

where:

F = the applied force (Newtons)

$\Delta(E)$ = the change in the output voltage (millivolts).

Equation (3.3) was used to convert the drag of the nets from millivolts to newtons. The combined mean standard error of the product of two measured quantities having means m_1 and m_2 and mean standard errors e_1 and e_2 is calculated using the following equation [27]:

$$e = \sqrt{(m_1 e_1)^2 + (m_2 e_2)^2} \tag{3.4}$$

The mean standard error of each *net*(N) as shown in appendix B was calculated using equation (3.4). Again, the mean standard error shown is the largest occurring at that angle of attack and is expressed as a percentage of the drag.

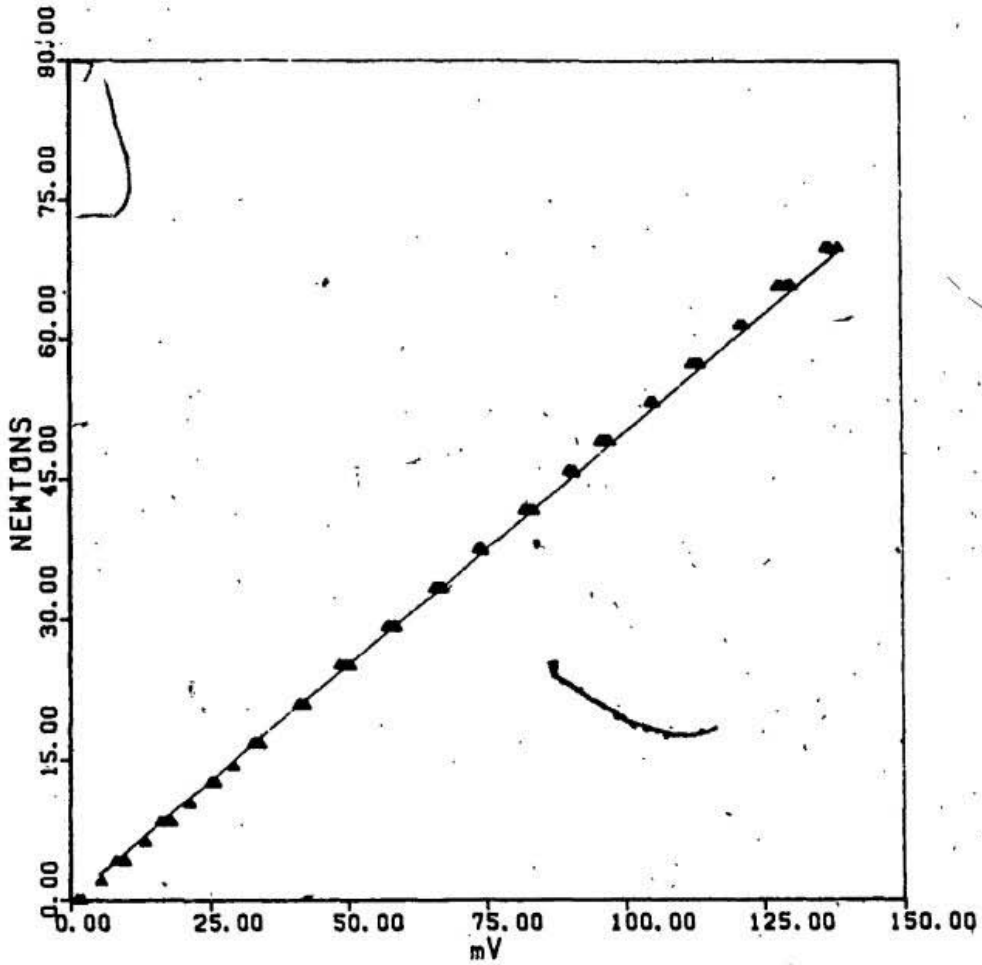

Figure 3-9: Calibration curve

Chapter 4

DERIVATION OF THE DRAG COEFFICIENT OF POLYETHYLENE NETTING

An analysis was made of the drag measurements reported in chapter 3.0 in terms of the projected twine area of the netting and the angle of attack. Empirical drag coefficients were derived which are shown to be a function of the projected twine area and the angle of attack. In the final section of this chapter these coefficients are used in empirical net drag calculations and found to give reasonable predictions of the drag of a trawl net made from polyethylene twine.

The following principles of Fluid Mechanics were considered in the analysis of the drag measurements.

4.1. Basic fluid mechanics principles

An object immersed in an incompressible flow experiences lift and drag forces resulting from localized pressure differences over its surface as well as frictional effects in the boundary layer around its surface. No lift force measurements were made and therefore these forces are neglected in the following analysis.

The total drag on an object immersed in a flow is the sum of pressure drag and friction drag. Friction forces originate from the dissipation of energy in

overcoming the resistance to flow within the boundary layer. These frictional forces are predominant at lower velocities. Pressure drag is dependent upon the form of the object but is also affected by the formation of the boundary layer. The momentum of the fluid particles within the boundary layer will be considerably less than those outside the boundary layer at corresponding positions in the flow. As the velocity of fluid particles in the boundary layer is slowed, a circular motion is induced by the surrounding flow. A discontinuity is formed which is characterized by the formation of a separation point and a wake zone behind the object.

Immediately outside the boundary layer the fluid will act as an ideal fluid, accelerating over the upstream section of the object and decelerating over the downstream side. High velocities associated with this acceleration and deceleration result in localized pressure reductions which are transmitted into the wake at the rear of the object. The result is a large drag force caused by the pressure difference immediately upstream and downstream of the object.

The pressure drag force acting on an object immersed in an incompressible flow is dependent upon its area, the density and viscosity of the fluid, and the velocity of flow around the object, i.e.

$$R = f(A, \rho, \upsilon, V). \tag{4.1}$$

where:

A = profile area

ρ = the density of the fluid

υ = the viscosity of the fluid

These variables are rearranged using dimensional analysis to give the following basic equation:

$$R = c_d A \rho V^2/2 . \tag{4.2}$$

where:

c_d = the drag coefficient of the object which is dependent upon the Reynolds number over a wide range of flow.

4.2. Drag coefficient analysis

Equation (4.2) can be represented by an equation of the following form:

$$R = K V^2 \tag{4.3}$$

where:

$$K = c_d A \rho/2 . \tag{4.4}$$

The profile area of a net taken as the projected twine area on the plane perpendicular to the direction of motion is given as follows [18]:

$$Ap = b d a + k \pi d_k^2/4 . \tag{4.5}$$

where:

b = number of bars

d = diameter of a bar

a = length of a bar

k = number of knots

d_k = diameter of a knot

This formula takes into account all the knots and twine bars making up the net

and leads to an accurate calculation of the projected twine area. The twine bars are assumed to be cylindrical in shape while the knots are assumed to have a circular profile area with a diameter three times that of the twine.

As the angle of attack of a net is reduced below 90°, its projected twine area to the flow also decreases. Intuitively, one might suspect that the projected twine area of a net varies with the sine of the angle of attack as in the case of a flat plate. However, the orientation of the mesh in the flow results in a unique relationship between the projected twine area and the angle of attack. A detailed analysis was made to derive this relationship and is described below.

Figure 4-1 shows a three-dimensional diagram of a single mesh as outlined by the twine bars AB, BC, CD and AD. The mesh forms an attack angle of α with the direction of motion, the x-axis, and has a mesh opening angle of θ. Also shown in figure 4-1 is the projection of the mesh in the plane perpendicular to the direction of motion, the y-z plane. At an angle of attack of 90° the mesh lies in the y-z plane and the projected twine area is given by equation (4.5). At angles of attack below 90° the projected length of the twine bars in the y-z plane is reduced and, therefore, the projected twine area of the mesh to the flow is reduced. There is also a variation in the projected knot area. However, considering that the knot is assumed spherical in shape it is reasonable to assume that the decrease in the projected knot area is negligible.

The projected length of bar AB in the y-z plane, AB_{y-z}, is given by the following expression:

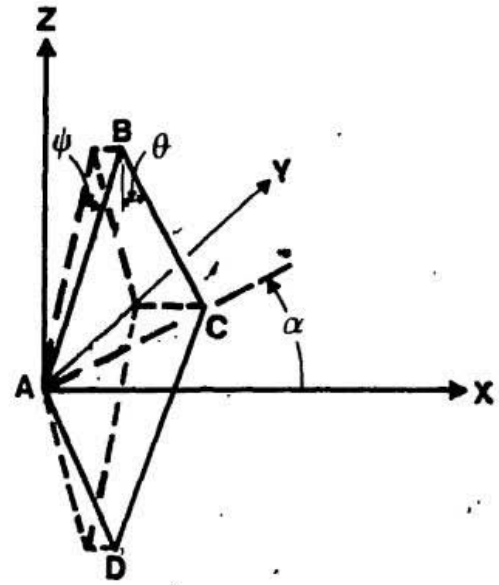

Figure 4-1: The projection of a mesh, held at an angle α to the x-axis, on the y-z plane

$$AB_{y-z} = AB\cos\psi \tag{4.6}$$

where:

$$\sin\psi = \sin\theta\cos\alpha\,. \tag{4.7}$$

AB_{y-z} is therefore written as follows:

$$AB_{y-z} = \sqrt{1-\sin^2\theta\cos^2\alpha}\;AB\,. \tag{4.8}$$

Upon substitution of equation (4.8) into equation (4.5), the projected twine area of a net becomes:

$$Ap = \sqrt{1-\sin^2\theta\cos^2\alpha}\;(b\,d\,a) + k\,\pi\,d_k^{\,2}/4\,. \tag{4.9}$$

The mean diameter of nominal 3 *mm* and 4 *mm* polyethylene twine samples

were measured and found to be $2.815 \pm .2mm$ and $3.558 \pm .3mm$ respectively. These measurements were made with a vernier caliper. Although optical methods are currently used to measure twine diameter very accurately [9], these methods could not be used to make the above measurements because of a lack of equipment. The degree of accuracy of the twine diameter measurements are, however, sufficient for illustrative purposes.

Measurements were made of the projected area of a twine knot at an angle of attack of 90°. The projected area of a knot made from 3 *mm* polyethylene twine was found to be $110.20 \pm 0.61mm^2$ while that of a knot made from 4 *mm* twine was found to be $126.90 \pm 0.23mm^2$. These measurements were taken from photographs of the respective knots using a high precision digitizer. Sample photographs are shown in figures 4-2 and 4-3.

Equation (4.9) was, therefore, modified to give the projected area of a net as follows:

$$Ap = \sqrt{1 - \sin^2\theta\cos^2\alpha}\,(b\,d\,a) + kA_k \qquad (4.10)$$

A least squares curve fitting computer program was developed to generate a smooth curve through each set of drag measurements using equation (4.3). The results are shown in figures 4-4 and 4-5 for 3 *mm* and 4 *mm* twine diameter nets with a mesh opening angle of 30°. These nets are numbers one and two in table 3.1. The correlation between the fitted curve and the experimental points is good in both cases.

Figure 4-2: The projected area of a knot made from 3 mm polyethylene twine. Scale, twice actual size.

Figure 4-3: The projected area of a knot made from 4 mm polyethylene twine. Scale, twice actual size.

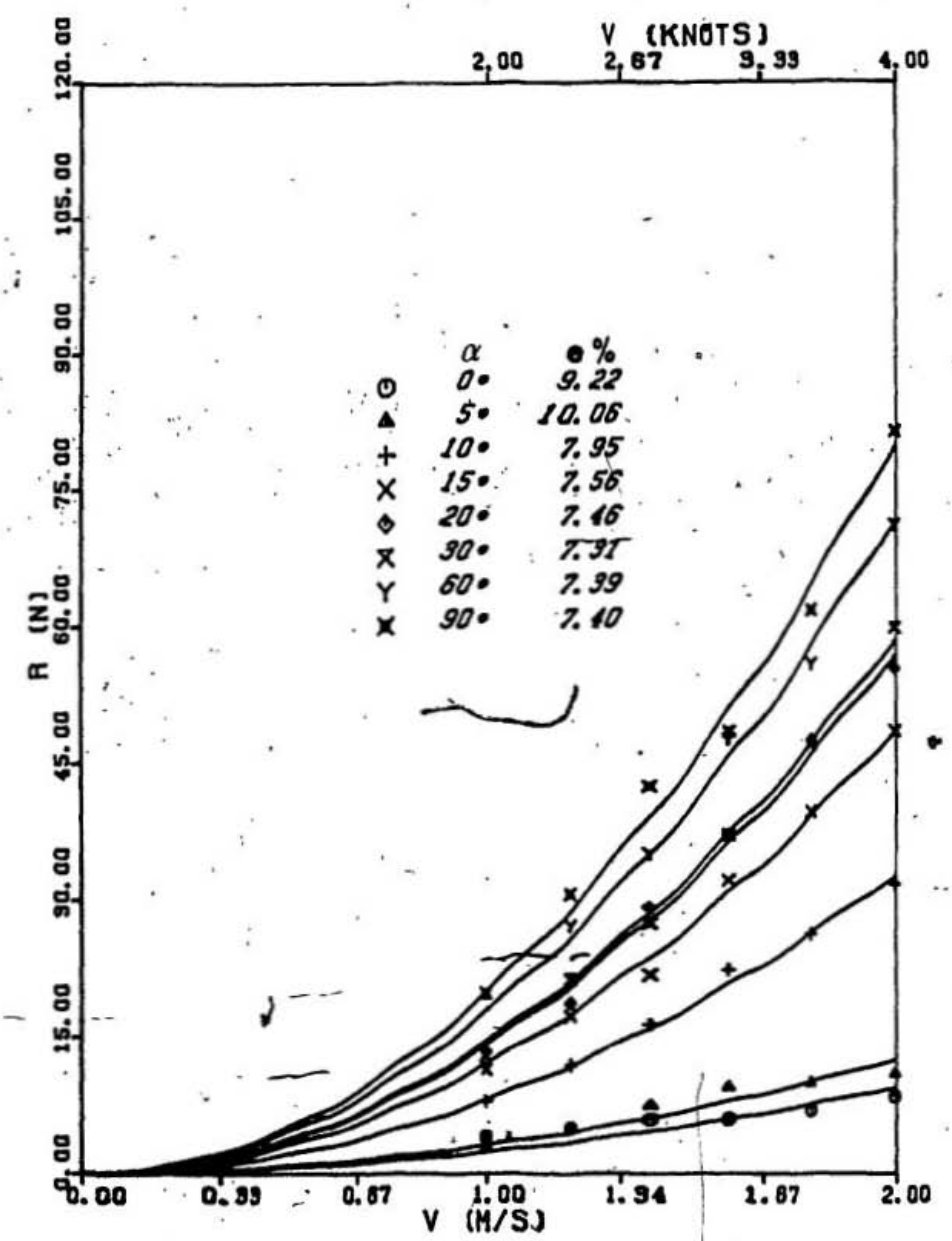

Figure 4-4: Net drag - 3mm polyethylene netting.

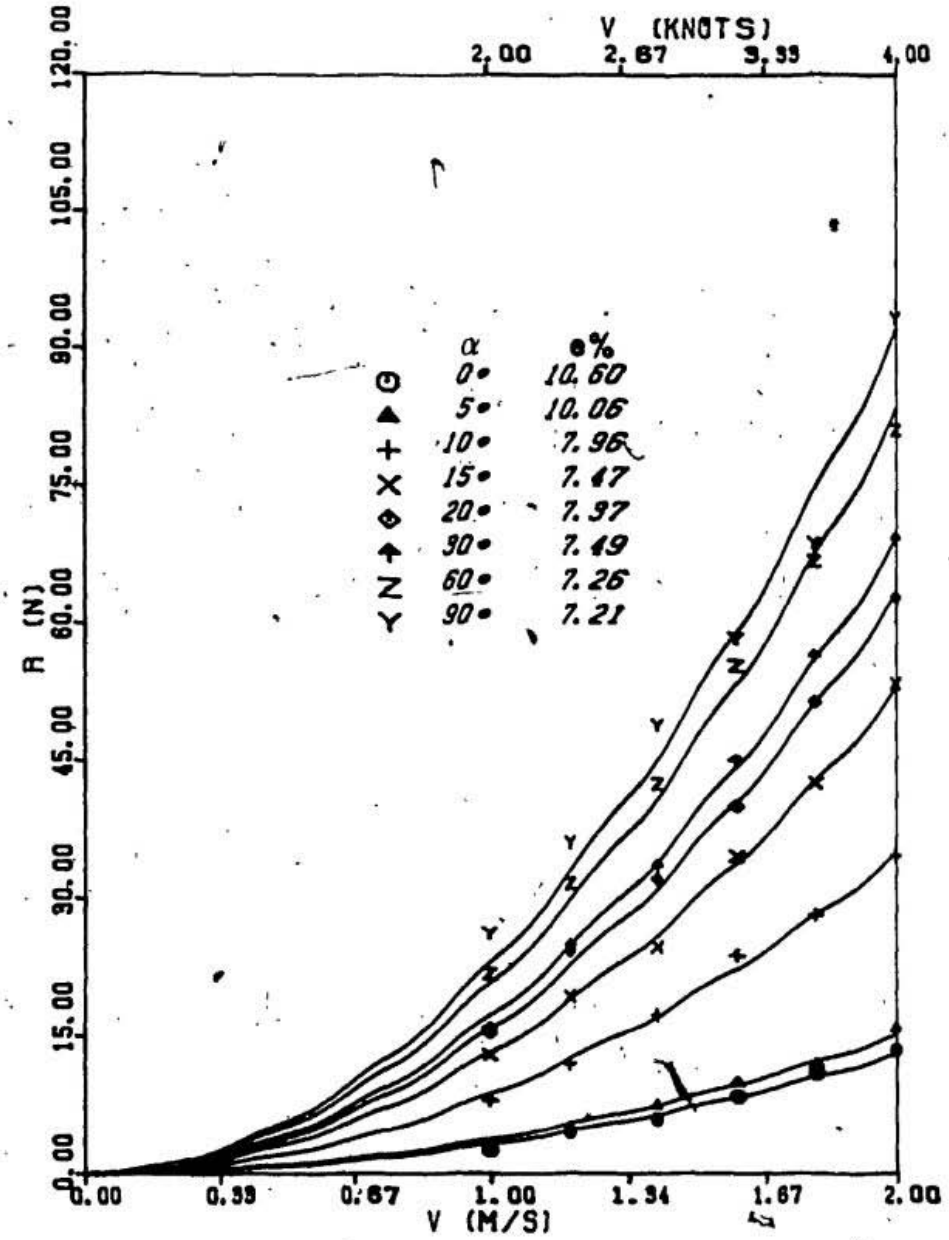

Figure 4-5: Net drag - 4 mm polyethylene netting.

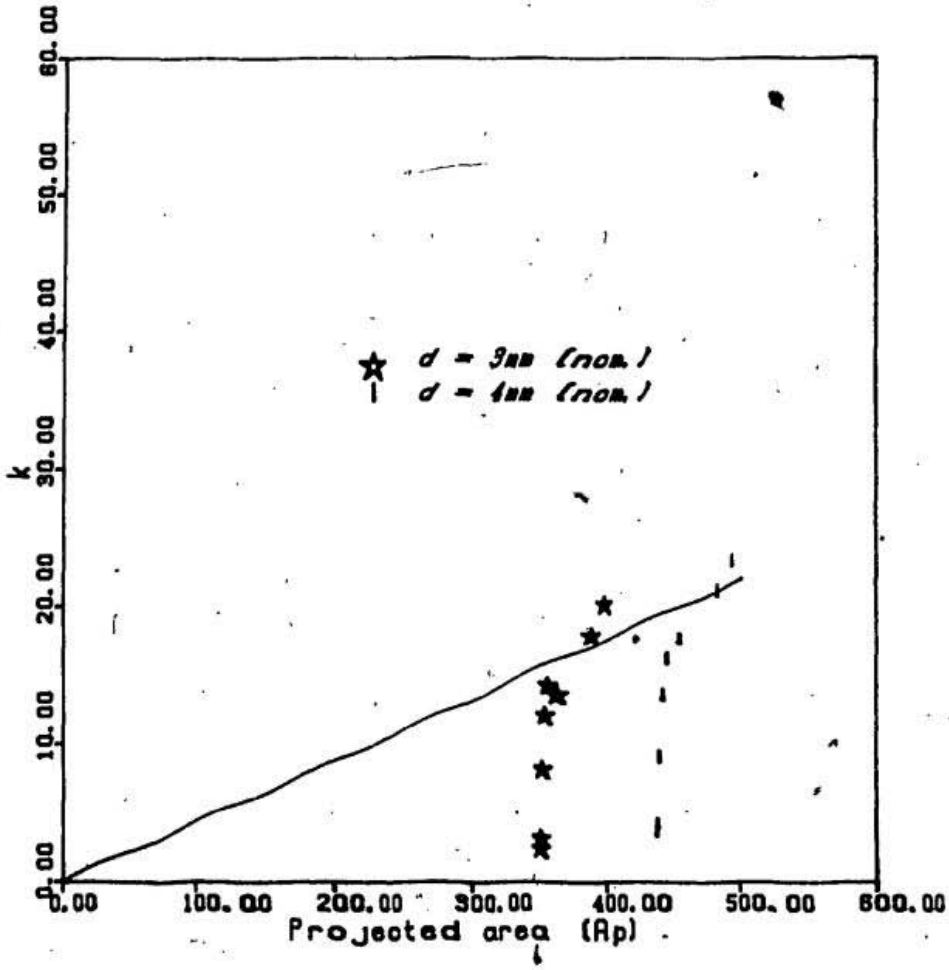

Figure 4-6: K versus projected twine area (Ap).

A plot of the curve fitting coefficient K and the projected twine area is shown in figure 4-6. Also shown in this figure is a straight line through the origin and the values of K at high angles of attack. The slope of this line represents a dimensionless theoretical drag coefficient which is a function of the projected twine area only. As shown by the marked points of the experimentally determined values of K differ significantly from those predicted by the theoretical line at low angles of attack.

The deviation of the experimental points from the theoretical line at lower angles of attack is a result of the twine bars lining up behind each other as the angle of attack is reduced. This effect is known as shielding or shadowing. As the angle of attack is reduced to a low value, it is to be expected that the flow around the twine bars behind the leading portion of the net will become increasingly turbulent. The development of turbulent flow could therefore lead to a reduced drag coefficient [1].

It is also clear that there is a reduction in the projected twine area of the net due to shielding. Imai [16] derived formulae to calculate the projected twine area of a net based on the assumption that the shielding effect begins when the projection of the knots touch in the plane perpendicular to the direction of motion. As shown in figure 4-7, the angle of attack at which the knots touch in this plane is calculated as follows:

$$\sin \alpha = \frac{y}{2a \sin \theta} \tag{4.11}$$

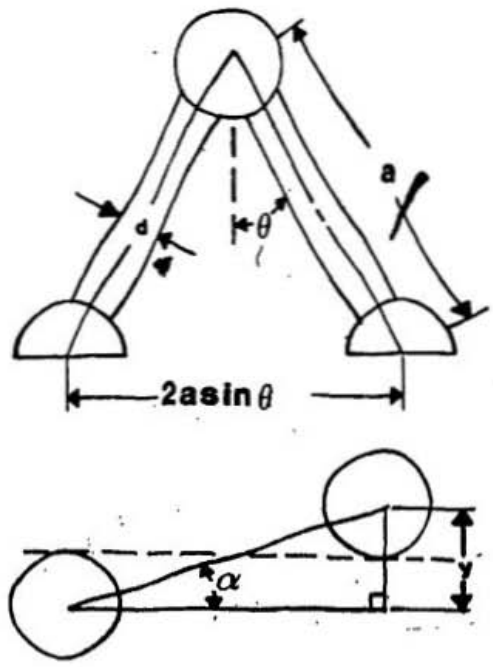

Figure 4-7: A diagram illustrating the beginning of shielding.

According to equation (4.11), shielding begins at an α of 6.89° with a bar length of 75 *mm* and an θ of 30°. Figure 4-6, however, indicates that a sudden decrease in the drag occurs at an α of approximately 30°. It is therefore likely that the development of turbulent flow is more significant than the shielding effect in reducing the drag of the nets at lower angles of attack or else shielding begins at angles of attack higher than predicted by the analysis.

The drag of polyethylene netting therefore does not appear to be proportional to its projected twine area only. Other researchers have drawn similar conclusions from measurements made on different types of netting [25]. It was intended that the strict calculation of the projected twine area of the nets

would lead to a linear relationship between the drag and the projected twine area. This is not the case, however, as it is apparent that the coefficient of drag of netting is a function of not only the projected twine area but also the angle of attack.

4.3. The calculation of the drag of the 350 I.C. trawl net

Trawl net drag calculations are made in this section using methods developed by Fridman and Dvernik [12], Kowalski and Gianotti [18] and Dickson [6]. These calculations give some insight into the difficulties arising when trawl net drag calculations are made and illustrate the usefullness of empirical net drag coefficients for making trawl net drag calculations.

4.3.1. Fridman's method

Trawl net drag calculations made by Fridman and Dvernik [12] are based on the hypothesis that the drag of a system of meshes is independent of the physical shape of the system. This hypothesis is stated mathematically for a trawl net constructed from individual panels as follows:

$$R = \frac{\rho}{2} \sum_{i=1}^{n} c_{di} A_i V^2 = \sum_{i=1}^{n} R_i \tag{4.12}$$

where:

R_i = the drag of the i^{th} panel

A_i = the area of the i^{th} panel

c_{di} = the coefficient of drag of i^{th} panel

n = the number of panels.

A further postulation by Fridman is that by calculating an average angle of attack from the angles of attack of the net panels making up the trawl net an average drag coefficient can be used in equation (4.12), i.e.

$$R = \frac{\rho}{2} c_{d\alpha} \sum_{i=1}^{n} A_i V^2 = \sum_{i=1}^{n} R_i \qquad (4.13)$$

It is impractical to count the number of twine bars and knots making up a trawl net in order to calculate its projected twine area at lower angles of attack using equation (4.10). A trawl net twine area was therefore calculated by multiplying the overall area of the net panels, as determined from the net drawings shown in figure 4-8, by the solidity of the meshes. Empirical net drag coefficients corresponding to this net area are shown in figure 4-9.

The calculation of the twine area is summarized in table 4-1. The solidity of the meshes were calculated using equation (1.4) assuming a mesh opening angle of 30°. An average angle of attack of 6.5° was estimated for the panels making up the trawl net from the sea measurements shown in figure 2-5. The empirical drag coefficient corresponding to this average angle of attack is 0.19 as shown in figure 4-9.

The results of the calculation of the drag of the I.C. trawl net using equation (4.13) and the variables given above are discussed in section 4.4.

4.3.2. Kowalski's and Gianotti's method

Trawl net drag calculations by Kowalski and Gianotti [18] are based on the hypothesis that the drag of the trawl net is directly proportional to the area of the mouth opening of the net, which is assumed to be conical in shape . This hypothesis was first tested by Crewe [5]. The drag of the net is calculated using the following equation:

$$R = c_{d90} (\pi A B) \rho S V^2/2 . \tag{4.14}$$

where:

c_{d90} = the coefficient of drag of the netting held at an angle of attack of 90 °. See figure 4-9.

$(\pi A B)$ = the frontal area of the elliptical mouth of the trawl net.

S = the mesh solidity.

Since the semiaxes, A and B, are measured at the wing tips a correction factor is applied to equation (4.14) to reduce the drag by an amount proportional to the space between the wings where there is no netting. Wind tunnel measurements made by Kowalski [17] indicated that the variation of the empirical net drag coefficient with the angle of attack, α, was proportional to the sine of the angle of attack, i.e.

$$c_{d\alpha} = \sin \alpha \, c_{d90} \tag{4.15}$$

The drag force that would act on the empty space between the wings if it were filled with netting is therefore given by the following equation:

$$R_{emptyspace} = \sin \alpha \, c_{d90} A_{emptyspace} \rho S V^2/2 . \tag{4.16}$$

The empirical drag coefficient $c_{d\alpha}$ was taken directly from figure 4-9 for the calculation of the drag of the I.C. trawl net using Kowalski's method. Equation (4.16) therefore becomes:

$$R_{emptyspace} = c_{d\alpha} A_{emptyspace} \rho S V^2/2 . \tag{4.17}$$

The ratio k_1 of equations (4.14) and (4.17) is given as follows:

$$k_1 = \frac{c_{d\alpha} A_{emptyspace} \rho S V^2/2}{c_{d90} (\pi A B) \rho S V^2/2} = \frac{c_{d\alpha} A_{emptyspace}}{c_{d90} (\pi A B)} \tag{4.18}$$

and equation (4.14) is therefore rewritten as follows:

$$R = (1 - k_1) c_{d90} (\pi A B) \rho S V^2/2 . \tag{4.19}$$

The angle of attack of the top and bottom portion of the I.C. trawl net was estimated to be approximately 3° and therefore a value of $c_{d\alpha}$ of 0.15 was taken from figure 4-8. The empty space between the wings was calculated using figure 4-8 and a value of 0.28 as calculated for k_1 using equation (4.18).

Kowalski calculates the drag on the codend using the following equation:

$$R = c_f \frac{\rho}{2} V^2 A_s \tag{4.20}$$

where:

c_f = the frictional drag coefficient of netting held parallel to the flow

A_s = the wetted surface area of codend.

The c_f used by Kowalski is 0.0005, which is given by Hoerner [15] as the frictional drag coefficient of a hollow cylinder the approximate size of a typical codend.

Calculations were made of the trawl net drag using the above procedure and are discussed in section 4.4. The semiaxes A and B were estimated from the performance measurements given in figure 2-5. An average solidity was calculated from the values shown in table 4-1 and the empty space between the wings was calculated from the net drawings shown in figure 4-8.

4.3.3. Dickson's method

This method is similar to Fridman's in that the drag of the trawl net is calculated by adding up the drag of the various panels. Dickson [6], however, uses theoretical drag coefficients calculated using theoretical formulae developed by Crewe [5]. According to this theoretical approach the drag coefficient of a sheet of netting held at some angle of attack, α, between 0° and 30° is calculated using the following equation:

$$c_{d\alpha} = (c_{d90} - c_{d0})\,\alpha/60 + c_{d0} \tag{4.21}$$

The drag coefficients c_{d90} and c_{d0} of a mesh consisting of two twine bars and a knot, are given as follows:

$$c_{d90} = c_{dsc}\,c_t\,2\,(a - d_k)\,d + c_k\,\pi\,d_k^2/4 \tag{4.22}$$

$$c_{d0} = [c_{dsc}\,c_t \sin^3\theta + c_f \cos^2\theta][2(a - d_k)d + c_k \pi d_k^2/4] \tag{4.23}$$

where:

c_{dsc} = the drag coefficient of a smooth cylinder (1.0)

c_t = a factor allowing for the type of twine (1.0)

c_k = the drag coefficient of a knot (0.47)

c_f = the twine skin friction coefficient (0.007)

θ = the mesh opening angle 30°

s = the solidity of a mesh

a = the twine bar length.

d = the twine diameter.

d_k = the knot diameter ($3d$).

A plot of the theoretical and empirical drag coefficients are shown in figure 4-10. Figure 4-10 indicates that the theoretical coefficients are larger than the empirical coefficients at lower angles of attack. It is apparent that the theoretical drag coefficients do not take into account the reduced drag of the net at the lower angles of attack.

The calculation of the drag of the I.C. trawl net using the theoretical drag coefficients and net panel areas as given in table 4-I are discussed in section 4.4.

4.4. Comparison of trawl net calculations with sea measurements

Drag curves were calculated for the I.C. trawl net using each of the above methods. These curves are shown in figure 4-11 along with the drag as derived from sea measurements made by King and Hearn [14].

In general the calculations give reasonable approximations of the sea measurements. The calculated drag, however, tends to increase more rapidly than the measured drag. This is particularly true in the case of the calculations made using Dickson's method. The reason for this is that the theoretical drag coefficients are larger than the empirical coefficients at lower angles of attack, as shown in figure 4-10.

It was concluded that the empirical drag coefficients given in figure 4-9 can be used to give reasonable approximations of the drag of other trawl nets similar to the 350 I.C. trawl net and made from polyethylene twine.

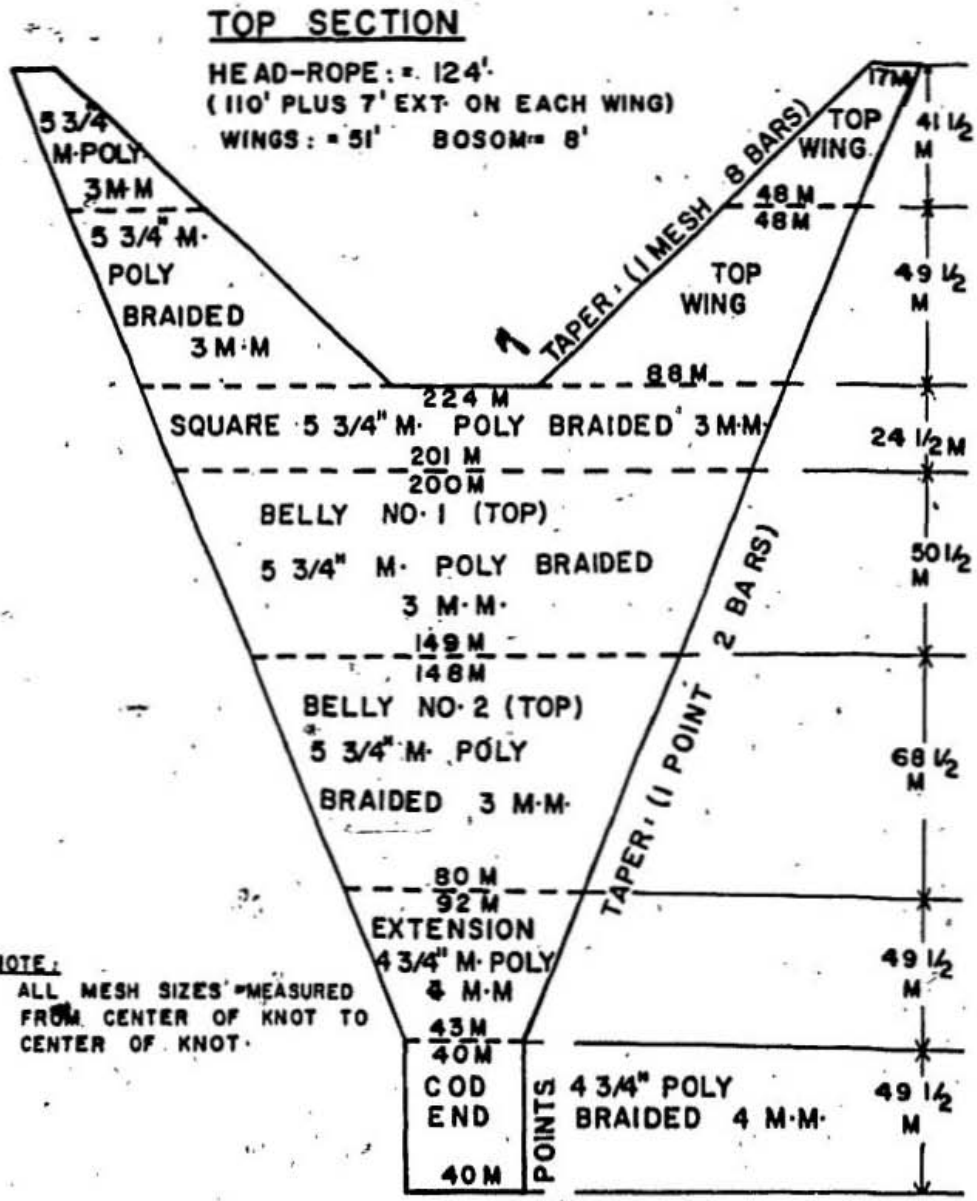

Figure 4-8: The 350 I.C. trawl net parameters.

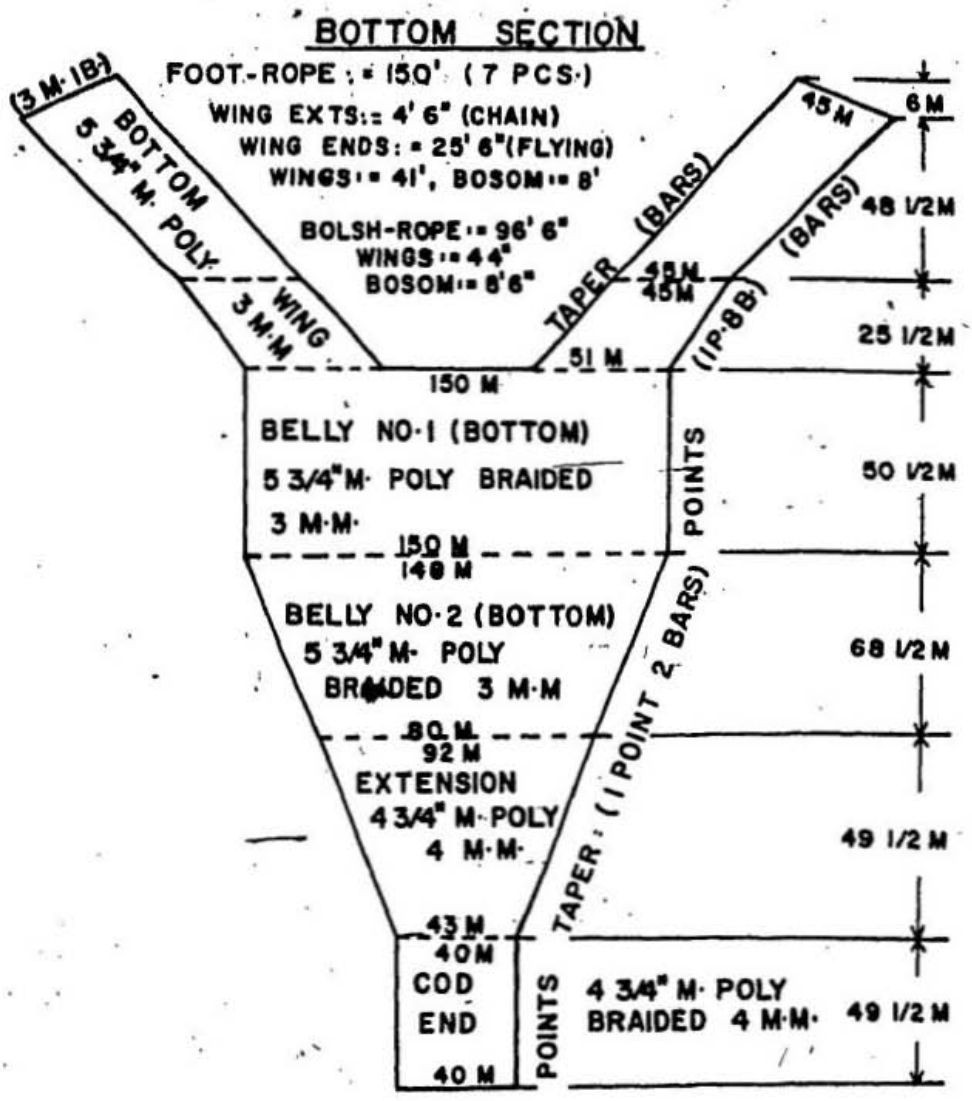

Figure 4-8, concluded

Table 4-1: Trawl net twine area calculations

Panel #	Panel area (m^2)	$d\,(mm)$	S	$A_p\,(m^2)$
1	13.14	3.0	.1054	1.38
2	32.79	3.0	.1054	3.46
3	13.14	3.0	.1054	1.38
4	32.79	3.0	.1054	3.46
5	50.72	3.0	.1054	5.35
6	85.85	3.0	.1054	9.05
7	76.08	3.0	.1054	8.02
8	29.66	4.0	.1464	4.34
9	21.26	3.0	.1054	2.24
10	11.18	3.0	.1054	1.18
11	21.26	3.0	.1054	2.24
12	11.18	3.0	.1054	1.18
13	75.79	3.0	.1054	7.78
14	76.08	3.0	.1054	8.02
15	29.66	4.0	.1464	4.34
16	19.29	4.0	.1464	2.82
17	19.29	4.0	.1464	2.82

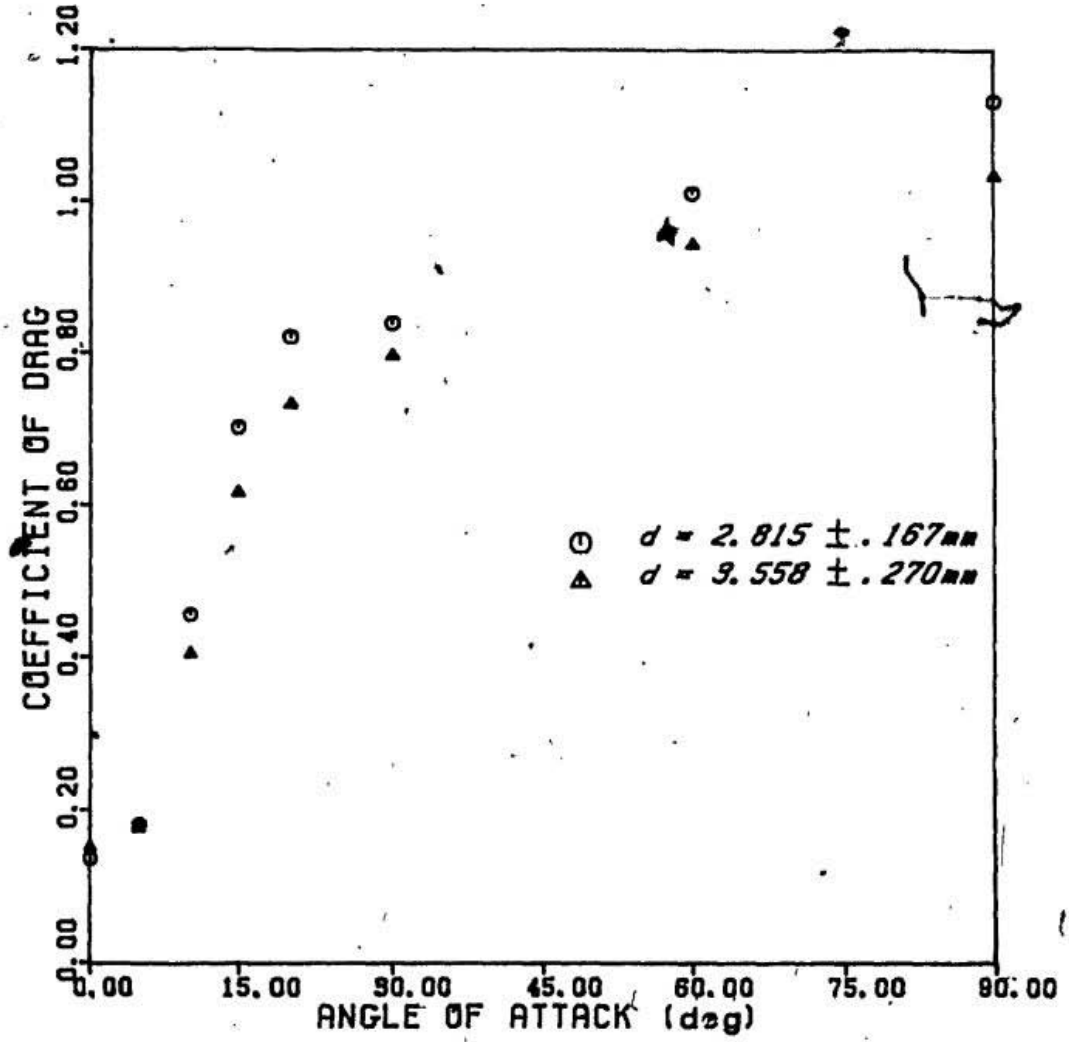

Figure 4-9: Empirical net drag coefficients.

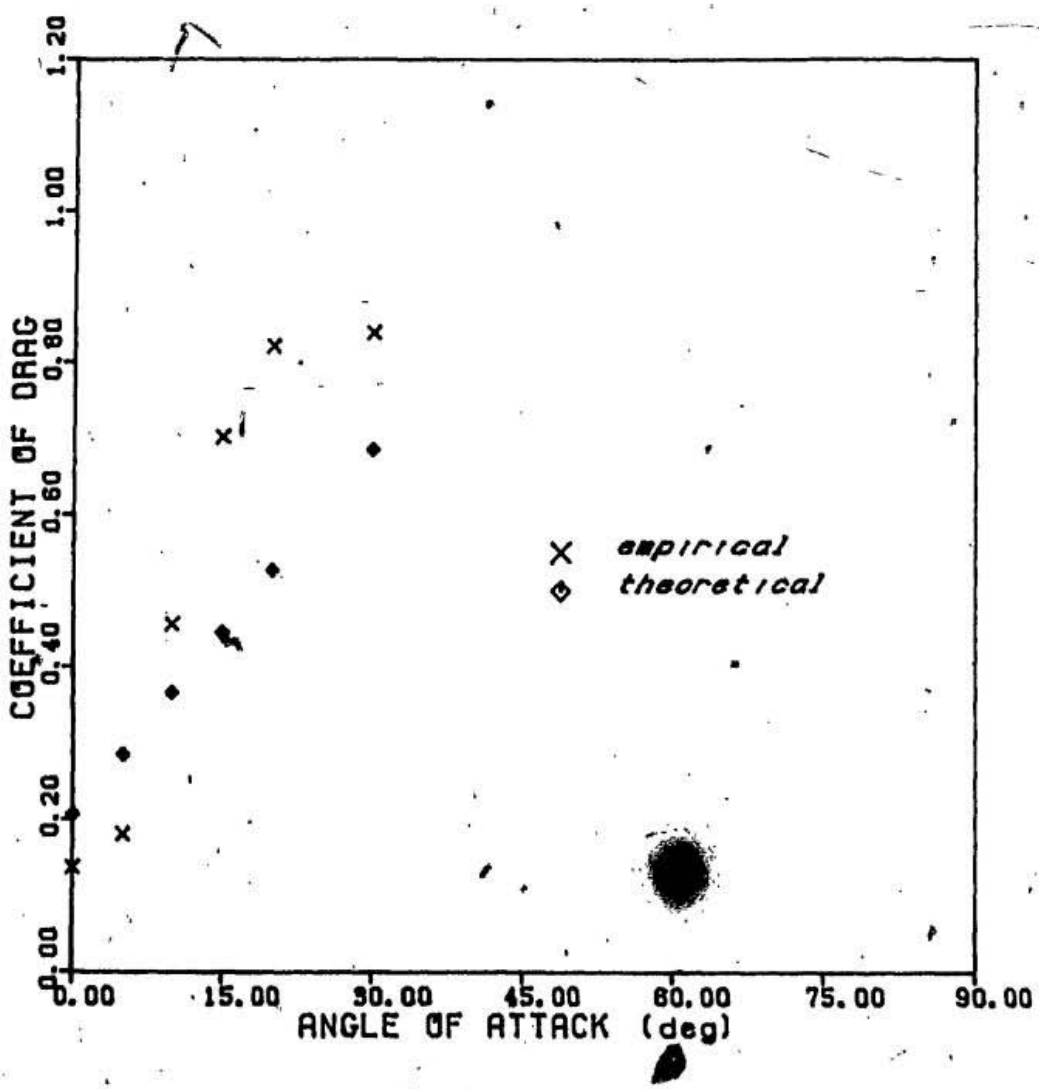

Figure 4-10: Empirical versus theoretical drag coefficients. (nominal 3mm twine)

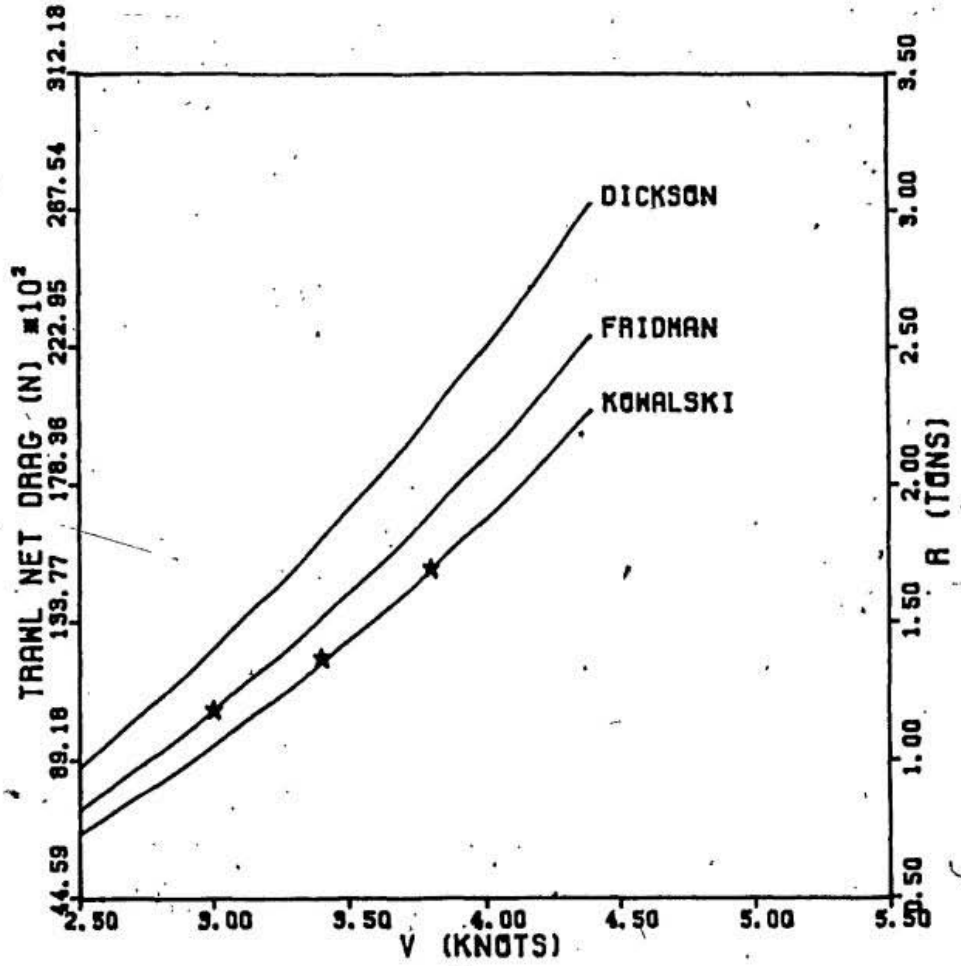

Figure 4-11: Comparison of sea measurements and empirical calculations.

Chapter 5

THE EFFECT OF THE MESH OPENING ANGLE ON THE DRAG OF NETS

This chapter contains further analysis of the net drag measurements. The work includes a full discussion of the effect of the mesh opening angle on the drag of nets. Theoretical calculations are also given which support the experimental measurements. Analysis of measurements made on square mesh nets, which have unique mesh opening angles, are also provided.

5.1. The drag of nets with different mesh opening angles

The drag coefficient of a net is dependent upon its mesh opening angle which ,along with the angle of attack, determines its orientation to the flow [25]. In the case of an angle of attack of 90° the variation of the drag coefficient is similar to that of the solidity at different mesh opening angles. Both the minimum drag coefficient and solidity occur at a mesh opening angle of 45° and both increase as the mesh opening angle increases. At angles of attack below 90°, Stengel's data shows a shift in the minimum drag coefficient away from 45° towards smaller mesh opening angles as illustrated in figure 5-1.

Since there is an increase in the solidity as the mesh opening angle is reduced below 45° there is a range of mesh opening angles for which there is an

increase in solidity and yet a decrease in the drag. In other words, the amount of netting is increasing but the drag is decreasing. Stengel attributes this behaviour to the orientation of the twine in the flow but no further analysis is given.

To investigate this behaviour measurements were made on a series of nets with different mesh opening angles. These nets are listed in table 3-1 as numbers four to seven. The measurements were made at angles of attack of 90° and 20°. Figures 5-2 and 5-3 show the drag of the different nets at each angle of attack. At an angle of attack of 90°, figure 5-2 indicates that the minimum drag occurs at a mesh opening angle of approximately 45°, as expected. Figure 5-3, however, shows that at an angle of attack of 20° the minimum drag occurs at a mesh opening angle greater than 48°. The projected twine area of a net with a mesh opening angle of 48° was calculated and found to be less than that of a net with a mesh opening angle of 45° at an angle of attack of 20°. Thus, the solidity of a net can increase although the projected twine area is not increasing. Also, the drag can decrease even though the solidity, which is representative of the amount of twine in the net, increases.

The projected twine area of a net as given by equation (4.9) is a function of the mesh opening angle θ. An expression for the minimum projected twine area can be found by minimizing equation (4.9) with respect to the mesh opening angle. Since the projected area of the knots is assumed to remain constant, equation (4.9) can be rewritten as follows:

$$Ap = \sqrt{1 - \sin^2\theta\cos^2\alpha}\ (b\,d\,a). \tag{5.1}$$

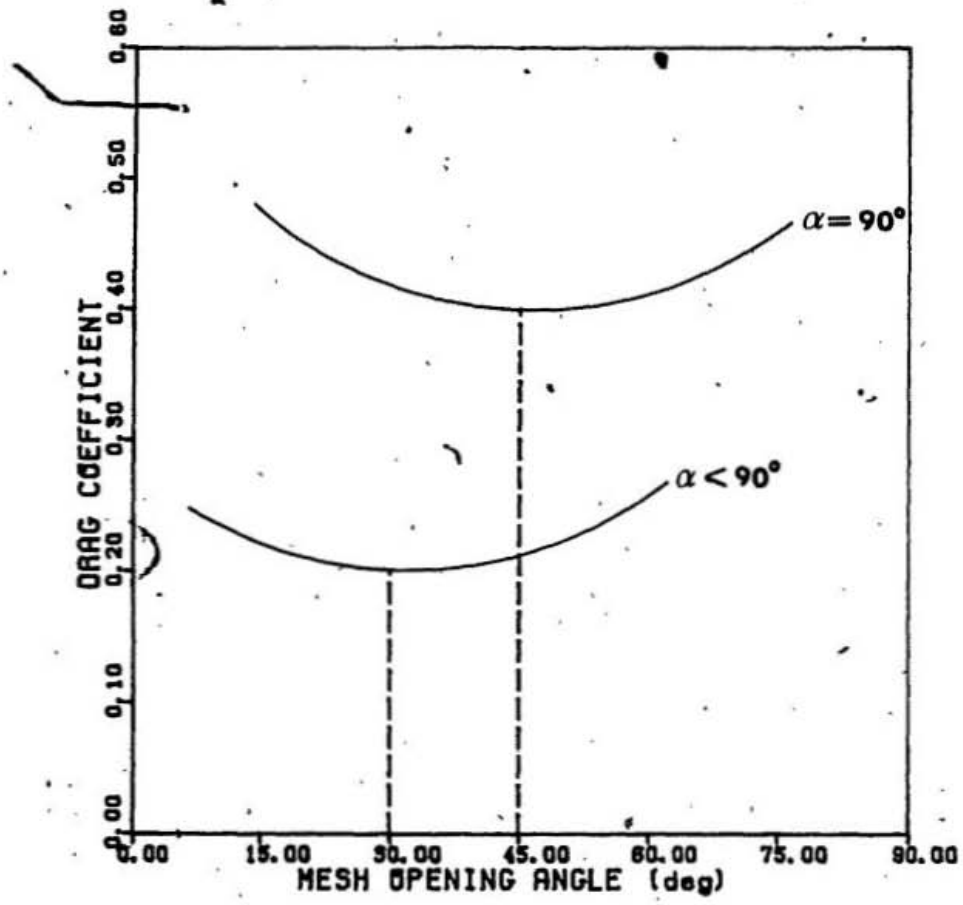

Figure 5-1: Drag coefficient versus mesh opening angle.

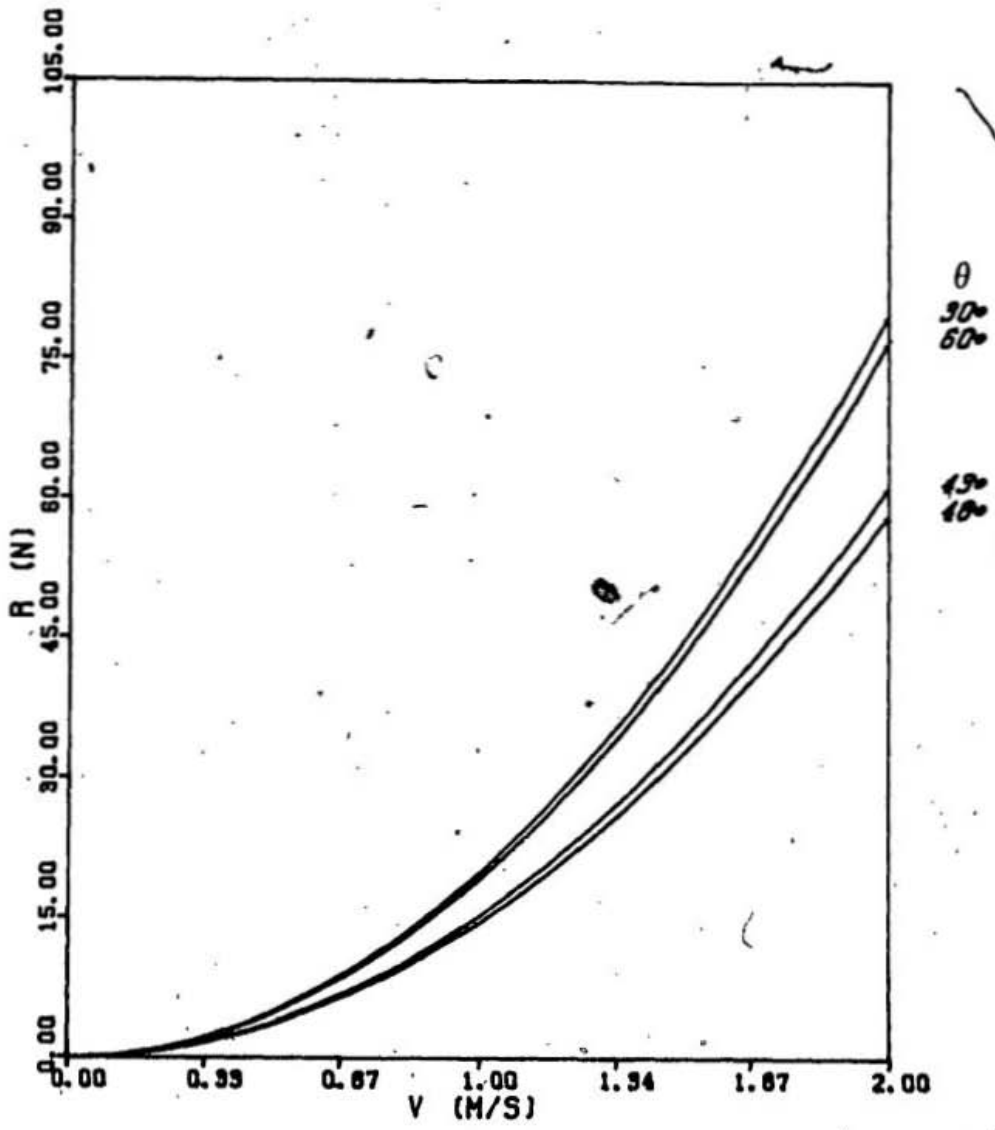

Figure 5-2: The drag of nets with different mesh opening angles at an angle of attack of ninety degrees.

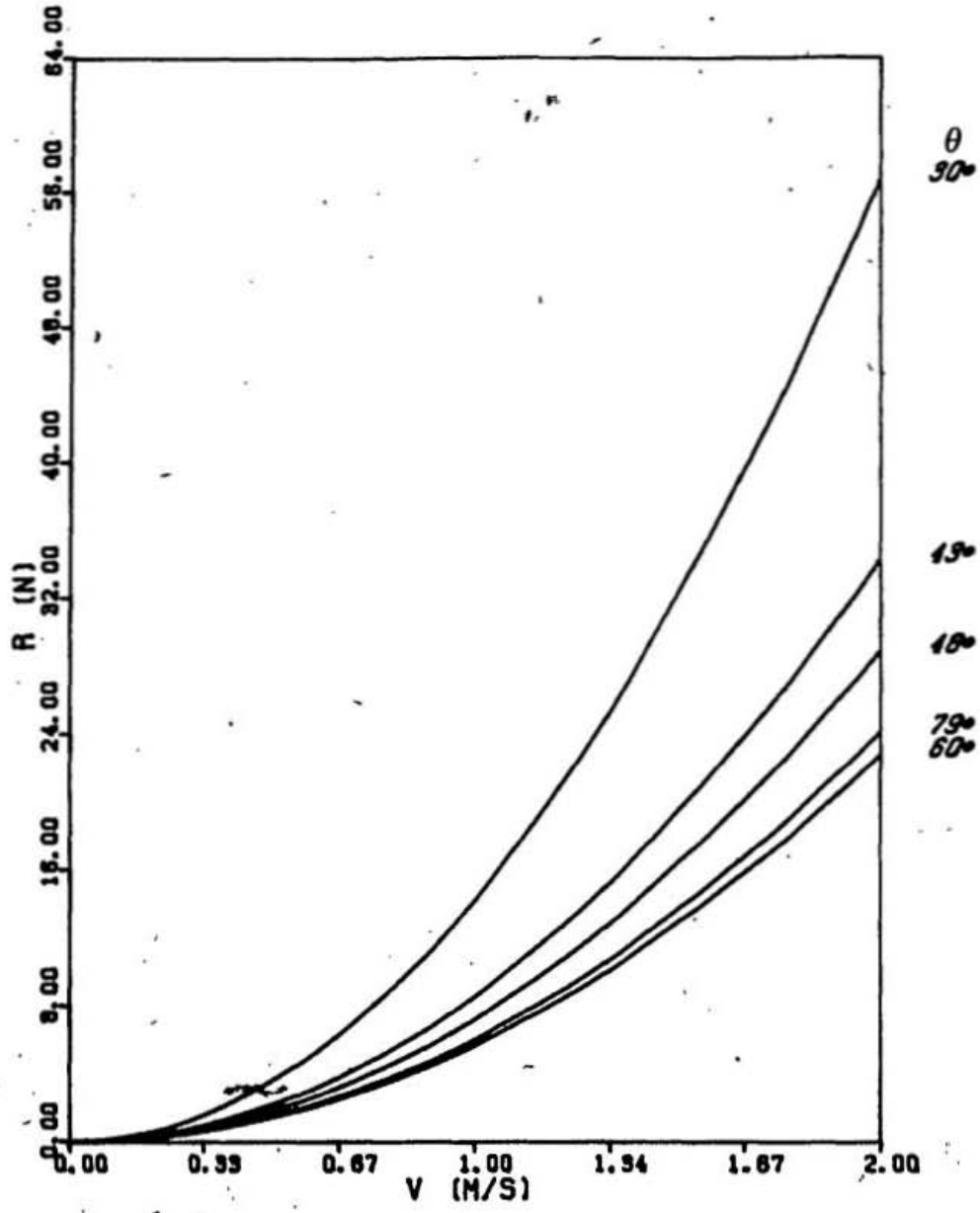

Figure 5-3: The drag of nets with different mesh opening angles at an angle of attack of twenty degrees.

The number of bars, b, is also dependent upon the value of θ. In the case of a flat net held in a frame the number of bars is equal to twice the number of mesh holes, i.e.

$$b = 2 \times (\#\ mesh\ holes)\,. \tag{5.2}$$

The number of mesh holes is found by dividing the inside area of the frame by the area of one mesh hole, i.e.

$$(\#\ mesh\ holes) = A_f / A_{mh}\,.$$

where:

A_f = the inside area of the frame

A_{mh} = the area of a mesh hole.

The area of a mesh hole is given by equation (1.3) as:

$$A_{mh} = 2 \sin\theta \cos\theta\, a^2\,.$$

Therefore the number of bars in a net is expressed as follows:

$$b = 2 A_f / 2 \sin\theta \cos\theta\, a^2 \tag{5.3}$$

which can be rewritten as:

$$b = 2 A_f / \sin 2\theta\, a^2\,. \tag{5.4}$$

Upon substituting for b in equation (5.1), the projected twine area becomes:

$$Ap = \sqrt{1 - \sin^2\theta \cos^2\alpha}\ (2 A_f / \sin 2\theta)\,(d/a). \tag{5.5}$$

Combining constants and noting that the angle α is also constant, equation (5.5) becomes:

$$Ap = c_1 \sqrt{1 - c_2 \sin^2\theta} \sin 2\theta \,. \tag{5.6}$$

where:

$$c_1 = 2 A_f d/a \qquad c_2 = \cos^2\alpha.$$

The derivative of Ap with respect to θ is therefore equal to

$$(d/d\theta)Ap = \frac{-c_1 c_2}{2\sqrt{1 - c_2 \sin^2\theta}} - \frac{2c_1 \cos 2\theta \sqrt{1 - c_2 \sin^2\theta}}{(\sin 2\theta)^2} \tag{5.7}$$

Equating $(d/d\theta)Ap$ to zero gives the following expression:

$$c_2 = -\cos 2\theta / \sin^4\theta \,. \tag{5.8}$$

Therefore the mesh opening angle required to give the minimum projected twine area at any angle of attack is given as follows:

$$\cos^2\alpha = -\cos 2\theta / \sin^4\theta \,. \tag{5.9}$$

According to equation (5.8) the minimum projected twine area occurs at a mesh opening angle of 45° for an attack angle of 90°. Also, as the angle of attack is reduced below 90° the mesh opening angle must be greater than 45° to minimize the projected twine area of the net. In fact, for angles of attack in the range of 0° to 90°, equation (5.9) is only valid for mesh opening angles greater than 45°.

A computer program was written to generate a curve representing equation (5.9). This curve is shown in figure 5-4. As shown by figure 5-4 the mesh opening angle required for minimum projected twine is 59.67° at an angle of attack of 20°. Therefore, in the range of mesh opening angles from 45° to 59.67° the solidity increases but the projected twine area and drag decrease.

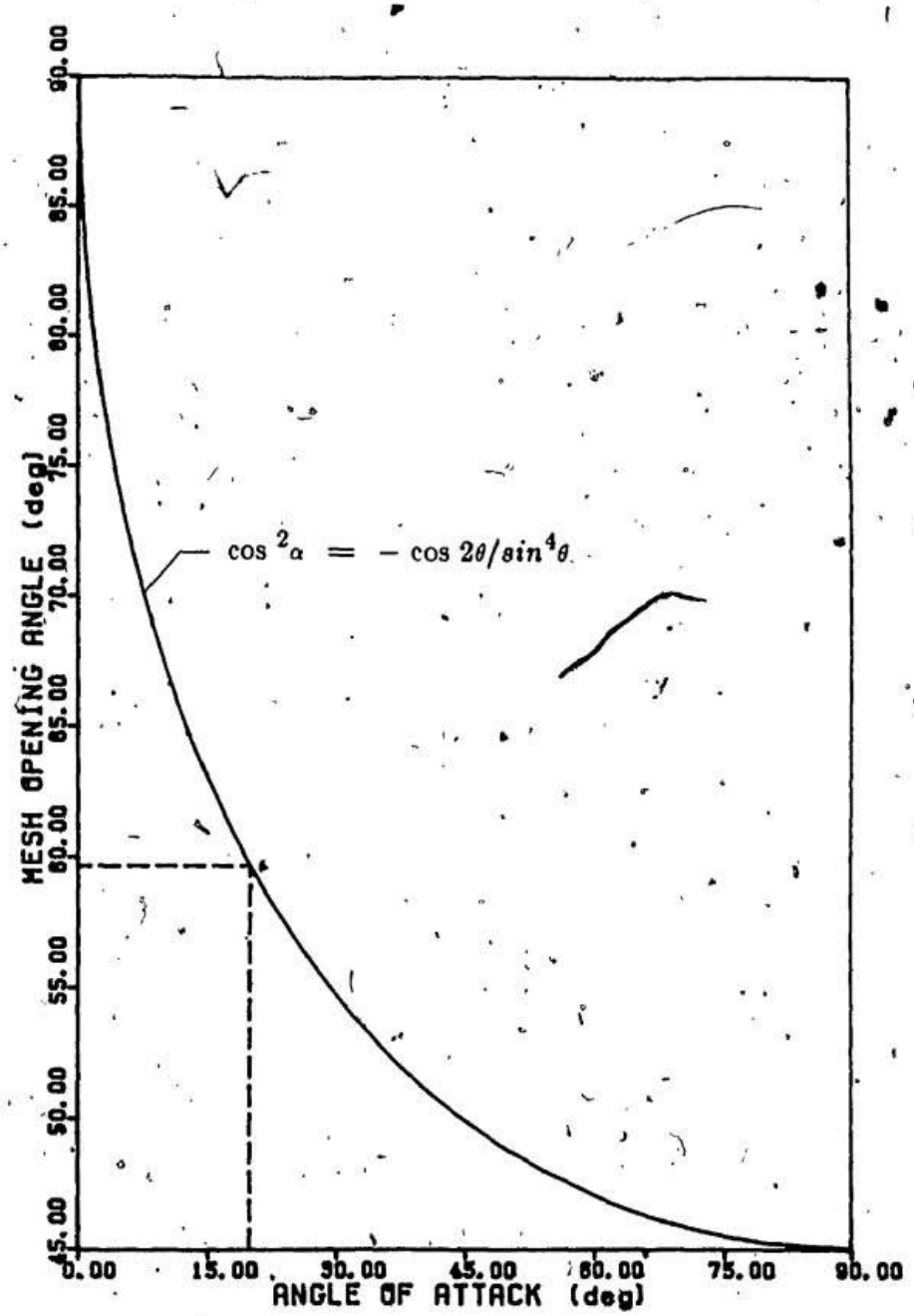

Figure 5-4: Mesh opening angles and angles of attack required for minimum projected twine area.

As mentioned previously, Stengel's data shows a minimum drag coefficient at a mesh opening angle less than 45° for angles of attack other than 90°. A possible explanation for this reversal is the difference in the definition of the angle of attack as used by Stengel and that given in chapter 3.0. In the analysis thus far, the angle of attack has been defined as the angle between the net and the vertical z-x plane as shown in figure 4-1. In Stengel's experiments the angle of attack was defined as the angle between the net and the horizontal y-x plane as shown in figure 5-5 below:

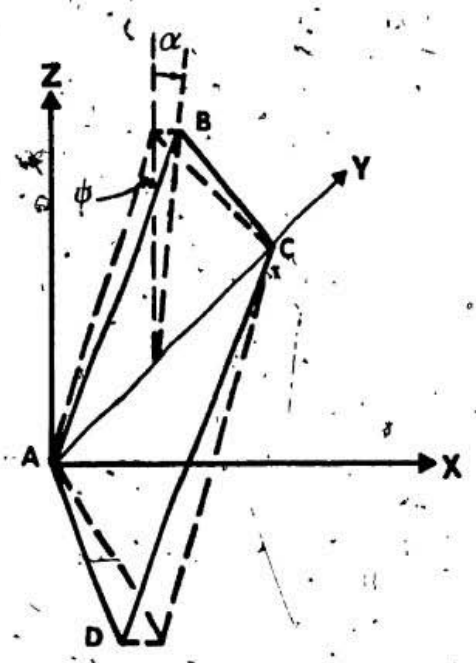

Figure 5-5: The projection of a mesh, held at an angle α to the z-axis, on the y-z plane.

As before, the projected length of the twine bar AB as shown in figure 5-5 is given as follows:

$$AB_{y-z} \triangleq AB\cos\psi \tag{5.10}$$

However, in this case the angle ψ is defined as follows:

$$\sin\psi = \cos\theta\sin\alpha \tag{5.11}$$

and the projected length of the twine bar becomes:

$$AB_{y-z} = AB\sqrt{1-\cos^2\theta\sin^2\alpha} \tag{5.12}$$

Applying the same procedure as before the following equation similar to equation (5.9) is obtained:

$$\cos^2\alpha = \cos 2\theta/\cos^4\theta \tag{5.13}$$

As before, the mesh opening angle must be 45° to minimize the projected twine area at an angle of attack of 90°. However, as the angle of attack decreases below 90° the mesh opening angle must also decrease if equation (5.13) is to be satisfied. Thus the minimum projected twine area of a net defined in this way will occur at some mesh opening angle below 45° for angles of attack below 90°.

5.2. Analysis of square mesh measurements

A square mesh net is a net with its meshes hung such that the twine bars are parallel to the sides of the net (see figure 5-7). This type of mesh is being investigated as a possible replacement for the conventional diamond mesh in the codend section of a trawl net [24]. The proposed advantage of square mesh over diamond mesh is that the square mesh remains open during trawling and therefore increases the escape area for small fish. It has also been reported that a trawl net tows easier when its codend is made with square mesh [24].

As part of the investigation of the effect of the mesh opening angle on the drag of nets a series of towing tank tests were made on a square mesh net constructed with the same amount of twine as diamond mesh net number one in table 3-1. The parameters of the square mesh net are listed as net number three in table 3-1.

Figure 5-8 shows the drag of both the diamond and the square mesh nets. Although both are made from nearly the same number of twine bars and knots the drag of the square mesh is clearly lower than that of the diamond mesh. The difference increases steadily as the angle of attack is decreased to 20°. It may be that the reduction in drag due to turbulent flow is not as severe for square mesh as for diamond mesh, or that there is reduced shielding of cross-flow bars in a square mesh net.

At an angle of attack of 90° the projected twine area of both nets are nearly equal and can be calculated using equation (4.5). As the angle of attack is reduced below 90°, the projected area of the diamond mesh net, as illustrated in figure 4-1, is calculated using equation (4.9). The projected twine area of a square mesh net at angles of attack below 90° is illustrated in figure 5-6 and is calculated using the following equation:

$$Ap = \sin\alpha\, b\, d\, a/2 + b\, d\, a/2 + k\,\pi\, d_k^{\,2}/4 \qquad (5.14)$$

or

$$Ap = (\sin\alpha + 1)\, b\, d\, a/2 + k\,\pi\, d_k^{\,2}/4 \,. \qquad (5.15)$$

Figure 5-9 shows a comparison of the projected twine area of the diamond

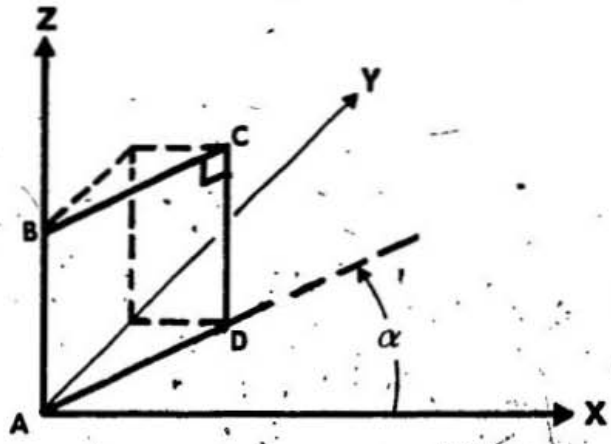

Figure 5-6: The projected area of a square mesh.

Figure 5-9 shows a comparison of the projected twine area of the diamond and square nets as calculated using equations (5.13) and (4.9) at angles of attack between 0° and 90°. The projected twine area and drag are nearly equal at an angle of attack of 90°. However the projected twine area of the square mesh net decreases dramatically below that of the diamond mesh net at angles of attack below 90°. It can therefore be concluded that the reduced drag of the square mesh net over the diamond mesh net is due to the fact that the projected twine area of the square mesh is less than that of the diamond mesh net.

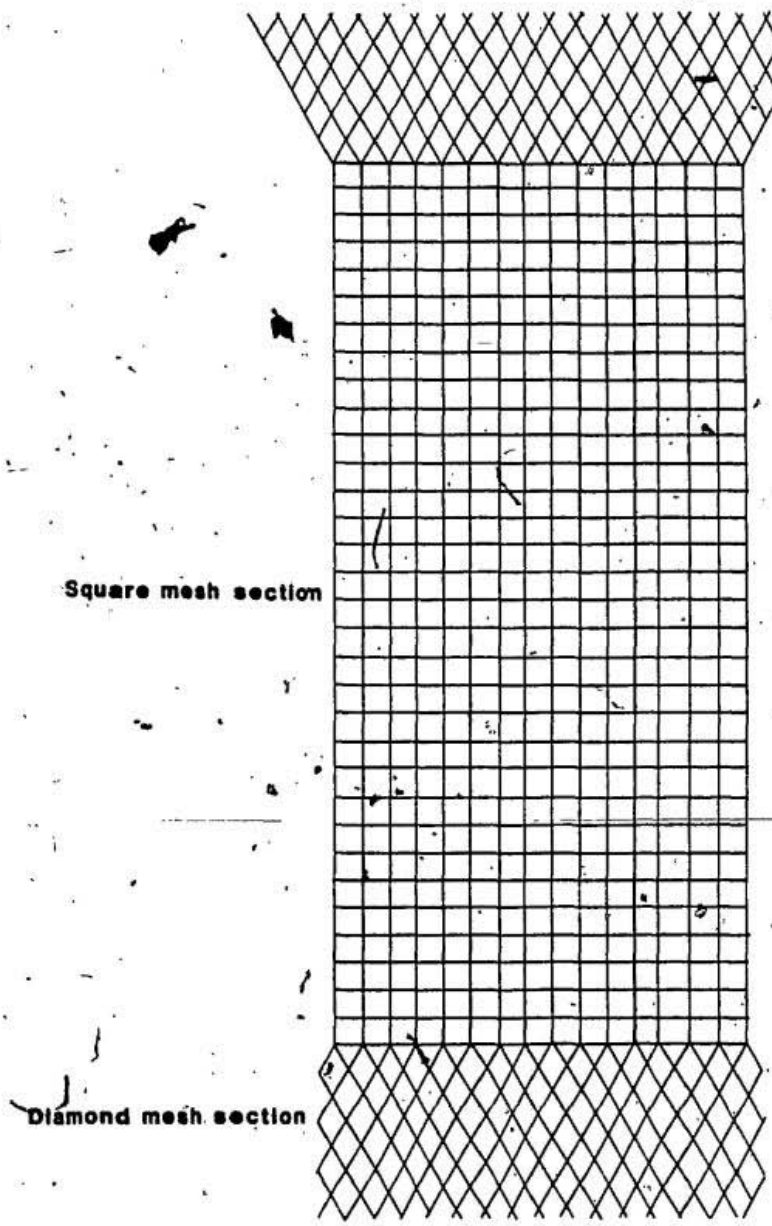

Figure 5-7: A diamond and square mesh codend.

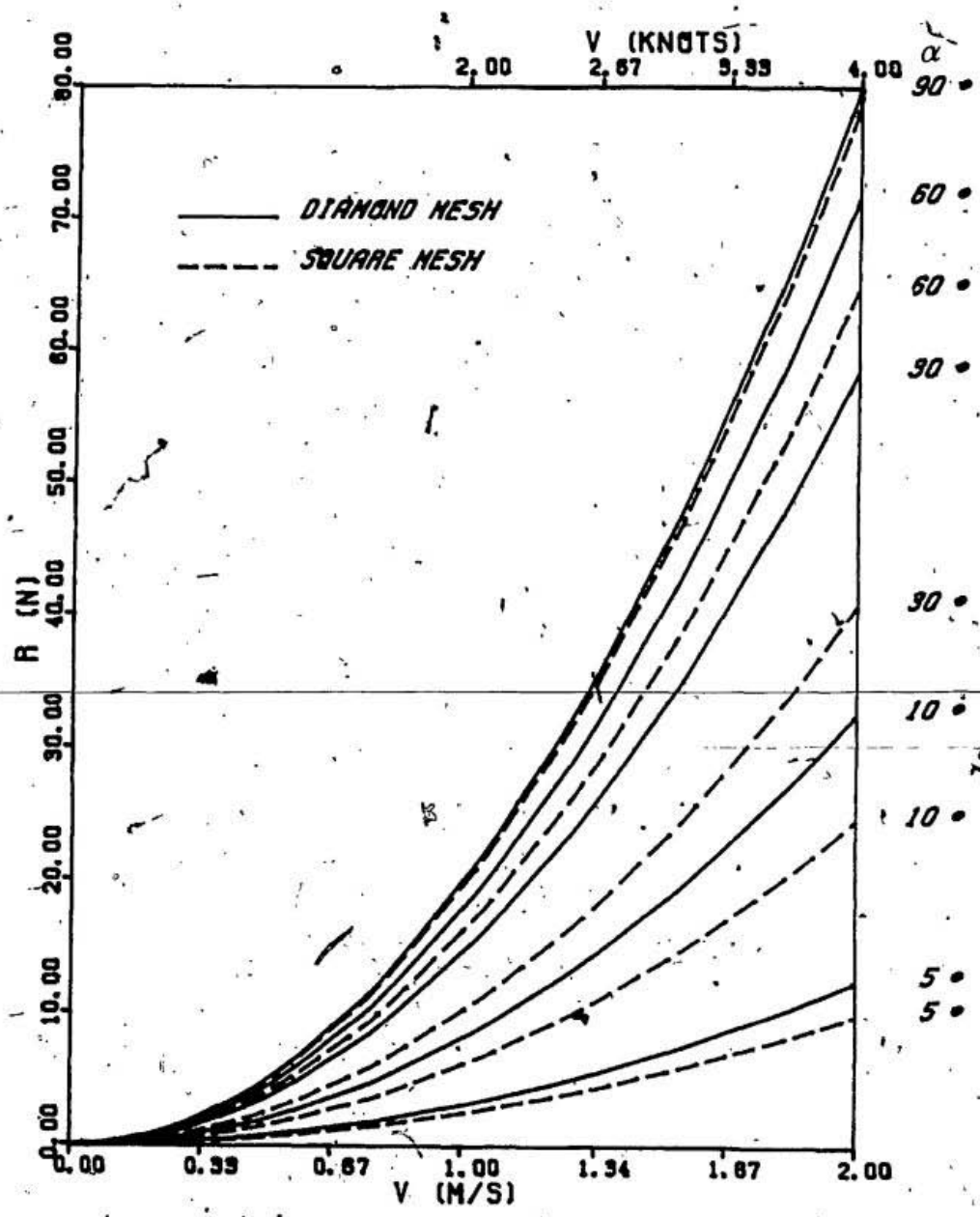

Figure 5-8: Diamond and square mesh drag.

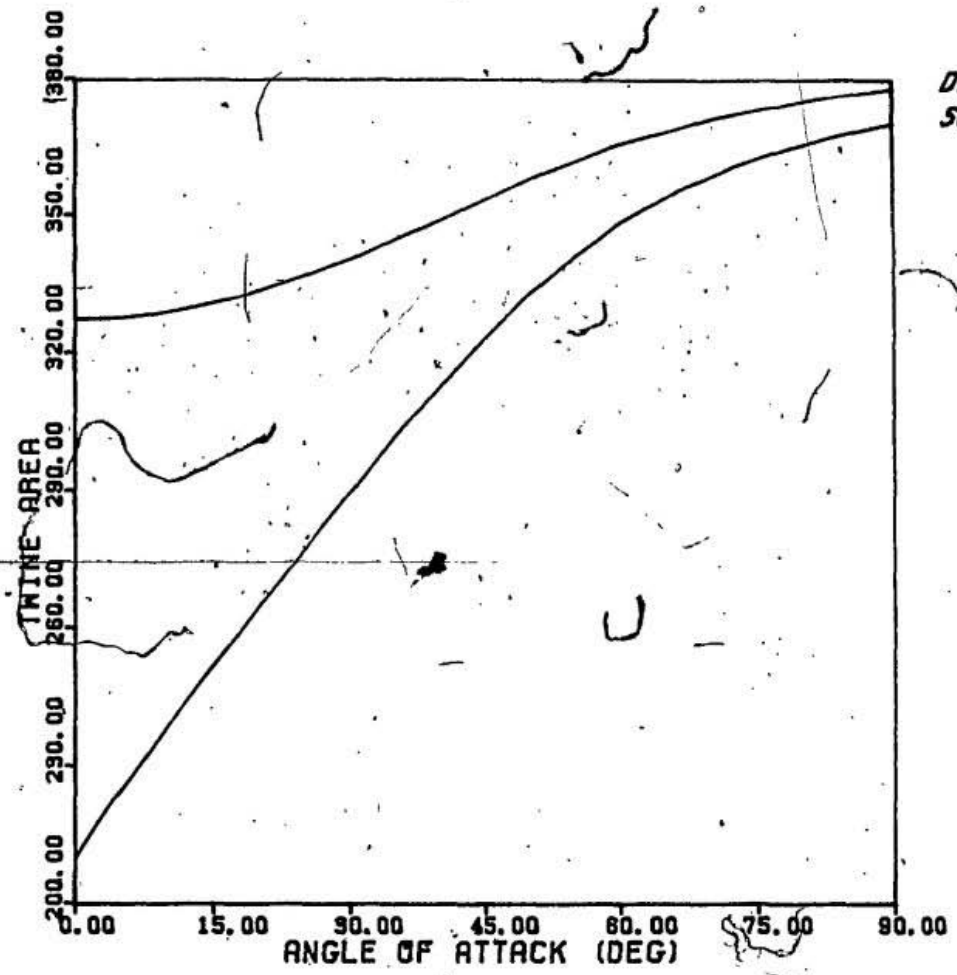

Figure 5-9. The projected twine area of diamond versus square mesh.

Chapter 6

COMPARISON OF VESSEL POWER AND GEAR DRAG

The derived drag of the I.C. trawl gear was compared to the available towing power of typical vessels used in the western Newfoundland inshore trawling fishery. Both wooden and steel vessels ranging from 15 to 20 meters in length are used in this fishery. The objective of the following chapter is to establish whether the towing power of these vessels matches the drag of the I.C. gear and if not, what changes in the gear size would improve this match.

6.1. Vessel propulsion analysis

Thrust and torque curves were developed for two typical vessels operating in this fishery. The propulsion analyses are based on procedures outlined by Kowalski [19] and Harvard [13].

6.1.1. Vessel descriptions

The two vessels for which calculations were made were the *Arctic Clipper* and the *Ocean Way*. The physical dimensions of each boat along with the engine and propeller specifications are given in Tables 6-1 and 6-2. The propeller specifications were suprisingly difficult to obtain. However, through discussions with suppliers and from records at the Provincial Department of Fisheries, the relevant information was assembled.

Table 6-1: *Arctic Clipper* specifications

LENGTH	16.5 *m*
BEAM	5.79 *m*
CONSTRUCTION	wood
ENGINE	365 hp
REDUCTION GEAR	4.5 : 1
PROPELLER	Wageningen type diameter 1219 *mm* pitch 1371.6 *mm* disk area ratio 0.50 3 blades

Table 6-2: *Ocean Way* specifications

LENGTH	19.8 *m*
BEAM	6.705 *m*
FRAME	steel
ENGINE	624 hp
REDUCTION GEAR	4.7 : 1
PROPELLER	Kaplan type diameter 1511.3 *mm* pitch 1409.7 *mm* disk area ratio 0.55 4 blades Kort nozzle

6.1.2. Vessel thrust and torque diagrams

The open water performance curves corresponding to each propeller are given in figures 6-1 and 6-2. These figures were used to calculate thrust and torque curves for each vessel which are shown in figures 6-3 and 6-4 [13] [22]. The following equations were used for these calculations [13]:

$$T = k_t \rho N^2 D^4 \tag{6.1}$$

$$Q = k_q \rho N^2 D^5 \tag{6.2}$$

where:

T = the thrust

k_t = the thrust coefficient

Q = the torque

k_q = the torque coefficient corresponding to delivered power

ρ = density

N = revolutions per second of the propeller

D = propeller diameter

The thrust and torque coefficients correspond to a particular advance coefficient, J, which is defined by the following equation:

$$J = \frac{V(1-w)}{ND} \tag{6.3}$$

where:

w = Taylor wake coefficient

N = propeller revolutions per second

D = propeller diameter

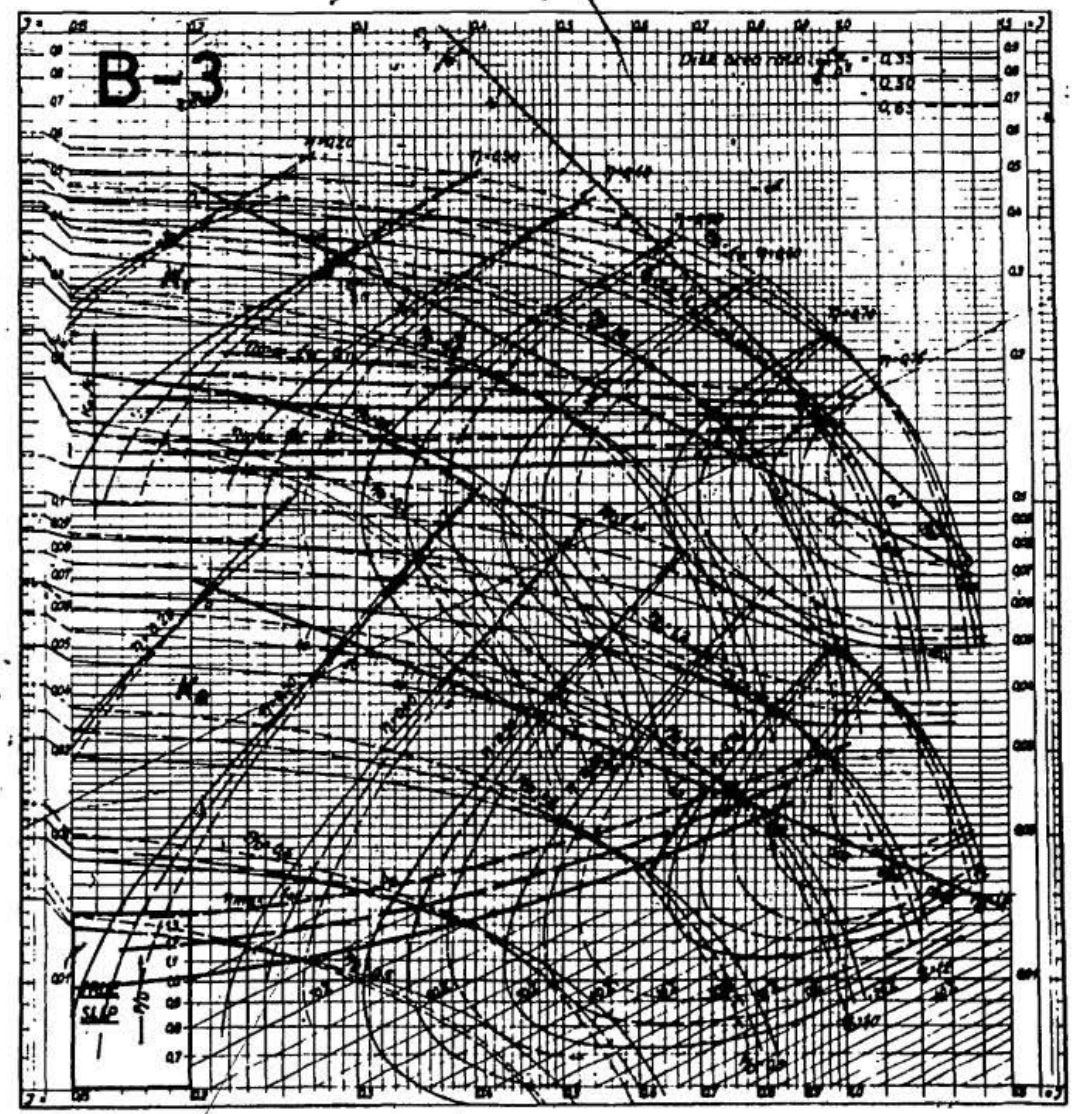

Figure 6-1 : Open water performance curves
(Wageningen B-3 series)
(Courtesy of Harvald (13))

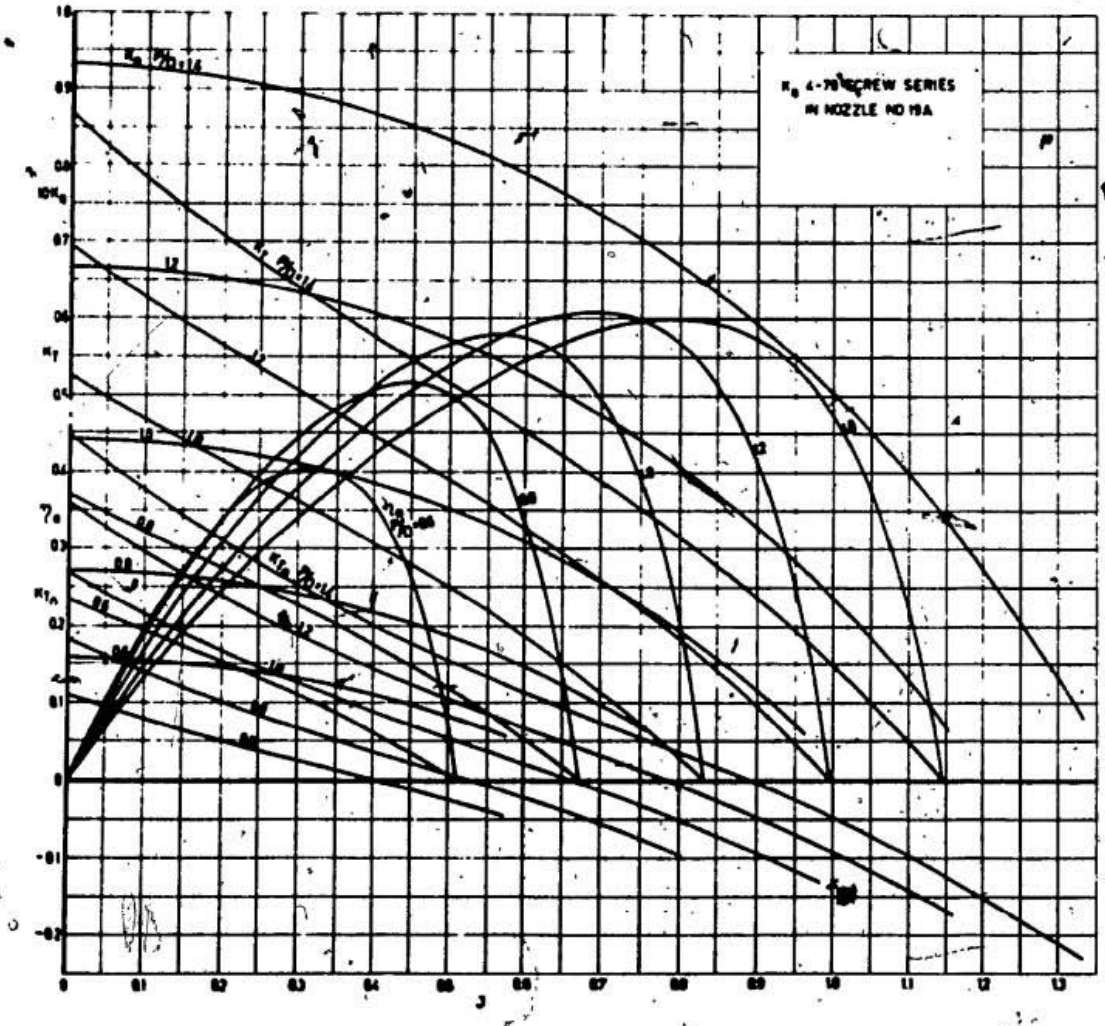

Figure 6-2 : Open water performance curves
(Ka 4-70 screw series with nozzle no. 19A)
(Courtesy of Oosterveld (22))

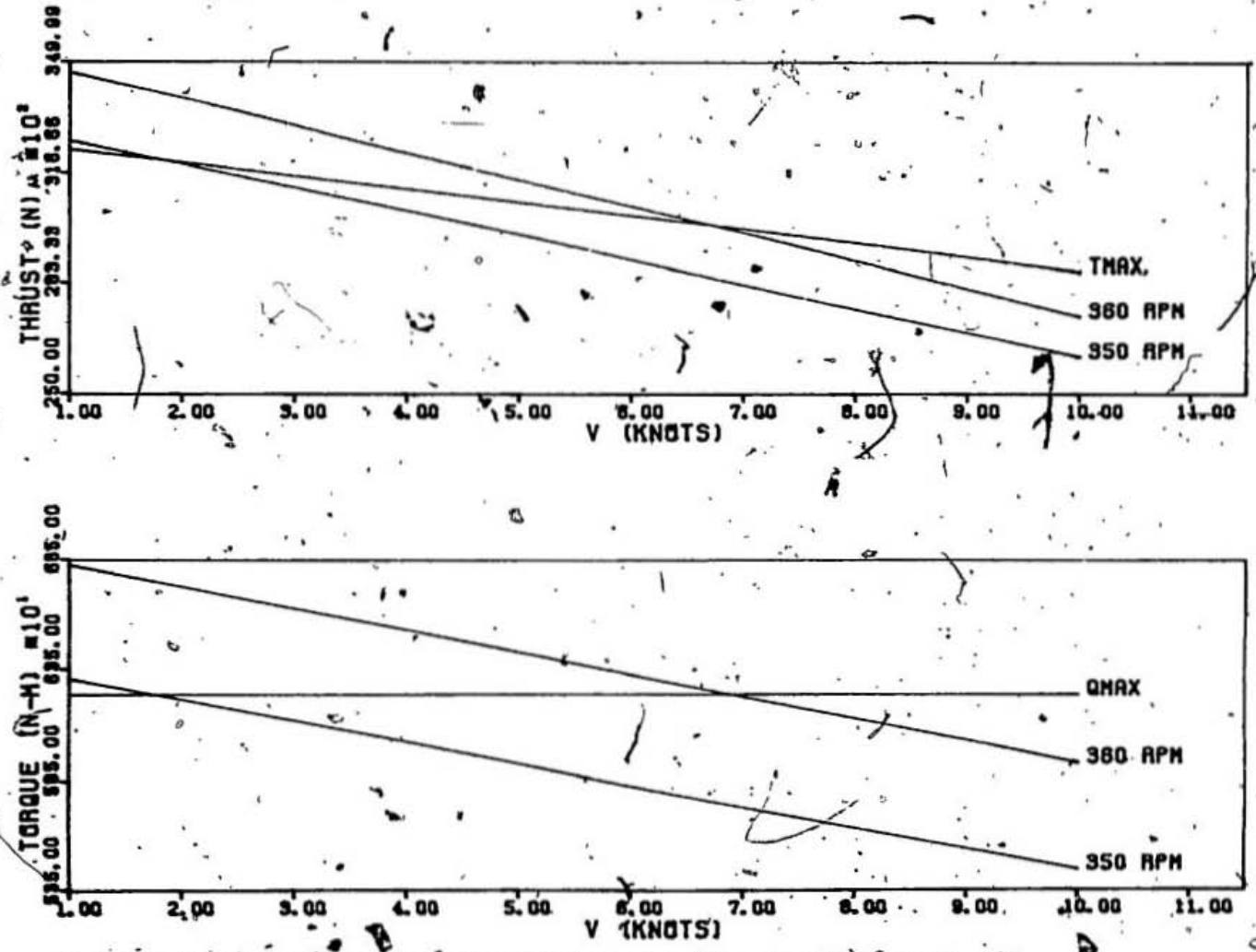

Figure 6-3: Torque and thrust limits (Arctic Clipper).

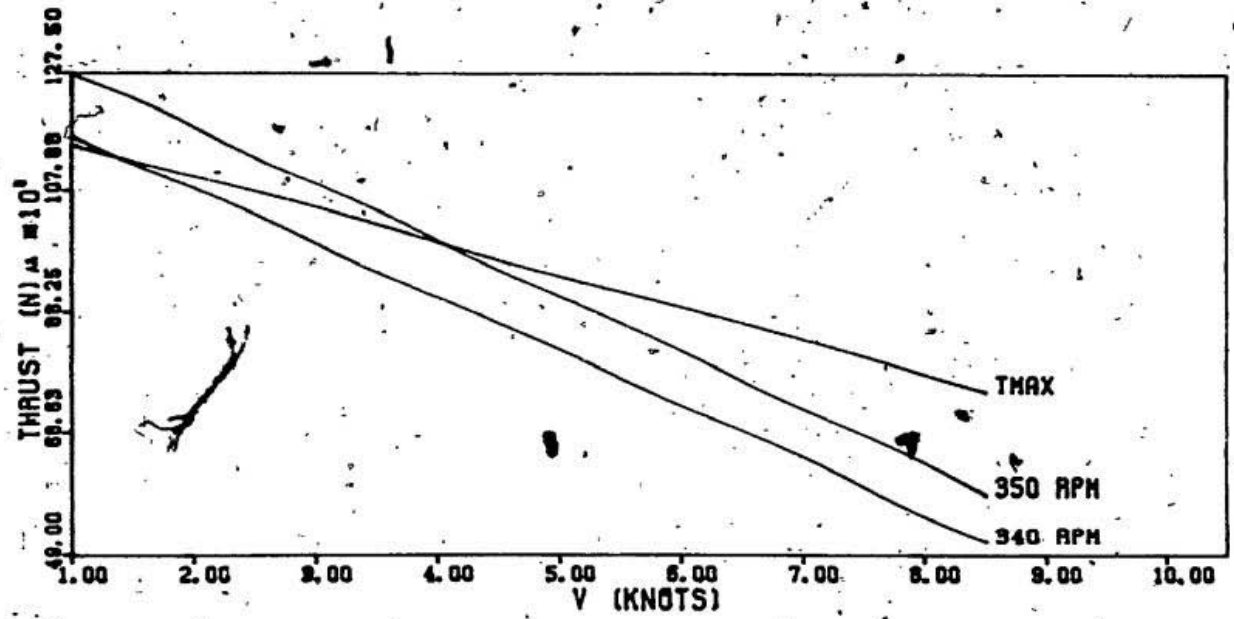

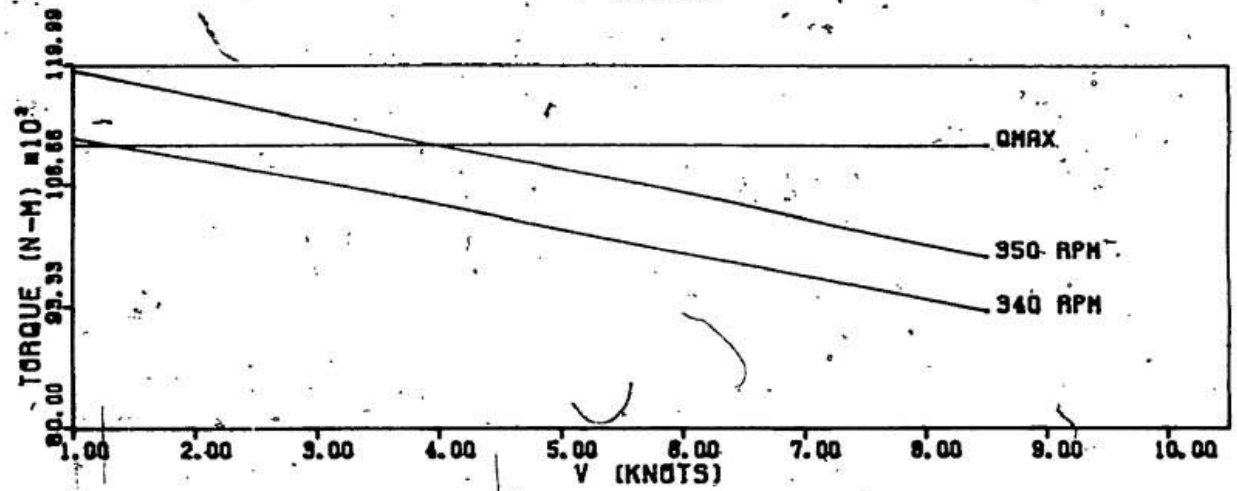

Figure 6-4: Torque and thrust limits (Ocean Hay).

A Taylor wake coefficient of 0.2 is typically used for trawler hull forms [19]. Equations (6.1) and (6.2) were evaluated over a range of engine rpms and advance coefficients to obtain the thrust and torque curves. As an example, the calculation of the thrust and torque curves at 350 rpm is summarized in table 6-3 for the Kurt nozzle unit of the *Ocean Way*.

Table 6-3: Calculations of thrust and torque curves of the *Ocean Way* at a propeller rpm of 350

V (*knots*)	2.0	2.5	3.0	3.5	4.0
V (*m/s*)	1.03	1.28	1.54	1.80	2.05
V(1 - w)	0.824	1.02	1.23	1.44	1.64
J	0.094	0.116	0.139	0.164	0.186
k_t	0.450	0.435	0.420	0.405	0.390
k_{tn}	.200	.190	.180	.170	.160
T (N)	118207	113661	109114	104568	100021
k_q	0.0425	0.0420	0.0415	0.0410	0.0405
Q (N-m)	11671	11533	11396	11258	11122

The thrust limit, *Tmax*, as shown in figures 6-3 and 6-4 is limited by the maximum torque, *Qmax*, placed on the propeller shaft by the engine. *Qmax* is also shown in figures 6-3 and 6-4. The maximum torque is assumed to be constant and is calculated using the following formula:

$$\text{Qmax} = \frac{33{,}000\ dhp}{2\pi\ \text{N}} \qquad (6.4)$$

where:

dhp = the delivered engine horsepower

N = shaft revolutions per minute

The delivered horsepower of the engine is estimated from its brake horsepower as follows:

$$dhp = bhp \times n \tag{6.5}$$

where:

bhp = the engine brake horsepower

n = the shaft efficiency (.96)

The maximum torque line, *Qmax*, intersects the rpm curves on the torque diagram as shown in figures 6-3 and 6-4. A thrust limit line, *Tmax*, is obtained by plotting two of these points, connected with a straight line, on the corresponding rpm curves on the thrust diagram.

As shown in figures 6-3 and 6-4 the available towing power, i.e. thrust, of the *Ocean Way* far exceeds that of the *Arctic Clipper*. For example, the maximum thrust of the *Ocean Way* at a towing speed of 3.5 knots is approximately three times that of the *Arctic Clipper*.

6.2. Hull resistance of typical inshore trawling vessels

Good data concerning the hull resistance of the particular type of vessels used in the western Newfoundland inshore trawling fishery was not identified despite a literature search. Drag curves for similar boats were therefore used. These curves were developed by Kowalski [19] and indicate that the hull resistance of the type of vessel in question is small compared to the total drag

resistance of the gear in the range of typical trawling speeds. The hull resistance curves are shown in section 6.3.

6.3. Available vessel power versus gear drag

The drag of the I.C. trawl gear, the hull resistance and thrust curves of the vessels are shown together in figures 6-5 and 6-6. The hull resistance is included in the total gear drag and is also shown separately.

Figure 6-5 shows that the thrust potential of a vessel such as the *Arctic Clipper* closely matches the I.C. gear drag. It may even be slightly undermatched since the maximum towing speed 4.5 knots.

It is apparent from figure 6-6, however, that the thrust potential of a vessel such as the *Ocean Way* is not fully developed when towing the I.C. trawl gear at typical trawling speeds. For example, at a speed of 3.5 knots only 20% of the available thrust is utilized. The thrust potential of vessels similar to the *Ocean Way* would be better utilized by towing a larger gear.

Assuming properly matched propulsion components with an overall efficiency typical of fishing vessels, the following conclusions were made:

- Vessels powered by engines with horsepower ratings in excess of 600 hp can tow a gear larger then the I.C. 350 mesh gear.
- Vessels powered by engines with horsepower ratings in the range of 350 hp are reasonably matched to the I.C. 350 mesh gear.

The increase in gear size permitted has been shown to increase catching efficiency [10].

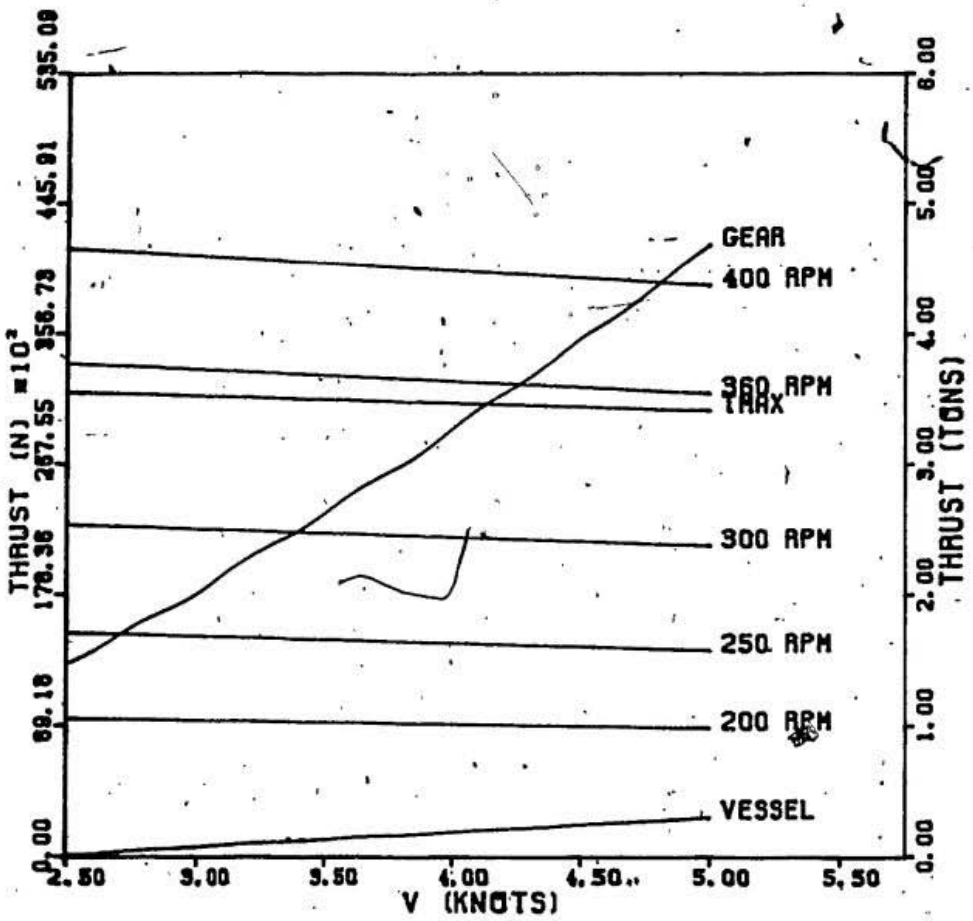

Figure 6-5: Vessel/gear interaction.
(Arctic Clipper)

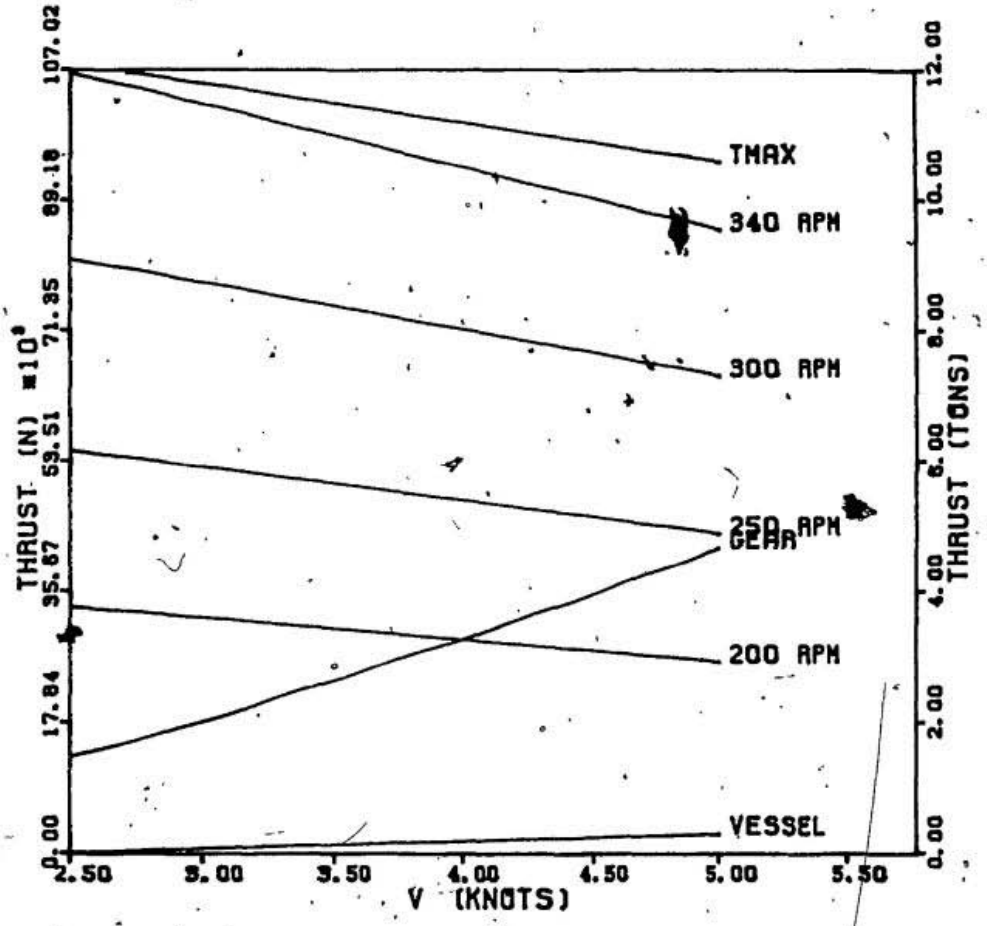

Figure 6-6: Vessel/gear interaction.
(Ocean Way)

Chapter 7

SUMMARY AND CONCLUSIONS

Newfoundland's trawlers are predominantly deep sea vessels which are owned and operated by large fishing companies. In recent times, however, private fishermen have begun trawling with small vessels in inshore waters. Investigations into the drag characteristics of the 350 I.C. trawl gear, which is commonly used in this fishery, are limited and not much relevant information has been published which could be used to help these fishermen match the towing power of their vessels to the drag of the gear.

A set of warp and bridle system tension measurements made by King [14] have been used in this thesis to derive data specifically for this purpose. Through an equilibrium analysis of the forces acting on these warps, the total drag of the gear and the drag of the trawl net have been determined. The total drag of the gear has been compared to the towing power of two vessels typical of those used in the Newfoundland fishery. A basic propulsion analysis was made to predict the towing power of both vessels. It was shown that vessels powered by engines in the range of 350 horsepower are closely matched to the I. C. gear while vessels with propeller nozzles and engines in the range of 600 horsepower could possibly tow a larger gear. Since a large number of vessels operating in this fishery are powered by the larger engines, it can be concluded that a significant number of vessel

could tow a bigger gear with a bigger mouth opening and thus a higher catch rate.

In addition, towing tank drag measurements were made on pieces of polyethylene nets. Very few other measurements have been reported on this type of netting. Analysis of these measurements indicates that the drag coefficient of polyethylene nets is dependent upon the projected twine area and the angle of attack of the netting. At high angles of attack the drag coefficient is directly proportional to the projected twine area but at low angles of attack it appears that turbulent flow decreases the drag coefficient. Empirical drag coefficients were derived from these measurements and used to calculate the drag of the 350 I.C. trawl net following procedures found in the literature. These coefficients are shown to give reasonable approximations of the drag of the 350 I.C. trawl net and it is concluded that the drag of other trawl nets made from polyethylene nets can be calculated using these coefficients.

Measurements were also made to investigate the effect of the variation of the mesh setting angle on the drag of a net. The mesh opening angle together with the angle of attack determines the orientation of the mesh in the flow. It was shown that the drag of a mesh depends more on the projected twine area than on its solidity, which corresponds to the surface area of the mesh. This is true even at low angles of attack where turbulent flow effects the drag of the net. For example, the measurements show that at an angle of attack of 20° the minimum drag of a series of nets with varying mesh opening angles occurs at a mesh opening angle of approximately 60°. The minimum projected twine area

was calculated at a mesh opening angle of 59.6° whereas the minimum solidity occurs at a mesh opening angle of 45°. Although it was physically impossible to construct and test a net with a mesh opening angle of 59.6°, the measurements indicate that the minimum drag corresponds to the minimum projected area and not solidity.

A series of measurements were also made on a net with its mesh hung square. The orientation of a mesh in this net is different than that of a mesh in a similar size diamond mesh net and therefore the drag of these nets should be different. Sea trials indicate that trawl nets made with square mesh codends tow easier than those with diamond mesh codends [24]. This also implies that the drag of square mesh nets is less then diamond mesh nets. The results of the drag measurements made on the square mesh netting were compared to the measurements made on the similar size diamond mesh net. The drag of the square mesh netting was found to be lower than that of the diamond mesh netting and particularly at low angles of attack. A formula was derived and used to calculate the projected area of a square mesh net at various angles of attack. The projected area of the square mesh net was found to be lower than that of the diamond mesh net at angles of attack below 90°. It was therefore concluded that the explanation of the difference in the drag of the square mesh and the diamond mesh was the difference in the projected twine area of each mesh.

References

1. Albertson, M. L., Barton, J. R., and D. B. Simons. *Fluid Mechanics For Engineers*. PRENTICE-HALL, INC., New York, 1960.

2. Baranov, F. J.. *Selected Works on Fishing Gear*. Pisceprom̆izdat, Moskva, 1948.

3. Bridger, J. P., Foster J. J., Margetts A. R. and E. S. Strange.. *Glossary of United Kingdom Fishing Gear Terms*. Fishing News Books Ltd., Farnham-Surrey-England, 1981.

4. Carrothers, P. J. G., Foulkes, T. J. and M. P. Connors. Data on the engineering performance of Canadian east coast groundfish otter trawls. 125, Fisheries Research Board of Canada, 1969.

5. Crewe, P. R. and T. A. Arlotte. Results of a systematic series of tank tests on plane webbing pieces; comparison with theory and earlier investigations. Westland Aircraft Ltd. Saunders Roe Division, 1964.

6. Dickson, W. Trawl drag area and netting geometry. Institute of Fishery Technology Research, Bergen, 1980.

7. Eames, M. C. "Steady State Theory of Towing Cables". *Transactions Royal Institute of Naval Archit. 3*, 110 (1958), 185-206.

8. Food and Agriculture Organization of The United Nations. *Otter Board Design and Performance*. FAO FISHING MANUALS, Rome, 1974.

9. Ferro, R. S. T. Report by the study group on twine thickness measurement. Marine Laboratory, Aberdeen, 1983.

10. Foster, J. J., Campbell C. M. and G. C. W. Sabin. "The fish catching process relevant to trawls". *Canadian Special Publication of Fisheries and Aquatic Sciences 58* (1981), 229-246.

11. Fridman, A. E.. *Theory and Design of Commercial Fishing Gear*. Israel Program For Scientific Translations, Jerusalem, 1973.

12. Fridman, A. L. and A. V. Dvernik. "Development of a method for the calculation of the resistance of a trawl net". *Fischerei-forschung 2*, 11 (1973), 7-68 and 79-101.

13. Harvald, SV. AA.. *Resistance and Propulsion of Ships*. John Wiley & Sons, New York, 1983.

14. Kingsley, R. and D. Hearn. Preliminary report on groundfish trawl experiments 1979-1981. Development Branch Report 25, Technology Division, Department of Fisheries, Government of Newfoundland and Labrador, 1981.

15. Hoerner, S. F.. *Fluid Dynamic Drag*. Published by the author, New York, NY, 1965.

16. Imai, T. "Experimental studies on the projective area of the weaver's knot-netting". *Bulletin of Japanese Society of Scientific Fisheries 50* (1984), 1823-1828 .

17. Kowalski, T. and J. Giannotti. Calculation of fishing net drag. Marine Technical Report 15, University of Rhode Island, 1974a.

18. Kowalski, T. and J. Giannotti. Calculation of trawling gear drag. Marine Technical Report 16, University of Rhode Island, 1974b.

19. Kowalski, T. and J. Giannotti. Calculation of trawling gear-trawler interaction. Marine Technical Report 17, University of Rhode Island, 1974c.

20. MacLennan, D. N. Hydrodynamic characteristics of trawl warps. 16, Marine Laboratory, Aberdeen, 1979.

21. MacLennan, D. N. "The drag of four-panel demersal trawls". *Fisheries Research 4*, 1 (1981), 23-33.

22. Oosterveld, Dr. Ir. M. W. C. Ducted propeller characteristics. Symposium on ducted propellers., 1973.

23. Revin, A. S. "Investigation of the effect of structure and shape of net panels for trawl nets on their drag in water currents". *Trudy Vniro 41* (1959), . Piscepromixdat.

24. Robertson, J. H. B. Square and hexagonal mesh codend design tests on FRV Goldseeker and commercial trials results with square mesh codends on Gem, Janeen II and Harvest Reaper. 3, Marine Laboratory, Aberdeen, 1982.

25. Stengel, H. and A. Fischer. "Results from studies of knotted net panels made from twisted nylon twine". *Fischerei-forschung 3*, 6 (1968), 45-50.

26. Tauti, M. "Drag of plane nets in water". *Journal of the Imperial Fishery Institute 21*, 2 (1925), .

27. Topping, J.. *Errors of Observation and Their Treatment*. The Institute of Physics, London, 1955.

Appendix A

EQUILIBRIUM WARP ANALYSIS PROGRAM

```
C*PROGRAM TO CALCULATE WARP SHAPE
C*************************************************************
C*       PROGRAM LISTING                                     *
C*************************************************************
C* CD = COEFFICIENT OF PRESSURE DRAG(1.1)                    *
C* CF = COEFFICIENT OF FRICTION DRAG(0.007)                  *
C* CL = DISTANCE DOWN WIRE                                   *
C* D  = WARP DIAMETER(.0127m)                                *
C* DEPTH = VERTICAL DEFLECTION OF WIRE IN Z DIRECTION        *
C* FX = FORCE IN X DIRECTION                                 *
C* FY = FORCE IN Y DIRECTION                                 *
C* FZ = FORCE IN Z DIRECTION                                 *
C* H = UNIT LENGTH OF CABLE ELEMENT                          *
C* LENGTH = HORIZONTAL DEFLECTION OF WIRE IN X DIRECTION     *
C* OMEGA = DIVERGENCE ANGLE IN DEGREES                       *
C* ROMEGA = DIVERGENCE ANGLE IN RADIANS                      *
C* RHO = FLUID DENSITY (1028 KG/mUP(3))                      *
C* SPREAD = HORIZONTAL DEFLECTION OF WIRE IN Y DIRECTION     *
C* BETA = DECLINATION ANGLE IN DEGREES                       *
C* RBETA = DECLINATION ANGLE IN RADIANS                      *
C* W = WEIGHT OF CABLE ELEMENT PER UNIT LENGTH               *
C* X = INCREMENTAL CHANGE IN X DIRECTION                     *
C* Y = INCREMENTAL CHANGE IN Y DIRECTION                     *
C* Z = INCREMENTAL CHANGE IN Z DIRECTION                     *
C*************************************************************
      DIMENSION A1(4),B1(4),C1(4),A2(4),B2(4),C2(4)
     1 ,A3(4),B3(4),C3(4),BETA(3000),OMEGA(3000),BOT(4)
     1 ,AK(4),Q(4),R(4),SIN3(4),T(3000),FX(4),FY(4),DEPTH(3000)
     1 ,FZ(4),RBETA(4),ROMEGA(4),TT(4),SPREAD(3000),CL(3000),LENGTH(3000)
      BYTE OUTPUT(15)
      DOUBLE PRECISION SPREAD,CL,LENGTH
C****** FORMULA TO CALCULATE THE DETERMINANT OF A MATRIX ****
      DET(X1,X2,X3,Y1,Y2,Y3,Z1,Z2,Z3)=(X1*Y2*Z3+X2*Y3*Z1+X3*Y1
     1 *Z2)-(X1*Y3*Z2+X2*Y1*Z3+X3*Y2*Z1)
C*************************************************************
      TYPE*,'INPUT CD,CF'
      ACCEPT*,CD,CF
      TYPE*,'INPUT V THE VELOCITY'
      ACCEPT*,V
      TYPE*,'INPUT DECLINATION(1),DIVERGENCE(1),TENSION(1)'
      ACCEPT*,BETA(1),OMEGA(1),T(1)
      RHO=1028.
      H=.1
      TYPE*,'INPUT W THE WEIGHT OF A CABLE ELEMENT'
      ACCEPT*,W
C****** INITIALIZE LENGTH, SPREAD AND DEPTH *****************
      LENGTH(1)=0.0
      SPREAD(1)=0.0
      DEPTH(1)=0.0
      CL(1)=0.0
      DO 10J=1,2311
      RBETA(1)=BETA(J)*3.14/180.
      ROMEGA(1)=OMEGA(J)*3.14/180.
      TT(1)=T(J)
      DO 15I=1,4
C******** COEFFICIENTS OF EQUILIBRIUM FORCE EQUATIONS *********
      A1(I)=-TT(I)*SIN(RBETA(I))*COS(ROMEGA(I))
      B1(I)=-TT(I)*COS(RBETA(I))*SIN(ROMEGA(I))
      C1(I)=COS(RBETA(1))*COS(ROMEGA(I))
```

```
      A2(I)=-TT(I)*SIN(RBETA(I))*SIN(ROMEGA(I))
      B2(I)=TT(I)*COS(RBETA(I))*COS(ROMEGA(I))
      C2(I)=COS(RBETA(I))*SIN(ROMEGA(I))
      A3(I)=TT(I)*COS(RBETA(I))
      B3(I)=0.0
      C3(I)=SIN(RBETA(I))
C*************************************************************
C****** EQUILIBRIUN FORCE EQUATIONS ********************
      FX(I)=-.5*RHO*V**2*D*(3.14*CF+CD*(SIN3(I)**3))
      FY(I)=.5*RHO*V**2*D*CD*(COS(RBETA(I)))**2*SIN(ROMEGA(I))*
     1 SQRT(1.-COS(RBETA(I))**2*COS(ROMEGA(I))**2)*COS(ROMEGA(I))
      FZ(I)=.5*RHO*V**2*D*CD*SIN(RBETA(I))*SIN3(I)*COS(RBETA(I))
     1 COS(ROMEGA(I))-W
C*************************************************************
C****** FOURTH ORDER RUNGE KUTTA METHOD ********************
      BOT(I)=DET(A1(I),A2(I),A3(I),B1(I),B2(I),B3(I),C1(I),C2(I),C3(I))
      AK(I)=H*DET(FX(I),FY(I),FZ(I),B1(I),B2(2),B3(I),C1(I),C2(I),C3(I))
     1 /BOT(I)
      Q(I)=H*DET(A1(I),A2(I),A3(I),FX(I),FY(I),FZ(I),C1(I),C2(I),C3(I))
     1 /BOT(I)
      R(I)=H*DET(A1(I),A2(I),A3(I),B1(I),B2(I),B3(I),FX(I),FY(I),FZ(I))
     1 /BOT(I)
      IF(I.EQ.3)GO TO 14
      RBETA(I+1)=RBETA(1)+(AK(I)/2.)
      ROMEGA(I+1)=ROMEGA(1)+(Q(I)/2.)
      TT(I+1)=TT(1)+(R(I)/2.)
      GO TO 15
14    CONTINUE
      RBETA(I+1)=RBETA(1)+AK(I)
      ROMEGA(I+1)=ROMEGA(1)+Q(I)
      TT(I+1)=TT(1)+R(I)
15    CONTINUE
      BETA(J+1)=BETA(J)+((AK(1)+2.*AK(2)+2.*AK(3)+AK(4))/6.)*180./3.14
      OMEGA(J+1)=OMEGA(J)+((Q(1)+2.*Q(2)+2.*Q(3)+Q(4))/6.)*180./3.14
      T(J+1)=T(J)+(R(1)+2.*R(2)+2.*R(3)+R(4))/6.
      X=COS(BETA(J+1)*3.14/180.)*COS(OMEGA(J+1)*3.14/180.)*H
      Y=COS(BETA(J+1)*3.14/180.)*SIN(OMEGA(J+1)*3.14/180.)*H
      Z=SIN(BETA(J+1)*3.14/180.)*H
      LENGTH(J+1)=LENGTH(J)+X
      SPREAD(J+1)=SPREAD(J)+Y
      DEPTH(J+1)=DEPTH(J)+Z
      CL(J+1)=CL(J)+.1
10    CONTINUE
C*************************************************************
C****** OUTPUT SECTION ***************
      TYPE*,'NAME OUTPUT FILE'
      ACCEPT25,OUTPUT
25    FORMAT(16A1)
      OUTPUT(16)=0.0
      OPEN(UNIT=1.0,NAME=OUTPUT,ACCESS='SEQUENTIAL',TYPE='NEW')
      WRITE(1,26)
26    FORMAT('1',' LENGTH    TENSION      b    w      X      Y
     1     Z')
      DO 351=1,2300,330
      IF(I.EQ.1)GO TO 27
      IF(I.EQ.1981)GO TO 28
      J=I-1
      GO TO 29
27    CONTINUE
      J=1
      GO TO 29
```

```
28      CONTINUE
        J=2811
29      CONTINUE
        WRITE(11,30)CL(J),T(J),BETA(J),OMEGA(J),LENGTH(J),DEPTH(J),SPREAD(J)
30      FORMAT(1H ,1X,F5.1,4X,F8.2,3X,F5.2,3X,F4.2,3X,F6.2,3X,F5.2,3X,
     1  F5.2)
35      CONTINUE
        CLOSE(UNIT=1)
        STOP
        END
```

Appendix B

EXPERIMENTAL NET DRAG

Table B-1: Net #1.0, $\alpha = 0°$

V (m/s)	(e)	1.00	1.20	1.40	1.60	1.80	2.00
NET/FRAME (mV)	(±.48%)	29.00	36.85	46.26	57.23	72.13	86.05
FRAME (mV)	(±.48%)	22.74	29.00	36.85	47.82	61.15	74.48
NET (mV)	(±2.82%)	6.26	7.85	9.41	9.41	10.99	11.57
NET (N)	(±2.83%)	3.98	4.94	5.93	5.95	6.92	8.38

Table B-2: Net #1.0, $\alpha = 5°$

V (m/s)	(e)	1.00	1.20	1.40	1.60	1.80	2.00
NET/FRAME (mV)	(±.48%)	28.22	39.20	53.31	68.21	82.32	99.57
FRAME (mV)	(±.48%)	23.52	31.36	41.55	53.31	66.64	82.32
NET (mV)	(±3.75%)	4.70	7.84	11.76	14.90	15.68	17.25
NET (N)	(±3.76%)	2.96	4.94	7.40	9.37	9.88	10.86

Table B-3: Net #1.0, $\alpha = 10°$

V (m/s)	(e)	1.00	1.20	1.40	1.60	1.80	2.00
NET/FRAME (mV)	(±.48%)	36.06	51.74	69.77	90.16	109.16	134.85
FRAME (mV)	(±.48%)	23.52	32.93	43.90	54.88	68.21	84.67
NET (mV)	(±1.64%)	12.54	18.81	25.87	35.28	41.55	50.18
NET (N)	(±1.65%)	7.90	11.85	16.30	22.22	26.17	31.60

Table B-4: Net #1.0, $\alpha = 15^\circ$

V (m/s)	(e)	1.00	1.20	1.40	1.60	1.80	2.00
NET/FRAME (mV)	(±.48%)	40.77	58.80	78.40	104.27	130.14	158.37
FRAME (mV)	(±.48%)	22.74	31.36	43.91	53.31	67.42	81.54
NET (mV)	(±1.24%)	18.03	27.44	34.49	50.96	62.72	78.83
NET (N)	(±1.26%)	11.36	17.22	22.27	32.10	39.50	48.39

Table B-5: Net #1.0, $\alpha = 20^\circ$

V (m/s)	(e)	1.00	1.20	1.40	1.60	1.80	2.00
NET/FRAME (mV)	(±.48%)	44.69	65.86	87.81	112.90	142.69	171.00
FRAME (mV)	(±.48%)	23.52	31.36	41.55	54.10	67.42	83.11
NET (mV)	(±1.14%)	21.17	34.50	46.26	58.80	75.27	87.89
NET (N)	(±1.16%)	13.32	18.64	29.13	37.04	47.40	55.30

Table B-6: Net #1.0, $\alpha = 30^\circ$

V (m/s)	(e)	1.00	1.20	1.40	1.60	1.80	2.00
NET/FRAME	(±.48%)	47.04	65.86	85.85	113.68	142.69	176.40
FRAME (mV)	(±.48%)	26.66	32.14	42.34	54.88	68.21	81.54
NET (mV)	(±1.27%)	20.38	33.72	43.51	58.80	74.48	94.86
NET (N)	(±1.29%)	12.83	21.24	27.40	37.03	46.92	59.75

Table B-7: Net #1.0, $\alpha = 60°$

V (m/s)	(e)	1.00	1.20	1.40	1.60	1.80	2.00
NET/FRAME (mV)	(±.48%)	54.45	79.97	108.19	143.67	180.32	225.79
FRAME (mV)	(±.48%)	25.09	36.85	52.53	68.21	91.73	112.89
NET (mV)	(±.48%)	29.36	43.12	55.66	75.46	88.59	112.90
NET (N)	(±.98%)	19.75	27.16	35.06	47.56	55.80	71.10

Table B-8: Net #1.0, $\alpha = 90°$

V (m/s)	(e)	1.00	1.20	1.40	1.60	1.80	2.00
NET/FRAME (mV)	(±.48%)	62.72	89.38	122.30	159.94	203.05	251.47
FRAME (mV)	(±.48%)	31.36	40.77	55.47	83.10	105.06	122.31
NET (mV)	(±1.07%)	31.36	48.61	66.83	67.16	97.99	129.16
NET (N)	(±1.09%)	19.75	30.61	42.46	48.39	61.72	81.35

Table B-9: Net #2.0, $\alpha = 0°$

V (m/s)	(e)	1.00	1.20	1.40	1.60	1.80	2.00
NET/FRAME (mV)	(±.48%)	26.66	37.63	50.17	65.07	83.10	101.92
FRAME (mV)	(±.48%)	22.74	30.58	40.77	51.75	65.85	80.75
NET (mV)	(±4.29%)	3.92	7.05	9.40	13.32	17.25	21.17
NET (N)	(±4.30%)	2.46	4.44	5.93	8.38	10.86	13.33

Table B-10: Net #2.0, $\alpha = 5°$

V (m/s)	(e)	1.00	1.20	1.40	1.60	1.80	2.00
NET/FRAME (mV)	(±.48%)	28.22	39.20	53.31	68.99	85.45	107.41
FRAME (mV)	(±.48%)	23.52	31.36	41.55	53.31	66.64	82.32
NET (mV)	(±3.75%)	4.70	7.84	11.76	15.68	18.81	25.09
NET (N)	(±3.76%)	2.96	4.94	7.40	9.88	11.85	15.80

Table B-11: Net #2.0, $\alpha = 10°$

V (m/s)	(e)	1.00	1.20	1.40	1.60	1.80	2.00
NET/FRAME (mV)	(±.48%)	36.06	51.75	71.34	92.51	112.89	139.50
FRAME (mV)	(±.48%)	23.52	32.93	43.90	54.88	68.21	84.67
NET (mV)	(±1.65%)	12.54	18.82	27.44	37.63	44.68	54.83
NET (N)	(±1.66%)	7.90	11.85	17.27	23.70	28.15	34.56

Table B-12: Net #2.0, $\alpha = 15°$

V (m/s)	(e)	1.00	1.20	1.40	1.60	1.80	2.00
NET/FRAME (mV)	(±.48%)	43.12	1.94	83.10	108.19	134.85	166.21
FRAME (mV)	(±.48%)	22.74	31.36	43.90	53.31	67.43	81.54
NET (mV)	(±1.15%)	20.38	30.58	39.20	54.88	67.42	84.67
NET (N)	(±1.17%)	12.84	19.25	24.69	34.56	42.46	53.33

Table B-13: Net #2.0, $\alpha = 20°$

V (m/s)	(e)	1.00	1.20	1.40	1.60	1.80	2.00
NET/FRAME (mV)	(±.48%)	47.82	69.78	92.51	117.60	148.96	182.67
FRAME (mV)	(±.48%)	23.52	31.36	41.55	54.09	67.43	83.10
NET (mV)	(±1.05%)	24.30	38.42	50.96	63.51	81.51	99.57
NET (N)	(±1.07%)	15.30	24.20	32.08	40.00	51.35	62.72

Table B-14: Net #2.0, $\alpha = 30°$

V (m/s)	(e)	1.00	1.20	1.40	1.60	1.80	2.00
NET/FRAME (mV)	(±.48%)	48.60	71.34	97.22	127.00	160.70	197.56
FRAME (mV)	(±.48%)	26.12	31.49	43.90	53.78	71.34	87.80
NET (mV)	(±1.17%)	22.48	39.85	53.32	73.22	89.36	109.76
NET (N)	(±1.19%)	15.80	24.82	33.58	44.83	57.03	69.13

Table B-15: Net #2.0, $\alpha = 60°$

V (m/s)	(e)	1.00	1.20	1.40	1.60	1.80	2.00
NET/FRAME (mV)	(±.48%)	61.94	88.59	121.52	158.36	202.27	250.88
FRAME (mV)	(±.48%)	27.44	38.42	54.09	70.56	96.43	122.30
NET (mV)	(±.94%)	34.50	50.17	67.43	87.80	105.84	128.58
NET (N)	(±.96%)	21.73	31.60	42.46	55.30	66.66	80.98

Table B-16: Net #2.0, $\alpha = 90^\circ$

V (m/s)	(e)	1.00	1.20	1.40	1.60	1.80	2.00
NET/FRAME (mV)	(±.48%)	70.56	101.92	139.55	183.45	233.63	289.29
FRAME (mV)	(±.48%)	29.00	44.69	61.94	90.94	124.65	141.12
NET (mV)	(±.88%)	41.56	57.23	77.61	92.51	108.98	148.17
NET (N)	(±.91%)	26.17	36.05	48.88	58.26	68.64	93.33

Table B-17: Net #3.0, $\alpha = 0^\circ$

V (m/s)	(e)	1.00	1.20	1.40	1.60	1.80	2.00
NET/FRAME (mV)	(±.48%)	26.66	37.63	52.53	65.86	76.83	92.51
FRAME (mV)	(±.48%)	22.74	30.58	40.77	51.75	65.85	80.75
NET (mV)	(±4.29%)	3.92	6.78	11.76	14.11	10.98	11.76
NET (N)	(±4.30%)	2.47	4.45	7.42	8.88	6.92	7.43

Table B-18: Net #3.0, $\alpha = 5^\circ$

V (m/s)	(e)	1.00	1.20	1.40	1.60	1.80	2.00
NET/FRAME (mV)	(±.48%)	31.36	37.63	48.61	64.29	78.40	97.22
FRAME (mV)	(±.48%)	23.52	31.36	41.55	53.31	66.64	82.32
NET (mV)	(±2.40%)	7.84	6.27	7.06	10.98	11.76	14.90
NET (N)	(±2.41%)	4.94	3.95	4.44	6.92	7.42	9.37

Table B-19: Net #3.0, $\alpha = 10°$

V (m/s)	(e)	1.00	1.20	1.40	1.60	1.80	2.00
NET/FRAME (mV)	(±.48%)	32.93	47.04	62.72	81.54	101.14	121.52
FRAME (mV)	(±.48%)	23.52	32.93	43.90	54.88	68.21	84.67
NET (mV)	(±2.06%)	9.41	14.11	18.82	26.66	32.93	36.85
NET (N)	(±2.07%)	5.92	8.88	11.85	16.78	20.74	23.21

Table B-20: Net #3.0, $\alpha = 15°$

V (m/s)	(e)	1.00	1.20	1.40	1.60	1.80	2.00
NET/FRAME (mV)	(±.48%)	34.50	50.17	68.99	90.16	112.11	137.98
FRAME (mV)	(±.48%)	22.74	31.36	43.90	53.31	67.43	81.54
NET (mV)	(±1.68%)	11.76	18.81	25.09	36.85	44.68	56.44
NET (N)	(±1.69%)	7.41	11.85	15.80	23.21	28.15	35.55

Table B-21: Net #3.0, $\alpha = 20°$

V (m/s)	(e)	1.00	1.20	1.40	1.60	1.80	2.00
NET/FRAME (mV)	(±.48%)	38.42	54.88	71.34	94.08	117.60	141.90
FRAME (mV)	(±.48%)	23.52	31.36	41.55	54.09	67.43	83.16
NET (mV)	(±1.45%)	14.90	23.52	29.79	39.99	50.17	58.81
NET (N)	(±1.47%)	9.38	14.81	19.82	25.19	31.60	37.03

Table B-22: Net #3.0, $\alpha = 30°$

V (m/s)	(e)	1.00	1.20	1.40	1.60	1.80	2.00
NET/FRAME (mV)	(±.48%)	39.20	57.23	76.23	99.57	122.30	150.53
FRAME (mV)	(±.48%)	23.52	31.49	43.96	53.78	71.34	87.80
NET (mV)	(±1.39%)	15.67	25.74	32.93	45.79	50.96	62.73
NET (N)	(±1.41%)	8.87	16.30	20.74	27.65	32.10	39.50

Table B-23: Net #3.0, $\alpha = 60°$

V (m/s)	(e)	1.00	1.20	1.40	1.60	1.80	2.00
NET/FRAME (mV)	(±.48%)	55.66	78.40	106.60	138.77	178.75	221.10
FRAME (mV)	(±.48%)	27.44	38.42	54.04	70.56	96.43	122.30
NET (mV)	(±1.05%)	28.22	39.98	52.56	68.21	82.32	98.79
NET (N)	(±1.07%)	17.77	25.18	33.08	42.96	51.85	62.21

Table B-24: Net #3.0, $\alpha = 90°$

V (m/s)	(e)	1.00	1.20	1.40	1.60	1.80	2.00
NET/FRAME (mV)	(±.48%)	65.86	95.65	131.71	170.91	215.60	264.99
FRAME (mV)	(±.48%)	29.0	44.69	61.94	90.94	124.65	141.12
NET (mV)	(±..93%)	36.86	50.96	69.77	79.97	90.95	123.87
NET (N)	(±.95%)	23.21	32.08	43.95	50.36	57.28	78.01

Table B-25: Net #4.0, $\alpha = 20^\circ$, $\theta = 43^\circ$

V (m/s)	(e)	1.00	1.20	1.40	1.60	1.80	2.00
NET/FRAME (mV)	(±.48%)	36.85	51.74	68.99	89.37	111.33	136.42
FRAME (mV)	(±.48%)	23.52	31.36	41.55	54.09	67.43	83.10
NET (mV)	(±1.57%)	13.33	20.36	27.44	35.28	43.90	53.32
NET (N)	(±1.58%)	8.40	12.84	17.28	22.22	27.65	33.57

Table B-26: Net #5.0, $\alpha = 20^\circ$, $\theta = 48^\circ$

V (m/s)	(e)	1.00	1.20	1.40	1.60	1.80	2.00
NET/FRAME (mV)	(±.48%)	34.50	48.61	65.07	83.10	104.27	128.58
FRAME (mV)	(±.48%)	23.52	31.36	41.55	54.09	67.43	83.10
NET (mV)	(±1.82%)	10.98	17.25	23.52	29.01	36.84	45.47
NET (N)	(±1.83%)	6.91	10.86	14.81	18.27	23.22	28.64

Table B-27: Net #6.0, $\alpha = 20^\circ$, $\theta = 60^\circ$

V (m/s)	(e)	1.00	1.20	1.40	1.60	1.80	2.00
NET/FRAME (mV)	(±.48%)	31.36	43.90	59.58	76.83	97.22	119.17
FRAME (mV)	(±.48%)	23.52	31.36	41.55	54.09	67.43	83.10
NET (mV)	(±2.40%)	7.84	12.54	18.03	22.74	29.79	36.07
NET (N)	(±2.41%)	4.93	7.90	11.36	14.31	18.76	22.72

Table B-28: Net #7.0, $\alpha = 20^\circ$, $\theta = 79^\circ$

V (m/s)	(e)	1.00	1.20	1.40	1.60	1.80	2.00
NET/FRAME (mV)	(±.48%)	32.14	45.47	61.15	78.40	98.78	120.74
FRAME (mV)	(±.48%)	23.52	31.36	41.55	54.09	67.43	83.10
NET (mV)	(±2.21%)	8.62	14.11	19.60	24.31	31.35	37.64
NET (N)	(±2.22%)	5.43	8.88	12.33	15.30	19.77	23.70

Table B-29: Net #4.0, $\alpha = 90^\circ$, $\theta = 43^\circ$

V (m/s)	(e)	1.00	1.20	1.40	1.60	1.80	2.00
NET/FRAME (mV)	(±.48%)	58.02	83.89	116.82	152.09	190.51	243.04
FRAME (mV)	(±.48%)	29.00	44.69	61.94	90.95	124.65	141.12
NET (mV)	(±1.07%)	29.02	39.20	54.88	61.14	65.86	101.92
NET (N)	(±1.09%)	18.27	24.68	34.56	38.51	41.47	64.18

Table B-30: Net #5.0, $\alpha = 90^\circ$, $\theta = 48^\circ$

V (m/s)	(e)	1.00	1.20	1.40	1.60	1.80	2.00
NET/FRAME (mV)	(±.48%)	57.23	84.67	116.82	148.96	188.16	230.50
FRAME (mV)	(±.48%)	29.00	44.69	61.94	90.95	124.65	141.12
NET (mV)	(±1.09%)	28.23	39.98	54.88	58.02	63.51	89.38
NET (N)	(±1.11%)	17.77	25.17	34.56	36.54	39.98	59.25

Table B-31: Net #6.0, $\alpha = 90^\circ$, $\theta = 60^\circ$

V (m/s)	(e)	1.00	1.20	1.40	1.60	1.80	2.00
NET/FRAME (mV)	(±.48%)	64.29	96.43	130.14	169.34	216.38	271.26
FRAME (mV)	(±.48%)	29.00	44.69	61.94	90.95	124.65	141.12
NET (mV)	(±.95%)	35.29	51.74	68.20	78.40	91.73	130.14
NET (N)	(±.97%)	22.22	32.59	42.95	49.38	57.77	81.96